AD-A063 847 AIR FORCE FLIGHT DYNAMICS LAB WRIGHT-PATTERSON AFB OHIO F/G 4/2
THE LASER LIGHTNING ROD SYSTEM: A FEASIBILITY STUDY.(U)
JUN 78 C W SCHUBERT

UNCLASSIFIED AFFDL-TR-78-60 NL

1 OF 2
AD A063 847

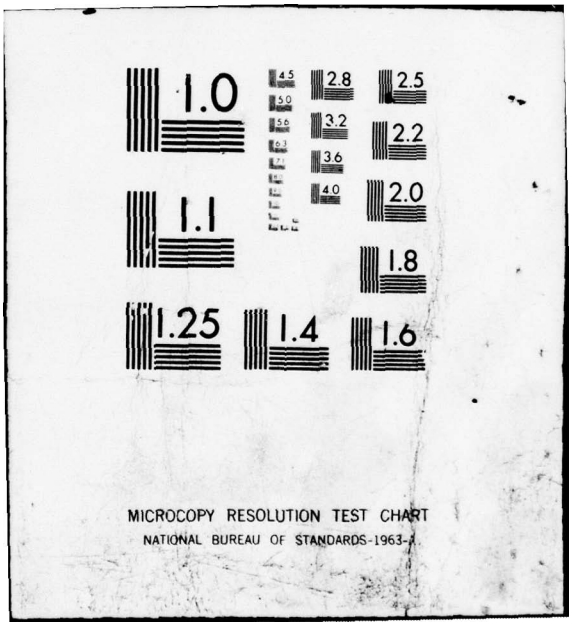
1.0
1.1
1.25
1.4
1.6
1.8
2.0
2.2
2.5
2.8
3.2
3.6
4.0
4.5
5.0
5.6
MICROCOPY RESOLUTION TEST CHART
NATIONAL BUREAU OF STANDARDS-1963-A

AFFDL-TR-78-60

LEVEL II

(2)

AD A063847

THE LASER LIGHTNING ROD SYSTEM: A FEASIBILITY STUDY

Survivability/Vulnerability Branch
Vehicle Equipment Division

June 1978

TECHNICAL REPORT AFFDL-TR-78-60

Final Report for the Period May through December 1977

AIR FORCE FLIGHT DYNAMICS LABORATORY
AIR FORCE WRIGHT AERONAUTICAL LABORATORIES
AIR FORCE SYSTEMS COMMAND
WRIGHT-PATTERSON AIR FORCE BASE, OHIO 45433

NOTICE

When Government drawings, specifications, or other data are used for any purpose other than in connection with a definitely related Government procurement operation, the United States Government thereby incurs no responsibility nor any obligation whatsoever; and the fact that the Government may have formulated, furnished, or in any way supplied the said drawings, specifications, or other data, is not to be regarded by implication or otherwise as in any manner licensing the holder or any other person or corporation, or conveying any rights or permission to manufacture, use, or sell any patented invention that may in any way be related thereto.

This report has been reviewed by the Information Office (IO) and is releasable to the National Technical Information Service (NTIS). At NTIS, it will be available to the general public, including foreign nations.

This technical report has been reviewed and is approved for publication.

Charles W. Schubert

CHARLES W. SCHUBERT, JR.
Captain, USAF

Vernon L. Mangold

VERNON L. MANGOLD
Chief, Electromagnetic Hazards Group
Survivability/Vulnerability Branch
Vehicle Equipment Division

FOR THE COMMANDER

Ambrose B. Nutt

AMBROSE B. NUTT
Director, Vehicle Equipment Division

Copies of this report should not be returned unless return is required by security considerations, contractual obligations, or notice on a specific document.

AIR FORCE/56780/31 August 1978 — 200

UNCLASSIFIED

SECURITY CLASSIFICATION OF THIS PAGE (When Data Entered)

REPORT DOCUMENTATION PAGE

READ INSTRUCTIONS BEFORE COMPLETING FORM

1. REPORT NUMBER: AFFDL-TR-78-60	2. GOVT ACCESSION NO.
3. RECIPIENT'S CATALOG NUMBER	
4. TITLE (and Subtitle): The Laser Lightning Rod System: A Feasibility Study.	5. TYPE OF REPORT & PERIOD COVERED: Final Report, May 1977 - December 1977
	6. PERFORMING ORG. REPORT NUMBER
7. AUTHOR(s): Captain Charles W. Schubert, Jr	8. CONTRACT OR GRANT NUMBER(s)
9. PERFORMING ORGANIZATION NAME AND ADDRESS: Air Force Flight Dynamics Laboratory, AF Wright Aeronautical Laboratories, Wright-Patterson AFB, Ohio 45433	10. PROGRAM ELEMENT, PROJECT, TASK AREA & WORK UNIT NUMBERS
11. CONTROLLING OFFICE NAME AND ADDRESS: Air Force Flight Dynamics Laboratory, AF Wright Aeronautical Laboratories, Wright-Patterson AFB, Ohio 45433	12. REPORT DATE: June 1978 13. NUMBER OF PAGES: 129
14. MONITORING AGENCY NAME & ADDRESS (if different from Controlling Office): 115 p.	15. SECURITY CLASS. (of this report): UNCLASSIFIED 15a. DECLASSIFICATION/DOWNGRADING SCHEDULE

16. DISTRIBUTION STATEMENT (of this Report)

Approved for public release; distribution unlimited

16 4363

17. DISTRIBUTION STATEMENT (of the abstract entered in Block 20, if different from Report)

17 Q1

18. SUPPLEMENTARY NOTES

19. KEY WORDS (Continue on reverse side if necessary and identify by block number)

Lightning Triggering
Laser Triggering

20. ABSTRACT (Continue on reverse side if necessary and identify by block number)

The feasibility of triggering lightning with an intense laser pulse is investigated. Physical mechanisms by which such triggerings might occur are examined, and criteria for lightning initiation with a laser beam established. A differential equation for determining the free electron distribution along a kilometer long laser beam is developed, based on the electron-cascade model of gas breakdown. Predictions are made of the electron distribution along laser beams of various focal lengths, wavelengths, pulse shapes, pulse lengths,

DD FORM 1 JAN 73 1473 EDITION OF 1 NOV 65 IS OBSOLETE

next page

SECURITY CLASSIFICATION OF THIS PAGE (When Data Entered)

Q12070

and flux intensities. The predicted densities are compared with the criteria for triggering lightning. A conclusion is drawn that the triggering of lightning with a laser pulse is feasible from the standpoint of the physics involved; but would require large laser apertures, short pulse lengths, and flux intensities at the aperture near the threshold for the breakdown of air.

FOREWORD

This report was prepared as a partial fulfillment of requirements for a degree of Masters of Science from the Air Force Institute of Technology (AFIT), WPAFB, Ohio. The program was conducted in support of an Air Force Flight Dynamics in-house work unit, 43630146 (LDF), "Laser Triggered Lightning (TRIP-77)."

The work reported was performed during the period June 1977 to October 1977, under the direction of the author, Charles W. Schubert, Jr. (Captain, USAF), principal investigator. The report was released by the author in December 1977.

The author wishes to thank his sponsors, Mr. Jack Lippert and Mr. Vernon Mangold of AFFDL/FES and Phil Nielsen (Captain, USAF) of the Air Force Institute of Technology who served as advisor.

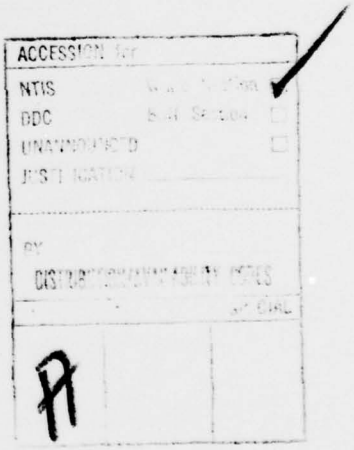

TABLE OF CONTENTS

TABLE OF CONTENTS (CONTINUED)

LIST OF ILLUSTRATIONS

LIST OF ILLUSTRATIONS (CONTINUED)

LIST OF TABLES

SECTION I

INTRODUCTION

The study of lightning and its effects has long been hampered because of the erratic nature of the lightning stroke. If lightning is to be studied well, it must be examined closely; from the point in a cloud at which it begins, to the location on the ground at which it ultimately strikes. Because of the impossibility of knowing exactly when or where the next stroke will take place, months and years are required to collect data even on distant lightning strikes.

To enable the study of lightning at close hand, experiments in the artificial triggering of lightning have been pursued. The most successful of these experiments, the rocket launching of a thin wire toward the base of a cloud, has achieved a lightning initiation success rate exceeding fifty percent. The lightning strokes initiated by this wire-and-rocket system, however, vaporize the wire and create a dense channel of metallic ions in the air. The lightning, in following this channel, acquires characteristics vastly different from the natural lightning stroke.

The demonstrated ability of high-powered lasers to produce ionized pathways in air, taken in conjunction with known facts about lightning initiation, suggests that lasers might be effective in the artificial triggering of lightning. The lightning stroke which might be initiated by a laser beam would follow a path of ionic species native to the air and to a natural lightning stroke. Consequently, if lightning can be triggered by a laser, the resultant stroke might be very similar to strokes which occur spontaneously.

1. PURPOSE

The purpose of this report is to determine whether the triggering of lightning with a laser-induced ionized pathway in air is indeed feasible.

To make this determination, analytical answers to the following questions will be required:

1. Can the physical mechanisms which occur in known methods of lightning initiation be duplicated through the use of an ionized column of air?

2. What external dimensions and internal ion density would such a column require?

3. Can lasers within our current level of technology create the appropriately configured ionized column?

4. What would be the best laser beam frequency, power, focal length, wavelength, pulse width, and pulse shape to perform the task?

2. SCOPE

The depth of the study will unfortunately be limited to some extent by the lack of knowledge concerning the general physics of lightning and the specific physics of laser-induced ionized pathways.

Theoretical models concerning the initiation and propagation of lightning are vague, and, at times, contradictory. Published information on experimentally determined electric fields, electron densities, and space-charge dimensions in a lightning channel are sparse or nonexistent. Because of this, the analysis of the known methods of lightning initiation can at best result in order-of-magnitude estimates of the parameters involved. No attempt will be made to extend the knowledge of lightning physics beyond that which is currently known. Furthermore, only cloud-to-ground lightning will be studied; cloud-to-cloud discharge will not be addressed.

The physics of laser-induced ionized pathways in air is currently in a state of active evolution. A large number of physical processes

are involved in the production of such pathways and a precise mathematical description of many of the contributing factors has yet to emerge. This study will be limited to those processes for which adequate mathematical models have been developed. The primary aim will be to extend these models to the specific problem of producing an ionized pathway on the order of one kilometer long.

The production of an ionized column of air with a specific configuration will involve a rather complicated system of lens and supporting hardware. This study will be limited, for the most part, to a description of laser beams which can be produced using hardware currently available. No attempt, therefore, will be made to discuss the specific systems or hardware that will be required. In essence, the study will focus on the physics involved beyond the final lens of the system producing the laser beam.

3. ORGANIZATION

In Section II, the mechanisms of lightning and its initiation are examined to determine criteria for the triggering of lightning with a laser beam. Sections III and IV are devoted to the development of an analytical expression for the electron distribution along a laser-induced ionized column of air. Significant parameters which affect the distribution and which impose limitations on a laser lightning rod system are analyzed in Section V. In Section VI, the theory developed in the preceding chapters is applied to specific laser lightning rod scenarios. The electron distribution along the beam in each scenario is determined, the results are compared to the criteria, and conclusions are drawn.

SECTION II

THE INITIATION OF LIGHTNING

To determine the feasibility of triggering lightning with a laser beam, it is necessary to identify the physical mechanisms which cause lightning to occur. The mechanisms discussed in this section fall into two categories: (1) natural causes of lightning, and (2) artificial methods of triggering lightning and sparks. The former category is presented via a discussion of theories about the lightning process; the latter, by descriptions of lightning and spark control experiments. Specific physical mechanisms through which a laser beam may initiate lightning are discussed at the end of the section.

1. THE LIGHTNING PROCESS

Lightning is an extremely complex phenomenon which is only partially understood at the present time. Lightning studies have been necessarily slow, since the acquisition of data must await the whim of nature to provide a lightning stroke at the right place at the right time for examination. In addition, since no two lightning strokes are identical, a correlation of acquired data from separate studies is somewhat sketchy and difficult to interpret.

Since an explanation of the lightning process must draw from available data, the theories concerning lightning tend to be vague, and, at times, contradictory. From a very elementary standpoint, however, lightning can be viewed as a huge spark discharge between the lower part of a cloud and the ground. As such, the earth and cloud may be regarded as parallel plates of a capacitor, with the intervening air serving as a dielectric. When the electric field between the cloud and the ground is sufficiently high, the air dielectric breaks down, and lightning occurs. In reality, however, this simple picture becomes greatly complicated.

Through mechanisms not yet completely understood, thunderclouds develop distinct oppositely charged regions on the order of kilometers in diameter (Reference 26: 2-3). Typically, the upper part of the cloud gathers a positive charge of perhaps 40 coulombs; the lower part, a negative charge of approximately the same magnitude. The exact size, shape, and charge of these regions is influenced by a turmoil of changing atmospheric conditions within the cloud. As a result, the electric fields in and around thunderclouds are strongly nonuniform, and change in intensity and in direction with the passage of time (Reference 8: 21-38).

The electric field required to produce the breakdown of air at ground level is approximately 3000 kV/m. Field intensities within active thunderclouds are much less: Fitzgerald reports an isolated high value of 390 kV/m (Reference 9: 839), and measurements of maximum fields by Gunn average 130 kV/m (Reference 10: 483). Field intensities on the ground are even smaller. A typical high value from data collected by Fitzgerald during surface measurements near a thunderstorm is on the order of only 1 kV/m (Reference 8: 26). A cursory glance at the data would thus indicate that lightning is impossible. That lightning does occur can be partially explained from the supposition that water droplets within a thundercloud, and the reduced pressure of higher altitude, lower the threshold for the breakdown of air to perhaps 200 kv/m within a cloud (Reference 20: 34). Thus, breakdown inside a cloud mass can easily occur. The mechanism by which lightning leaps from a cloud to the ground, however, remains somewhat a mystery.

Photographic studies of cloud-to-ground lightning strokes show that lightning begins the downward trek through a series of weakly luminous steps, each about 50 meters long, and each with a velocity of about 1.5×10^5 m/sec (Reference 26: 4-11). After each step, a pause of approximately 50 microseconds occurs. When this initiating stroke, or stepped leader, reaches the near vicinity of the ground, it is met by a highly luminous upward-travelling return stroke. The return stroke, moving with a velocity of about 5×10^7 m/sec, follows the path forged through the air by the stepped leader, and enters the cloud. After a

pause of 100 milliseconds or less, a dimly luminous dart leader may then traverse the original path downward at a speed of approximately 2×10^6 m/sec and initiate a second return stroke. The process is repeated until the flow of charge within the cloud can no longer support a dart leader. The highly luminous upward-moving return strokes produce the bright flash associated with lightning. Other varients of lightning exist in which the initiating stroke moves upward. These are most often observed in lightning strikes to tall objects.

Explanations of the observed characteristics of lightning are many and varied. Uman summarizes most of the suggested theories in his book on lightning (Reference 26: 216-222). It can serve no useful purpose to recount the assorted explanations here since none has been proved valid (or altogether invalid), and all are rather lengthy. It is generally agreed, however, that lightning begins with a localized breakdown in the cloud. The manner in which the breakdown leaves the cloud is the matter of controversy. Estimates of the leader radius and of the electron density within the leader from two of the more recent theories are listed below:

1. Leader radius: 500 cm
   Electron density: 10^9 cm^{-3} (Ref. 12: 867)

2. Leader radius: less than 100 cm
   Electron density: 10^{10} cm^{-3} (Ref. 26: 221)

The most accurate summary statement that may be made about the start of a lightning stroke is that it begins as a result of electric-field nonuniformities within a region of easily ionized air. A leader with a radius less than 500 cm and an electron density of at least 10^9 electrons/cm^3 is then somehow propelled to the earth.

2. ARTIFICIAL TRIGGERINGS OF LIGHTNING AND SPARKS

Three methods of triggering lightning and two methods of controlling sparks have been successfully employed. An examination of these

methods, and how they work, suggests the physical characteristics that a laser beam would require in order to initiate lightning. A brief outline of the methods, and the physical mechanisms underlying each, follows.

a. Common Lightning Rods

Although the ordinary lightning rod is not generally regarded as a lightning-triggering device, it must at least qualify as a lightning gatherer. Many statistics are available which substantiate the effectiveness of lightning rods in protecting structures by absorbing lightning strokes (Reference 27: 202). The Empire State Building, 381 meters tall, was struck an average of 22.7 times a year during studies in the nineteen-thirties. Figure 1, adapted from Viemeister and based on Westinghouse data, shows the number of times an object is struck per year, as a function of object height.

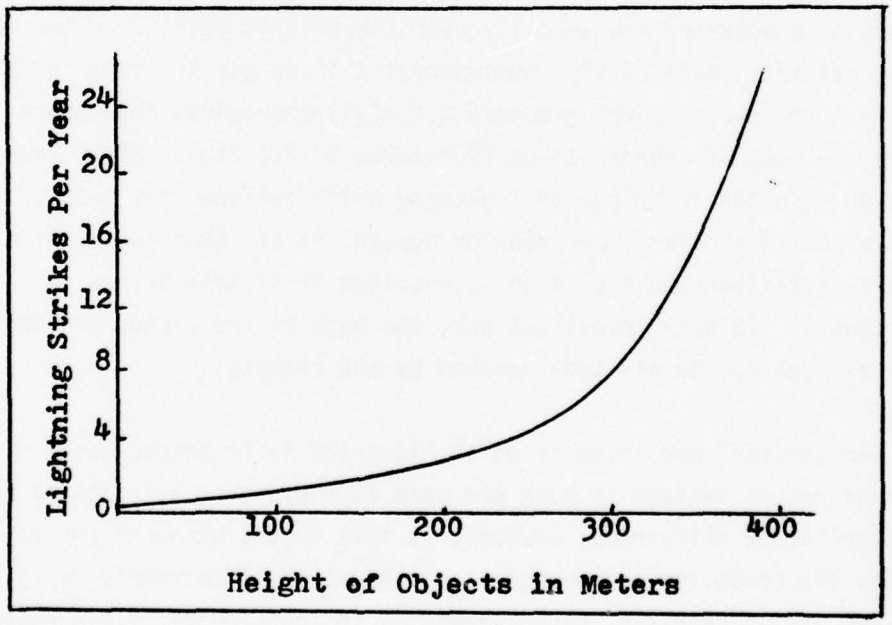

Figure 1. Annual Number of Lightning Strikes to Tall Objects

The principle underlying the lightning r an most easily be explained through the use of the parallel-plate capacitor model of lightning initiation mentioned earlier. If the plates (earth and cloud) are separated by a distance d, and a voltage V is applied, the electric field between the plates is given by the elementary expression on $E = \frac{V}{d}$. The potential difference between the earth and the cloud is established by the amount of charge that each possesses, and is approximately constant. However, the lightning rod, being a conductor, elevates the ground charge, and thereby diminishes the separation distance d. This results in an increased electric field at the top of the rod compared to the field at the ground. The small radius of curvature at the top of sharply pointed lightning rods serves to further increase the electric field by a small factor. Since air is more easily broken down in regions of high E, the lightning tends to follow a path to the top of the lightning rod.

b. Wire and Rockets

Experiments attempting to trigger lightning with wire-and-rocket systems have occurred sporadically over the past 40 years. In the most recent attempts, made by the Commissariat à l'Energie Atomique in France, rockets were used to carry grounded 0.2 millimeter wires 700 meters toward the base of thunderclouds (Reference 7: 212-213). Of 30 launches made, 20 resulted in triggered lightning which followed the path of the steel wire. A similar experiment by Newman, et al. (Reference 17: 4761), using rockets launched from a ship, resulted in 17 triggerings in 23 attempts. In both investigations, the base of the clouds was at least twice as high as the altitude reached by the rockets.

The physical mechanism by which lightning is triggered using wire-and-rocket systems is much the same as that for the lightning rod. One significant difference, however, is that in the wire-and-rocket systems the conductor is brought to a high altitude extremely rapidly. This results in transient nonuniformities in the electric field which may increase the probability of lightning initiation.

c. Sphere-Tipped Rockets

Investigating a theory developed by H. W. Kasemir, the New Mexico Institute of Mining and Technology attempted to discharge lightning by firing rockets tipped with metal spheres into the peak electric-field regions of thunderclouds. According to Kasemir, rockets with a suitable body-length to sphere-radius ratio can distort the electric field at the base of a thundercloud. Such distortion produces a localized air breakdown which then develops into a normal lightning discharge (Reference 11: 237). In the New Mexico experiment, rockets a meter long were tipped with metal spheres five, seven, or ten centimeters in diameter. The rockets were air-launched into thundercloud regions having electric fields on the order of 100 kV/m. Lightning discharges in the vicinity of the rocket flight paths were then monitored, and the results tabulated. Lightning discharges within 61 seconds of launch occurred following 9 of 12 launches. A possibility exists, however, that some or all of the discharges may have occurred regardless of the rocket flights (Reference 6: 623-627).

d. Laser-Produced Rarefication Channels

The guidance of an electrical spark by a laser-produced rarefication channel in a gas was reported in 1972. In an experiment performed by Saum and Koopman (Reference 22: 2077-2079), the distance that a spark would travel between two electrodes at a given voltage was measured. A 75-watt continuous wave CO_2 laser beam was then directed between the electrodes, from one to the other, and the maximum spark gap allowable again measured. It was found that the length of the spark could be increased from 14 centimeters to 20.4 centimeters by use of the laser beam. In addition, the spark followed the linear path of the laser beam, and lost the crooked shape usually associated with electrical discharge.

The experiments were performed with the electrodes in an atmosphere of air doped with NH_3. The NH_3 molecules, excited by the laser irradiation, increased the kinetic energy of air molecules as a result of collisions, and the gas became heated.

The physical basis for spark guidance by rarefication channels is that the laser-heated gas expands and leaves a transient cylinder of low-density air between the two electrodes. Since the electrical field required to cause breakdown is inversely proportional to air density, the spark preferentially follows the path of the laser beam.

e. Laser-Produced Channels of Ions in Air

Experiments by Koopman and Saum (Reference 13: 5328-5336) have shown that electrical sparks can be guided in laser-induced ionized channels of air. Using a Nd-glass laser with a focused power density of 10^{10} to 10^{11} W/cm^2, and a beam diameter of a few millimeters, Koopman and Saum ionized a column of air between two electrodes separated by as much as a meter. A potential difference of breakdown, or near breakdown, intensity was then applied across the electrodes. It was found that the electrical discharges produced followed the straight path of the laser beam rather than the twisted trail that sparks normally take.

The principle underlying the spark guidance is that the air is partially broken down by the laser beam. The spark then follows the path of least resistance. An analysis presented by Koopman and Saum indicates that an upper limit for the guidance of sparks in air is 10^{10} to 10^{11} electrons/cm^3.

3. MECHANISMS OF LASER-TRIGGERED LIGHTNING

Some physical mechanisms must underlie the triggering of lightning with a laser beam. The mechanisms discussed in the preceding sections are some possibilities. Others may exist which have not yet been determined or exploited. From the mechanisms which are known, however, it is possible to establish the characteristics that a laser beam in air would require in order to trigger lightning.

From the theories describing natural lightning, it appears that lightning could be triggered by producing a premature localized breakdown in the region within the cloud where lightning first begins. The size and shape of the ionized volume required is a matter of conjecture, since conditions in the initial breakdown region are not precisely known. Most likely, the required volume would depend upon the charge configuration within the cloud at the moment it is irradiated by the laser, the diameter of the laser beam, and the position of the laser beam relative to the charged regions of the cloud. Although this may be a promising mechanism to exploit, no numerical estimate of the laser beam characteristics which may be required can be established at this time.

The theories concerning lightning leaders, although vague, do seem to agree roughly on the amount of charge within a leader, and on the leader diameter. The production of a column of air with equivalent ionization and size could serve to trigger lightning. To be completely effective, an artificial leader of this type would have to persist in the air long enough for the stepped leader or a dart leader to traverse to the ground, or for a return stroke to travel to the cloud. Since leader velocities range from 1.5×10^5 to 5×10^7 m/sec, an ionization persistence time of 10^{-2} to 4×10^{-5} seconds would be required with a cloud base one or two kilometers in altitude. An ideal approach would be to generate a laser-induced artificial leader from the ground into the cloud. The portion of the beam inside the cloud could then produce the localized breakdown which naturally initiates lightning, and the remainder of the beam could direct the stroke to a desired location on the ground.

A second method of triggering lightning may be to duplicate the principle of the common lightning rod. To accomplish this, an ionized column of air with a conductivity equivalent, or nearly equivalent, to a lightning rod would be needed. The conductivity of copper, a typical lightning rod metal, is 2×10^{-6} ohm-cm. A fully ionized plasma at a temperature of 880 eV possesses a conductivity of this same order of magnitude. The wire-and-rocket systems also hinge on the existence of a conductive path. The conductivity of stainless steel, the material

generally used for the wires, is 7×10^{-5} ohm-cm. Duplication of this conductivity would require a fully ionized plasma with an electron temperature of about 100 eV (Reference 4: 162). It may, of course, be possible to duplicate the mechanisms involved by using an ionized column of air with less conductivity. But this, again, is a matter of conjecture. In any case, unless the laser-generated ionized column of air reaches all the way to the cloud, a strong possibility exists that the initial lightning leader would travel upward. For lightning-target interaction studies, this would be somewhat undesirable, since the more common lightning strikes begin with downward-moving leaders.

The qualified success of the sphere-tipped rocket experiments suggests that a laser beam might succeed in initiating lightning by creating a transient distortion of the high E-field regions within, or near, a cloud. The mechanism by which the distortion would occur cannot be quantitatively assessed, however, until more is known about the initial breakdown process of natural lightning.

The laboratory experiments with spark gaps confirm that a laser beam can initiate and guide an electrical discharge. Although it is not certain that the experimental results are scalable to an earth-cloud system, Koopman and Saum's estimate of the free electron density needed to guide a spark cannot be ignored. The feasibility of initiating lightning within a laser-generated rarefied column of air is discussed in Appendix A.

With the exception of the use of rarefied channels, all of the mechanisms which might be used to trigger lightning involve, in one way or another, the creation of free electrons in air. Furthermore, the electron density required for the guidance of sparks is fairly near the estimated density of electrons in a lightning leader. Many of the mechanisms involve a transient distortion of the atmospheric electric field. The fact that a laser beam can generate a distortion with virtually the speed of light is a major factor lending support to the feasibility of a laser lightning rod system. It would appear from a review of all

of the mechanisms that an ionized channel of air with an electron density of 10^9 to 10^{11} electrons/cm^3 or more, extending from near ground level to the base of a cloud, would have a high probability of triggering lightning. The radius of the channel may be less important than the electron densities within it, judging from the success of the wire-and-rocket experiments with the millimeter diameter wires. Based on the time required for natural discharges to traverse the cloud-earth distance, a channel persistence time of 10^{-2} to 4×10^{-5} seconds would be required to guide lightning to a specific location on the ground. The ability of a dart leader to traverse a return stroke channel after a pause of tens of milliseconds suggests, however, that the initial fractional ionization need not be maintained for the entire persistence time. It will be shown in Section V that after 10 milliseconds most of the electrons recombine or attach, so the dart-supporting channel consists, instead, of perhaps 10^8 ions/cm^3. Thus, the feasibility criterion of 10^9 to 10^{11} electrons/cm^3 is probably an upper limit to the fractional ionization required.

SECTION III

LASER-INDUCED IONIZATION - BACKGROUND

If the electron distribution along a laser-induced ionized column of air is to be analyzed, it is necessary to first understand the physical processes which take place when air is irradiated by an intense laser beam. Furthermore, it is necessary to develop mathematical relationships which describe those processes so that predictions of probable electron densities can be made. The purpose of this section is to establish the fundamental relationships upon which the more predictive models of the following sections can be developed. To this end, the section begins with a qualitative discussion of the breakdown process. Basic equations which describe the breakdown of air are then developed. In conclusion, a qualitative and quantitative analysis of radiation transfer is presented.

1. THE IONIZATION PROCESS

A laser pulse will produce an ionized region in air if, at any time during the duration of the pulse, the laser-generated ionization processes overcome all mechanisms which inhibit ionization. The generation of ions may result from two laser-supported mechanisms, photoionization and electron-cascade ionization. The first process, photoionization, occurs when an atom absorbs one or more photons and emits an electron. The second, electron-cascade ionization, results when "heated" electrons collide inelastically with atoms, causing the release of new electrons. Mechanisms which inhibit ionization encompass an extremely large number of naturally occurring atomic interactions. These interactions establish a sharply defined threshold flux level which must be exceeded by the pulse if ionization is to ensue. Once the threshold level is reached, ionization growth is a function of laser flux intensity.

Photoionization is believed to play a rather insignificant role in the large scale ionization (breakdown) of atmospheric air by laser beams of infrared frequencies. In order for photoionization to take place, the energy of the individual photons must exceed the ionization potential

of the atoms undergoing the reaction. For lasers of interest here, photon energies range from 0.12 eV for the CO_2 laser to 1.2 eV for the neodymium laser. Unexcited oxygen and nitrogen, the primary constituents of air, possess ionization potentials of about 15 eV. Clearly then, a single photon cannot ionize the typical atom of air. Several photons may, however, interact simultaneously with an atom through a process of multiphoton absorption. A simultaneous absorption of at least 13 photons would be needed to detach electrons from unexcited oxygen or nitrogen using radiation from the aforementioned lasers. The theoretical laser flux required to produce this rate of simultaneous photon absorption is two or three orders of magnitude higher than fluxes which have been experimentally observed to cause gas breakdown (Reference 21: 655). This indicates that mechanisms other than multiphoton absorption are the primary agents in the breakdown of air. It is possible that multiphoton ionization may be enhanced by the use of mode-locked lasers (Reference 1: 2292-2295). However, the theory of breakdown by mode-locked laser pulses is still in the embryo stage, and it is unlikely that confident predictions of the resulting ion distribution can be made until more is known about the process. One remaining photoionization mechanism is that of multi- or single-photon ionization of excited atoms. The ionization potentials of excited atoms may be quite low, allowing photoionization through the absorption of a small number of photons. However, the density of excited atoms is low until the latter stages of breakdown; and it is precisely during this phase that the second ionization mechanism, the electron cascade, becomes overwhelmingly predominant.

Electron-cascade ionization, unlike photoionization, propagates through a "chain-reaction" of atomic interactions. The cascade begins with a small number of initial electrons, which may be present from cosmic-ray bombardment of the atmosphere, multiphoton ionization, or laser-beam vaporization of impurity particles in the air. Free electron-atom pairs absorb photons of laser flux through the process of inverse bremsstrahlung, with the excess energy of the reaction being converted into an increased translational energy of the electrons. The process of stimulated bremsstrahlung emission, also occurring, will cause

electrons to lose kinetic energy. However, the inverse process is more likely, so that a net absorption of energy from the beam by the electrons results. If the cascade-inhibiting processes which are discussed later are sufficiently small, the electrons will eventually gain enough energy to ionize atoms. The electrons released as a result of the ionizations are, in turn, heated by the laser beam. The process repeats itself for the duration of the laser pulse. If t_g is the average time between ionizing collisions for each electron, the number of ionizations generated per second by each electron is t_g^{-1}. The incremental increase in the electron density after a time dt is thus given by

$$dn = t_g^{-1} n(t) dt \tag{1}$$

where n(t) is the electron density at time t. Integration of Equation 1 results in

$$n(t) = n_{eo} \exp(t/t_g) \tag{2}$$

where n_{eo} is the initial electron density. The electron growth, or e-folding time t_g, is governed by the rate at which the electrons gain energy from the laser beam, and the rate at which the same electrons lose energy as a result of various cascade-inhibiting processes. To gain an insight on the factors affecting t_g, it is necessary to examine the specific loss processes involved.

Cascade-inhibiting, or loss, processes may be divided into the following two categories: (1) those which reduce the translational energy of electrons, and (2) those which eliminate electrons from the ensemble altogether. Collisional processes which diminish the electron translational energy include excitations of atomic electronic levels, excitations of molecular vibrational levels, and ionizations of atoms.

Processes which remove electrons from the cascade are electron-ion recombinations, electron-atom (or molecule) attachments, and electron diffusion from the laser beam volume. The most significant cascade inhibitor at low laser flux levels is the excitation of molecular vibrational levels, chiefly of N_2. This loss, reinforced somewhat by attachments to O_2 molecules, establishes the sharply defined threshold level which must be exceeded by the laser flux before an electron cascade can begin. Experiments establish the threshold in clean air to be (Reference 2: B-1, B-2)

$$S_T = 3 \times 10^9 \times (\lambda/10.6)^2 \text{ W/cm}^2 \qquad (3)$$

where λ is the laser wavelength in microns. At flux intensities, S, between $3 \times 10^9 \times (\lambda/10.6)^2$ to about $3 \times 10^{10} \times (\lambda/10.6)^2$ W/cm^2, atomic excitations dominate as the primary cascade inhibitor, although the other loss mechanisms are not entirely negligible. Above $3 \times 10^{10} \times (\lambda/10.6)^2$ W/cm^2, all electron loss processes become insignificant. Beginning at this point, the cascade becomes dependent only upon the rate at which the electron gas can be heated by the laser flux, and the rate at which ionization of atoms can occur. When all of the losses are taken into account, a dependence of the e-folding time on laser flux intensity shown in Figure 2 for CO_2 laser radiation results. Corresponding curves for other laser wavelengths can be found by using the λ^2 scaling law evident in Equation 3.

2. THE BOLTZMAN EQUATION AND ITS MOMENTS

An analysis of electron-cascade ionization can be most easily approached through the use of the Boltzman equation, which describes the change in the distribution, f, of particles in space and time. Using this equation, a theoretical expression for the electron growth rate can be derived.

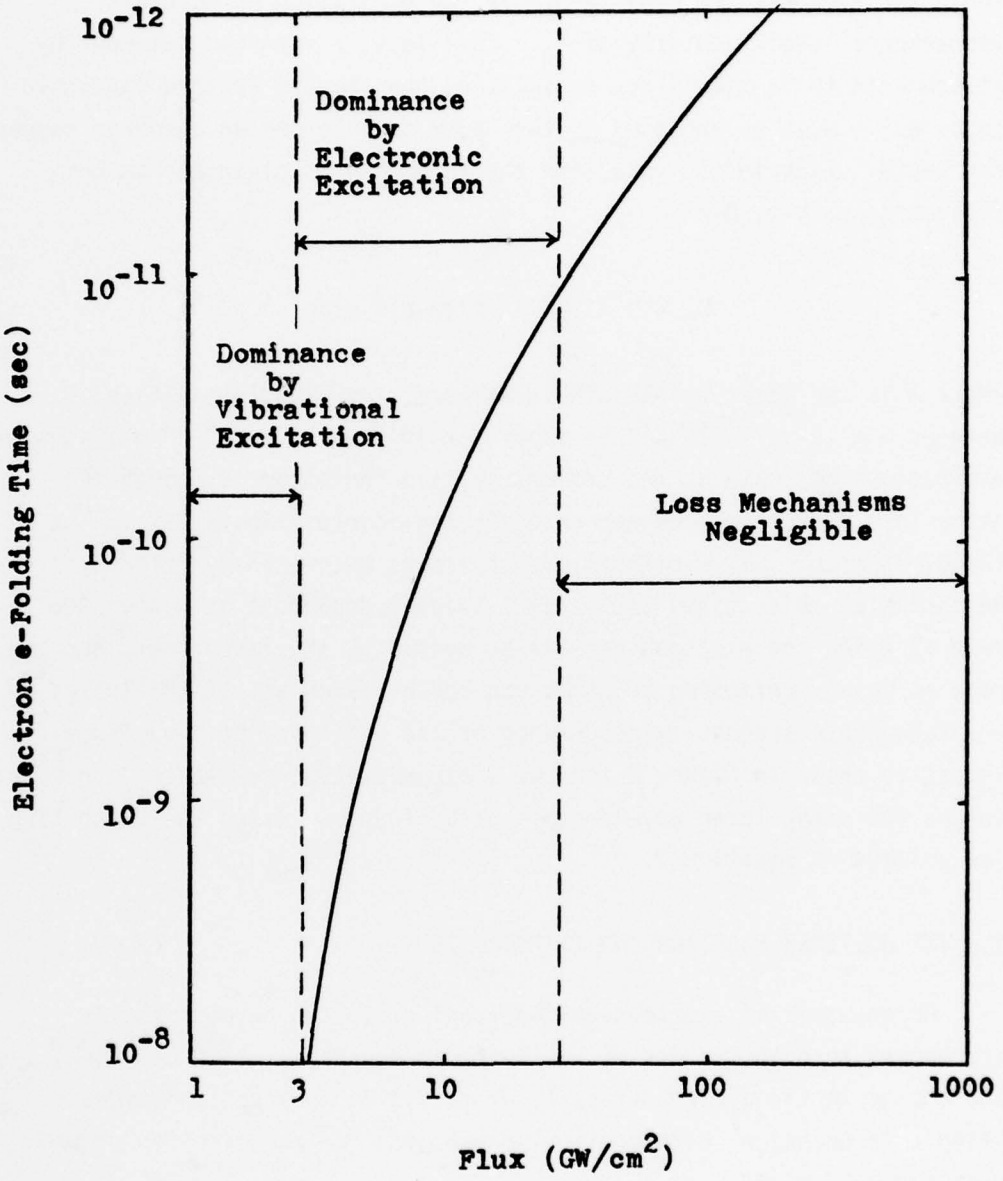

Figure 2. Electron e-Folding Time for λ = 10.6 Microns
Adapted from Triplett (Ref 25: 7)

The Boltzman equation for free electrons in space is

$$\frac{\partial f}{\partial t} + \bar{v}\cdot\nabla f + \bar{a}\cdot\nabla_v f = \left.\frac{\partial f}{\partial t}\right|_{coll} \tag{4}$$

where $\bar{v}$ is the electron velocity, $\bar{a}$ is the electron acceleration, and $\frac{\partial f}{\partial t}_{coll}$ is the time change in f due to collisional processes. Assuming an isotropic velocity distribution, the third term on the left-hand side of Equation 4 may be re-expressed in energy parameters as $\dot{\varepsilon}\,\frac{\partial f(\varepsilon)}{\partial \varepsilon}$, where $\dot{\varepsilon}$ is the time rate of change of the electron energy. A diffusion term, added to the right-hand side of the equation, can substitute for the $v\cdot\nabla f$ term. If these changes are made, and the collision terms specified, the Boltzman equation becomes

$$\frac{\partial f(\varepsilon)}{\partial t} + \dot{\varepsilon}\,\frac{\partial f(\varepsilon)}{\partial \varepsilon} = + \text{Collisional gains to } f(\varepsilon) \text{ due to three-body recombinations, atomic excitations, molecular vibrational excitations, ionizations, and diffusion} \tag{5}$$

$$- \text{Collisional losses from } f(\varepsilon) \text{ due to ionizations, attachments, diffusion, molecular vibrational excitations, atomic excitations, and recombinations.}$$

A zeroth moment to the Boltzman equation, acquired by integrating Equation 5 over all energy, produces a differential equation for electron growth. Taking the moment, the two terms on the left-hand side of Equation 5 integrate straightforwardly to become $\frac{\partial n}{\partial t}$ and zero, respectively. An exact integration of the terms implied by the right-hand side of the equation can be extremely lengthy. The recombination component alone, for example, must include all two- and three-body recombining interactions between electrons and all species of unexcited and excited atomic and molecular ions. Table III in Section V of this report gives a short list of the more significant reactions involved. For purposes of development at this point, the result of the integration can be symbolized

$$\frac{\partial n}{\partial t} = \begin{matrix}\text{electron gains} \\ \text{due to collisions}\end{matrix} - \begin{matrix}\text{electron losses} \\ \text{due to collisions}\end{matrix} \tag{6}$$

Electron gains may arise from photoionizations or from electron-atom ionizing collisions, with the latter process dominating the former during most of the cascade. Integrating the Boltzman term for electron-atom ionizing collisions (Appendix B) and substituting the result into Equation 6 yields

$$\frac{\partial n}{\partial t} = n_o n\langle R_I \rangle - \begin{matrix}\text{electron losses} \\ \text{due to collisions}\end{matrix} \qquad (7)$$

where n_o is the density of atoms and $\langle R_I \rangle$ is the energy-averaged rate of ionization.

A differential equation for the average electron energy, $\langle \varepsilon \rangle$, emerges by taking the first energy moment of the Boltzman equation. The first moment is acquired by multiplying the Boltzman equation by the electron energy, ε, and integrating over all energy. A problem of evaluating the large number of collisional terms again arises. The first moment of the ionizing collision term is derived in Appendix B. For present purposes, the remaining terms may be represented by an average electron energy loss rate, $- n\langle \dot{\varepsilon}_L \rangle$. Thus, the first moment contribution by the collisional terms is $- In_o n\langle R_I \rangle - n\langle \dot{\varepsilon}_L \rangle$. The non-collisional terms of the Boltzman equation (Equation 5) may be explicitly multiplied by ε and integrated. The first moment then becomes

$$\langle \varepsilon \rangle \frac{\partial n}{\partial t} + n \frac{\partial \langle \varepsilon \rangle}{\partial t} - n\langle \dot{\varepsilon} \rangle - n\left\langle \varepsilon \frac{\partial \dot{\varepsilon}}{\partial \varepsilon} \right\rangle = - In_o n\langle R_I \rangle - n\langle \dot{\varepsilon}_L \rangle \qquad (8)$$

The two terms in Equation 8 involving $\dot{\varepsilon}$ may be replaced by a single quantity $n\langle \dot{\varepsilon}_H \rangle$. Then if the equation is divided by n, and the terms rearranged, the following expression is obtained:

$$\frac{\partial \langle \varepsilon \rangle}{\partial t} = \langle \dot{\varepsilon}_H \rangle - \left[\frac{\langle \varepsilon \rangle}{n} \frac{\partial n}{\partial t} + In_o \langle R_I \rangle + \langle \dot{\varepsilon}_L \rangle \right] \qquad (9)$$

A physical interpretation of Equation 9 is that the time change in average electron energy is equal to the increase in energy due to laser heating, $\langle \dot{\varepsilon}_H \rangle$, minus the decrease in energy from collisional interactions (Reference 18).

The heating of electrons in a laser beam is, strictly speaking, a quantum effect. It has been shown by Raizer, however, that the effect is equivalent to classical microwave heating (Reference 21: 658). The microwave heating term, found widely in the literature, and specifically in Raizer's paper is

$$\langle \dot{\varepsilon}_H \rangle = KS \tag{10}$$

where

$$K = \frac{e^2 \nu}{m_e c \varepsilon_o (\omega^2 + \nu^2)} \tag{11}$$

and where

e = electron charge

ν = electron-atom collision frequency

m_e = electron mass

c = speed of light

ε_o = permittivity constant

ω = angular frequency of the laser field

By substituting the heating rate given by Equation 10 into Equation 9, and assuming that the average electron energy equilibrates rapidly so that $\frac{\partial \langle \varepsilon \rangle}{\partial t}$ is approximately zero at any instant of time, the following energy balance is obtained:

$$KS = \frac{\langle \varepsilon \rangle}{n} \frac{\partial n}{\partial t} + \langle \dot{\varepsilon}_L \rangle + I n_o \langle R_I \rangle \tag{12}$$

An expression for the electron e-folding time as a function of S can now be derived, at least for the special case of high laser flux intensities. As mentioned earlier, when the laser flux reaches levels of about $3 \times 10^{10} \times (10.6/\lambda)^2$ W/cm^2, electron growth losses due to collisions are negligible. Thus, in this high flux limit, Equation 7 becomes

$$\frac{\partial n}{\partial t} = n n_o \langle R_I \rangle \tag{13}$$

Since, in the high flux limit, most of the laser input energy is being used to produce ionizations, all other energy loss mechanisms due to collisions may be neglected. Consequently, Equation 12 reduces to

$$KS = \frac{\langle\varepsilon\rangle}{n}\frac{\partial n}{\partial t} + In_o\langle R_I\rangle \tag{14}$$

With the assumption that the average electron energy $\langle\varepsilon\rangle$ is much less than the ionization energy I, Equations 13 and 14 may be combined to yield

$$\frac{1}{n}\frac{\partial n}{\partial t} = \frac{KS}{I} \tag{15}$$

The solution to Equation 15 for constant K is

$$n(t) = n_{eo} \exp \frac{K}{I}\int_0^t S\, dt' \tag{16}$$

Thus, for a variable flux intensity, the electron growth in the high flux limit is dependent upon the fluence, $\int_0^{t_p} S\, dt$, of the pulse.

For constant S, Equation 16 can be integrated straightforwardly to yield

$$n(t) = n_{eo} \exp(\frac{KSt}{I}) \tag{17}$$

A comparison of Equation 17 with Equation 2 shows that the e-folding time in the high flux limit is given by

$$t_g = \frac{I}{KS} \tag{18}$$

3. RADIATION TRANSFER

The propagation of laser flux in space and time is described by a radiation transfer equation. Since the free electron density at any

position is dependent upon the laser flux at that position, radiation transfer considerations will ultimately provide a framework for determining the electron distribution along the entire laser beam.

As radiation travels from a position z to a position z + dz in a time dt, an incremental change of flux intensity may occur. For a pulse of arbitrary shape, the change may be represented by

$$dS(z,t) = \frac{\partial S(z,t)}{\partial z} dz + \frac{\partial S(z,t)}{\partial t} dt \qquad (19)$$

It is convenient to employ a reference frame in which timing begins with the arrival of the front edge of a pulse to a position z. In such a reference frame, the second term on the right-hand side of Equation 19 can be set to zero, and a pulse "mapped" from one position to another. A rather simple example can clarify the concept involved. Suppose the sole factor modifying the flux intensity is atmospheric attenuation. Then $\frac{\partial S}{\partial z} = - A_T S$, where A_T is the atmospheric attenuation coefficient. If, in addition, $\frac{\partial S}{\partial t} = 0$, the solution to Equation 19 is

$$S(z) = S(0)\exp(-A_T z) \qquad (20)$$

which is Beer's law for the attenuation of radiation in the atmosphere. Now, consider Figure 3, in which the solid line represents the time variation of flux intensity of a radiation pulse emerging from a laser. The time variation of flux at some later position, z', downstream may be obtained by applying Beer's law to each point of the original pulse, and plotting the results on the same S versus t coordinate frame. A new flux distribution in time will result, such as that shown by the dotted line. Hence, an entire pulse is mapped from one position to another.

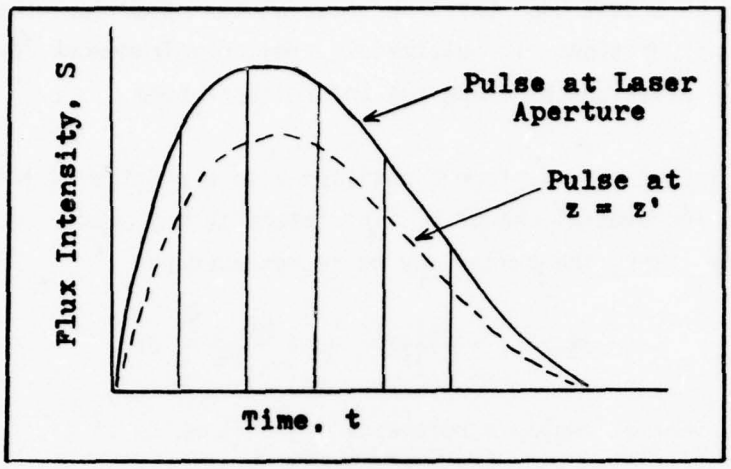

Figure 3. Pulse Mapping

For situations of practical interest, optical focusing becomes important. Representing the effects of focusing by F(z) and using the moving coordinate system, the radiation transfer equation becomes

$$\frac{dS(z,t)}{dz} = [\ F(z) - A_T\ ]\ S(z,t) \qquad (21)$$

If the flux intensity exceeds the threshold value for the breakdown of air, a significant portion of the flux will be consumed in the microwave heating of free electrons. The loss in flux per unit distance due to microwave heating is given by $-Kn(z,t)S(z,t)$, where K is the microwave heating coefficient introduced in Equation 10. Adding the microwave heating term to Equation 21 yields

$$\frac{dS(z,t)}{dz} = [\ F(z) - A_T\ ]\ S(z,t) - Kn(z,t)S(z,t) \qquad (22)$$

as the radiation transfer equation for fluxes above S_T.

Using radiation transfer Equations 21 and 22 along with electron cascade Equations 15 and 16, a differential equation for the free electron density in a high flux laser beam can be derived. The derivation required is somewhat lengthy, and is the subject of the next section.

SECTION IV

THE PRODUCTION OF IONIZED PATHWAYS IN AIR

Two fundamental equations for determining the free electron distribution along any laser beam of breakdown intensity are derived in this chapter. To begin this chapter, the concept of beam regions, necessary in the derivations, is introduced. A detailed development of the fundamental equations is then presented. A summary of the equations, and a brief discussion of possible limitations, is given in conclusion.

1. LASER BEAM REGIONS

In any laser lightning rod system of practical interest, it is highly desirable to begin the breakdown of air at a distance well separated from the laser aperture. Unless some separation is maintained, a likelihood exists that a lightning stroke could follow the beam to the laser and its associated optics, destroying both. Thus, any laser beam of interest here can be divided, for the purpose of analysis, into the three spatial regions illustrated in the lower part of Figure 4.

In the first, or prebreakdown, region the maximum intensity of the radiation pulse remains below the threshold S_T, and air breakdown cannot occur. This region extends from the final focusing element of the optical system producing the beam to the position z_B, where the maximum intensity of the pulse reaches a value S_T. At this point, the breakdown region begins. In the breakdown region, a portion of the pulse maintains an intensity greater than S_T, and an electron cascade is produced. Cascade conditions are maintained until position z_E, where the maximum flux intensity of the pulse falls below S_T. The third, or postbreakdown, region extends from position z_E onward. In this region, the maximum flux remains below the threshold, and breakdown is not possible. The minigraphs in the upper part of Figure 4 illustrate a pulse as it might appear in each of the three regions and at the positions z_B and z_E.

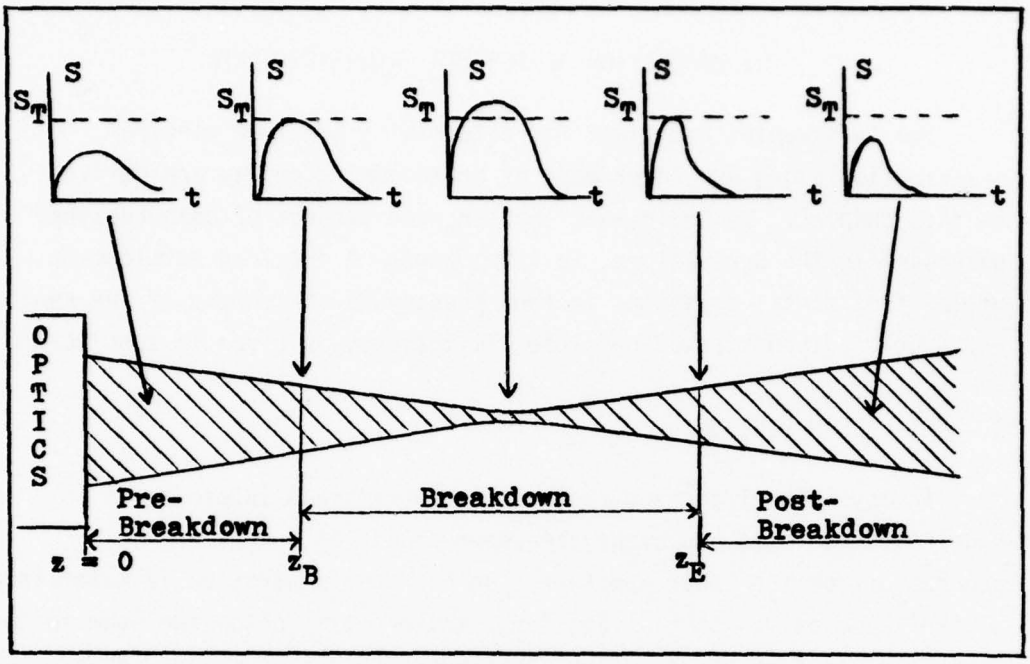

Figure 4. Beam Regions

Following the convention established in the preceding section, the timing in each of the minigraphs begins with the arrival of the front edge of the pulse at the z position indicated. The same convention is used throughout this section.

2. THE BREAKDOWN INITIATION EQUATION

The maintenance of a specific breakdown initiation point, z_B, requires a careful blend of optical focusing and maximum laser power output. If focusing is too strong, or the pulse intensity too high, z_B may rest dangerously near the laser. If focusing is weak, or the pulse intensity too low, breakdown of air may not occur at all. The breakdown initiation equation establishes the relationship between optical focusing, maximum pulse intensity at the laser, and the position z_B.

A radiation pulse emerging from a laser reaches a maximum value at some time t_{max} after the front edge of the pulse leaves the aperture. Because focusing and attenuation effects are linear, the maximum value of the pulse at any later position, up to and including the position z_B, also occurs when $t = t_{max}$, and is represented by $S(z,t_{max})$. As the pulse moves from $z = 0$ to $z = z_B$, the maximum flux intensity increases and eventually reaches the threshold value. The condition for the initiation of breakdown is thus $S(z_B, t_{max}) = S_T$.

The growth of the pulse as it moves through the prebreakdown region is given by the radiation transfer equation

$$\frac{dS(z,t)}{dz} = [\, F(z) - A_T \,]\, S(z,t) \tag{21}$$

Solving Equation 21 for $S(z,t)$ and specifying the time t_{max} results in

$$S(z,t_{max}) = S_{max} \exp \int_0^z [\, F(z') - A_T \,]\, dz' \tag{23}$$

where S_{max} is the maximum flux intensity at the final optical element producing the beam. At the position $z = z_B$, Equation 23 becomes

$$S_T = S_{max} \exp \int_0^{z_B} [\, F(z) - A_T \,]\, dz \tag{24}$$

Equation 24 is the fundamental equation for the determination of breakdown initiation criteria. If $F(z)$ is specified, and the integration performed, an explicit relationship between S_{max} and z_B is obtained. Since the growth of free electrons first begins at z_B, Equation 24 establishes the functional relationship between the starting point of the free electron distribution (in effect, the ion distribution, since the electrons promptly attach), the focusing configuration, and the maximum flux intensity at the laser.

3. THE ELECTRON DISTRIBUTION EQUATION

An exact determination of the free electron distribution within the breakdown region of a laser beam can theoretically be made by simultaneously solving the radiation transfer equation and the first two moments of the Boltzman equation. In practice, however, the situation is less than ideal, since the collisional terms of the Boltzman equation are extremely difficult to evaluate analytically. One possible approach to the problem is to bypass the collisional terms altogether, and to use an empirically determined expression for the electron e-folding time. This approach, used in a simplified form by Triplett (Reference 25: 10-19), results in a lengthy integrodifferential equation which has a large number of variable parameters: pulse length, pulse shape, laser aperture size, focal point, breakdown initiation point, and laser wavelength. To determine the effect of each of these on the electron distribution would require a large number of solutions, and a prohibitive amount of computer time. The electron distribution equation developed in this section is a compromise between the desire to determine the exact electron distribution, and the need to know the effect of the variable parameters on that distribution. The simplicity of the equation permits many computer solutions in a relatively short amount of time. The predicted densities can, however, be inaccurate, and care must be taken in analyzing the results. In general, several computations must be made, and the results compared for consistency.

The free electron density produced by a laser pulse in the breakdown region is, from Equation 16 and Figure 2, dependent upon the pulse intensity S, and the amount of time that the intensity is above the threshold S_T. Thus, even in the breakdown region, only a portion of the pulse is capable of maintaining an electron cascade. As seen in Figure 5, breakdown first begins at a time t_1 after the pulse encounters position z. Breakdown continues until a time t_2, with the number of electrons generated being dependent upon the fluence between times t_1 and t_2. After time t_2, flux is insufficient for further production of electrons. The beam, however, will continue to be sharply attenuated

by the electrons produced by the early part of the pulse. For reference purposes, the three following temporal regimes may be established: time 0 to t_1, temporal prebreakdown; time t_1 to t_2, temporal breakdown; and time t_2 to t_3, temporal postbreakdown. The derivation of the electron distribution equation centers upon determining the fluence in the breakdown regime, and relating the fluence to the electron density.

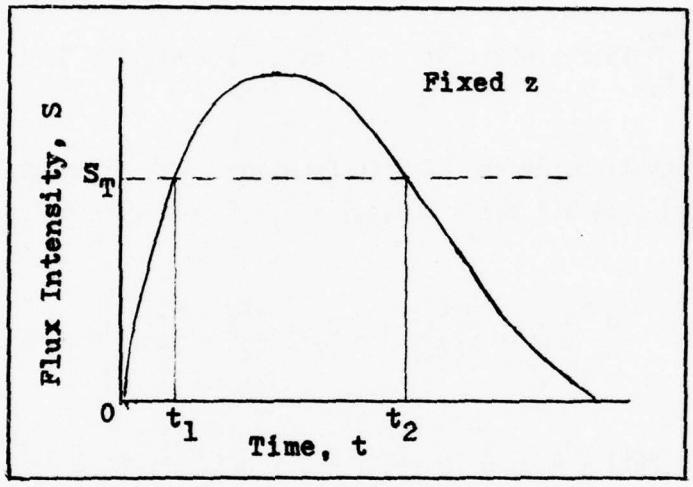

Figure 5. Pulse in Breakdown Region

Within the temporal breakdown regime, the radiation transfer equation is

$$\frac{dS(z,t)}{dz} = [\ F(z) - A_T\ ]\ S(z,t) - Kn(z,t)S(z,t) \qquad (22)$$

Equation 22 may be integrated from time t_1 to time t_2 to yield

$$\frac{d}{dz}\int_{t_1}^{t_2} S(z,t)dt - S(z,t_2)\frac{\partial t_2}{\partial z} + S(z,t_1)\frac{\partial t_1}{\partial z} =$$

$$[\ F(z) - A_T\ ]\int_{t_1}^{t_2} S(z,t)dt - \int_{t_1}^{t_2} Kn(z,t)S(z,t)dt \qquad (25)$$

where Liebnitz's rule for the differentiation of integrals has been used to expand the left-hand side of the equation.

From Equation 16, assuming constant K, and designating a position z,

$$\int_{t_1}^{t_2} S(z,t)\, dt = \frac{I}{K} \ln \frac{n(z,t_2)}{n(z,t_1)} \tag{26}$$

And from Equation 15,

$$\int_{t_1}^{t_2} KS(z,t)n(z,t)dt = I \left[n(z,t_1) - n(z,t_2) \right] \tag{27}$$

Substituting Equations 26 and 27 into Equation 25 to eliminate S(z,t); and recognizing that $S(z,t_1) = S(z,t_2) = S_T$ (from Figure 5) results in

$$\frac{d}{dz} \left[\frac{I}{K} \ln \frac{n(t_2)}{n(t_1)} \right] - S_T \left[\frac{\partial t_2}{\partial z} - \frac{\partial t_1}{\partial z} \right] =$$

$$\left[F(z) - A_T \right] \frac{I}{K} \ln \frac{n(t_2)}{n(t_1)} - I \left[n(t_2) - n(t_1) \right] \tag{28}$$

At time t_1, the electron cascade has not yet begun to build. Thus, $n(z,t_1) = n_{eo}$, where n_{eo} is the ambient-air free-electron density. The electron cascade will grow between the times t_1 and t_2, reaching a maximum value at time t_2. Hence, $n(z,t_2) = n(z)$, where n(z) represents the final electron density at position z. In terms of n(z) and n_{eo}, Equation 28 can be written as

$$\frac{1}{n(z)} \frac{dn(z)}{dz} = \frac{KS_T}{I} \left[Dt_2 - Dt_1 \right]$$

$$+ \left[F(z) - A_T \right] \ln \frac{n(z)}{n_{eo}} - K \left[n(z) - n_{eo} \right] \tag{29}$$

where the symbol D has been used to represent the partial derivative with respect to z.

Equation 29 can be used to determine the free electron density at any position within the breakdown region. In order for the equation to be useful, however, it is necessary to express Dt_1 and Dt_2 in terms of parameters which are known, or which can be measured. To accomplish this, it is desirable to first establish the physical meaning of Dt_1 and Dt_2. An insight on the matter can be acquired from Figure 6, which shows a pulse at two separate positions, z and z_1, within the breakdown region.

At position z, the flux intensity of the pulse reaches threshold after a time t_1, then falls below threshold at a time t_2. As the pulse moves forward from position z, it is magnified as a result of optical focusing. It is also distorted, particularly on the trailing edge, because of non-linear losses which occur in the microwave heating of electrons. Consequently, when the pulse reaches position z_1, the flux intensity reaches threshold after a time t_1' and falls below threshold at a time t_2', where $t_1' \neq t_1$ and $t_2' \neq t_2$. It is seen, then, that $Dt_2 - Dt_1$ establishes the rate of change, with respect to distance along the laser beam, of the cascade-producing pulse length. To express Dt_1 and Dt_2 in terms of known parameters a separate analysis of each is necessary.

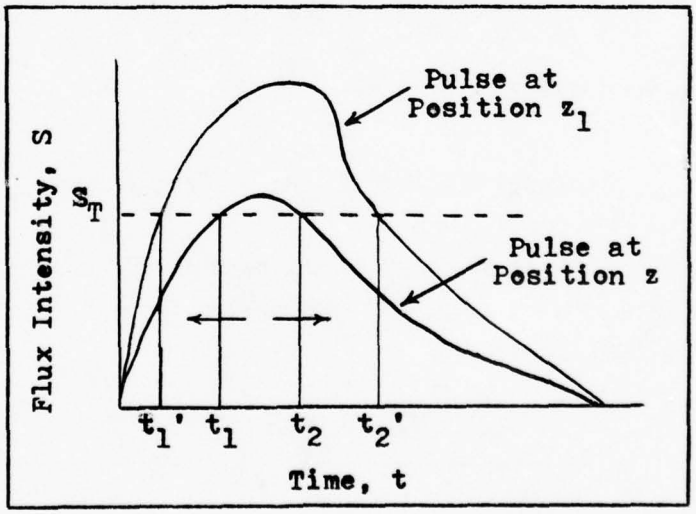

Figure 6. Motion of Dt_1 and Dt_2

a. Determination of Dt_1

If losses due to atmospheric attenuation and electron heating are negligible, the flux intensity of a pulse will increase steadily until the pulse reaches the most narrow part, or waist, of the laser beam. The pulse as a whole is magnified, and the time t_1 moves toward t = 0, as seen in Figure 6.

Electron heating will distort the portion of the pulse which rests in the temporal breakdown regime. However, since the pulse must be continuous, the end of the prebreakdown time regime and the beginning of the breakdown time regime must occur at the same time t_1. Consequently, Dt_1 can be determined from the radiation transfer equation applicable to the prebreakdown time regime:

$$\frac{dS(z,t)}{dz} = [\ F(z) - A_T\ ]\ S(z,t) \tag{21}$$

An integration of Equation 21 over z yields an expression for S(z,t) at position z

$$S(z,t) = S(0,t)\ \exp \int_0^z [\ F(z') - A_T\ ]\ dz' \tag{30}$$

Then at time t_1, since $S(z,t_1) = S_T$,

$$S(0,t_1) = S_T\ \exp \int_0^z [\ A_T - F(z')\ ]\ dz' \tag{31}$$

An expression for Dt_1 is acquired by taking a partial derivative of Equation 31 with respect to z, and rearranging terms. The following expression is then obtained:

$$Dt_1 = \frac{[\ A_T - F(z)\ ]\ S_T\ \exp \int_0^z [\ A_T - F(z')\ ]\ dz'}{\partial S(0,t_1)/\partial t_1} \tag{32}$$

Substituting $S(0,t_1)$ from Equation 31 for the applicable factors in the numerator of Equation 32 yields the following, more compact, equation for Dt_1:

$$Dt_1 = \frac{S(0,t_1)\ [\ A_T - F(z)\ ]}{\partial S(0,t_1)/\partial t_1} \tag{33}$$

It will be shown in the following section under "Pulse Shapes" that $S(0,t_1)$ can be expressed in terms of known parameters, namely, $F(z)$, A_T, and the initial pulse shape.

b. Determination of Dt_2

The microwave heating of electrons has a significant effect on the time, t_2, that the trailing edge of the pulse falls below threshold. If the electron density is small, microwave heating losses are negligible. In this case, the pulse will be magnified as a whole as it approaches the beam waist, and t_2 will move steadily outward, in a direction opposite to the motion of t_1 (Figure 6). The portion of the pulse above threshold increases, so to speak, from both ends. On the other hand, if the electron density is large, flux losses due to electron heating compete with flux gains due to optical focusing. The direction of t_2 then depends upon whether the flux gain or the flux loss dominates at a given position and time. In either case, the radiation transfer equation for the breakdown time regime must be used to determine the rate of change with position of t_2. The appropriate equation is (from Section III)

$$\frac{dS(z,t)}{dz} = [\ F(z) - A_T]\ S(z,t) - Kn(z,t)S(z,t) \tag{22}$$

Equation 22 may be solved for $S(z,t)$ with the result

$$S(z,t) =$$

$$S(z_B,t)\ \exp \int_{z_B}^{z} [\ F(z') - A_T\ ]\ dz'\ \exp \int_{z}^{z_B} Kn(z',t)dz' \tag{34}$$

From Equation 30 the flux intensity at position z_B is given by

$$S(z_B,t) = S(0,t) \exp \int_0^{z_B} [\, F(z') - A_T \,]\, dz' \tag{35}$$

Substituting this value for $S(z_B,t)$ into Equation 34, and then specifying the time t_2 yields

$$S_T = S(0,t_2) \exp \int_0^{z} [\, F(z') - A_T \,]\, dz' \exp \int_z^{z_B} Kn(z')dz' \tag{36}$$

Differentiation of Equation 36 with respect to z results in

$$Dt_2 =$$

$$\frac{S_T[A_T - F(z) - Kn(z)]\exp \int_0^{z} [A_T - F(z')]dz' \exp \int_{z_B}^{z} Kn(z')dz'}{\partial S(0,t_2)/\partial t_2} \tag{37}$$

which may be simplified, using Equation 36, to yield

$$Dt_2 = \frac{S(0,t_2)\, [A_T - F(z) + Kn(z)\,]}{\partial S(0,t_2)/\partial t_2}$$

The quantity $S(0,t_2)$ is cast in terms of known parameters in the following section.

4. THE FUNDAMENTAL EQUATIONS AND THEIR LIMITATIONS (SUMMARY)

The free-electron distribution along any laser beam may be computed through the use of the breakdown initiation equation and the electron distribution equation.

The breakdown initiation equation establishes the position, z_B, at which the free-electron distribution begins. The equation is

$$S_T = S_{max} \exp \int_0^{z_B} [\, F(z) - A_T \,]\, dz \tag{24}$$

The electron distribution equation, upon solution, predicts the electron distribution beyond the point z_B. The equation is

$$\frac{1}{n(z)}\frac{dn(z)}{dz} = \frac{KS_T}{I}\left[Dt_2 - Dt_1 \right]$$

$$+ \left[F(z) - A_T \right] \ln \frac{n(z)}{n_{eo}} - K\left[n(z) - n_{eo} \right] \qquad (29)$$

where

$$Dt_1 = \frac{S(0,t_1)\left[A_T - F(z) \right]}{\partial S(0,t_1)/\partial t_1} \qquad (33)$$

and

$$Dt_2 = \frac{S(0,t_2)\left[A_T - F(z) + Kn(z) \right]}{\partial S(0,t_2)/\partial t_2} \qquad (38)$$

Three limitations to the electron distribution equation exist. First, the equation applies only to the high flux limit, since the high flux limit relationships (Equations 15 and 16) were instrumental in the derivation. This limitation can be overcome somewhat by the use of a "modified" high flux limit, which is discussed in the section on Electron Heating in the next chapter. Second, the fundamental equation is strictly applicable only in the portion of the breakdown region prior to the beam waist. Beyond the beam waist, the expression for Dt_1 may become inaccurate. Third, under some focusing conditions, the expression for Dt_2 may become invalid. The limitations involving Dt_1 and Dt_2 occur in essence because of lack of pulse shape distortion information in the equations. Fortunately, the limitations are minor, and can generally be ignored, as will be discussed under "Pulse Shapes" in the next section.

To apply the fundamental equations to specific situations, the terms heretofore symbolized $F(z)$, A_T, $S(0, t_1)$, $S(0,t_2)$, and K must be explicitly determined. These determinations are made in the next section.

SECTION V

SIGNIFICANT PARAMETERS

The free-electron distribution produced by a laser beam in air is influenced by a large number of parameters. The purpose of this section is to analyze the most significant of these, with the primary aim being to establish specific relationships or values for use in the electron distribution equation. Some of the analyses in themselves reveal limitations which must be considered in the design of a practical laser lightning rod system. These limitations are analyzed as they arise. Factors which will be considered, in turn, are electron heating, optical focusing, pulse shape (and pulse length), atmospheric attenuation, and free-electron losses.

1. MICROWAVE HEATING OF ELECTRONS

The microwave heating of electrons provides the link between laser flux intensity and the rate at which free electrons are generated. The linkage is established in the electron distribution equation by the microwave heating coefficient K. Since the distribution equation is based on the assumption of a high flux limit, the microwave heating coefficient which corresponds to high laser fluxes would seem most appropriate in any calculations. For many cases of practical interest, however, laser flux intensities may fall well below those which qualify as "high." In such cases, a value for K based on a "modified" high flux limit can be more realistic.

In the high flux limit, the electron growth is related to the flux intensity by (from Section III)

$$t_g = \frac{I}{KS} \tag{18}$$

The ionization potential of air is approximately 2.4×10^{-18} joules, and K is of the order of 10^{-17} cm^2 for CO_2 laser fluxes of high intensity. Consequently,

$$t_g \approx \frac{2.4 \times 10^{-1}}{S} \text{ sec} \tag{39}$$

The dependence of electron e-folding time on S predicted by Equation 39 is shown in Figure 7. It can be seen from the figure that the agreement between Equation 39 and the true electron e-folding time is excellent at fluxes above 3×10^{10} W/cm^2. At fluxes below 3×10^{10} W/cm^2, however, the high flux limit approximation of t_g is consistently lower than the true value, with the disparity exceeding two orders of magnitude near 3×10^{9} W/cm^2. It will be shown later that laser-lightning-rod fluxes are on the order of 10^{10} W/cm^2, and are frequently lower. In this realm of S, the high flux limit approximation underestimates t_g by at least an order of magnitude. Since the rate of electron growth is inversely proportional to the e-folding time (Equation 18), the high flux limit consistently overestimates the rate of electron growth.

In the modified high flux limit approximation, the value of K is adjusted to diminish the disparity between the true and the approximated e-folding times. Figure 7 shows two such approximations, labeled Modification A and Modification B.

Modification A is established by using a value of K slightly smaller than that of the true high-flux limit. Using this modification, the electron e-folding time is underestimated by an order of magnitude or less for fluxes below 8×10^{9} W/cm^2. Above 8×10^{9} W/cm^2, the electron e-folding time is slightly overestimated. Thus, this modification predicts a lower, more realistic electron growth rate for fluxes of the order of 10^{10} W/cm^2.

In Modification B, the value of K is decreased still further. As shown in Figure 7, Modification B results in an overestimation of e-folding time for all fluxes above 4×10^{9} W/cm^2. Consequently, this

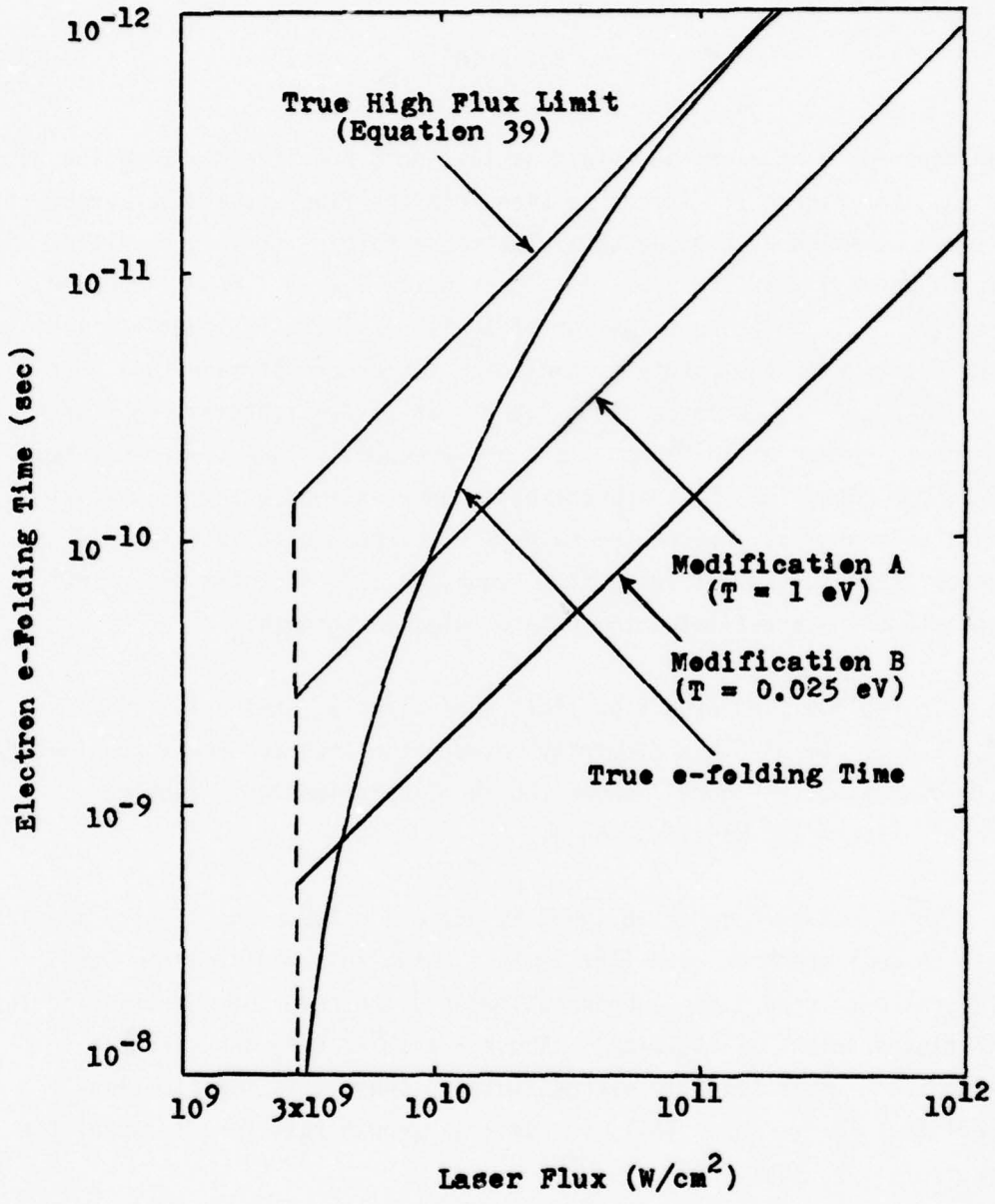

Figure 7. Modified High Flux Limits

modification, in contrast to the true high flux limit given by Equation 39, consistently underestimates the electron growth rate. A slight improvement to both modifications can be acquired by taking into account the effect of electron-ion collisions.

The electron heating coefficient is given by

$$K = \frac{e^2 \nu}{m_e c \varepsilon_o (\omega^2 + \nu^2)} \tag{11}$$

where ν is the electron-atom collision frequency. In a heated gas, the electrons will collide with both neutral atoms and with ions; however, because of Coulomb attraction, the electron-ion collision frequency is much greater than the electron-neutral atom collision frequency in a gas of given ion or neutral-particle density. Thus, assuming that ω is much greater than ν, Equation 11 will yield a higher value of K for ion collisions than for neutral atom collisions. Since the specification of K is equivalent to the selection of a given modified high-flux limit, it is possible to move from one modified limit to another by taking electron-ion collisions explicitly into account.

For a gas which contains both neutral atoms and ions, the total electron-heavy particle collision rate is

$$\nu = \nu_N + \nu_I \tag{40}$$

where ν_N is the electron-neutral collision frequency and ν_I is the electron-ion collision frequency. Using expressions for ν_N and ν_I adapted from Tannenbaum (Reference 24: 348), the total electron-atom collision frequency becomes

$$\nu = 2.8 + 10^{-8} n_{0T} T_e^{\frac{1}{2}} + n[2.9 \times 10^{-5} T_e^{-3/2} - 2.8 \times 10^{-8} T_e^{\frac{1}{2}}] \tag{41}$$

where T_e is the electron temperature in electron volts, and n_{0T} is the total heavy particle density. As before, n is the electron density.

At CO_2 laser fluxes below 10^{11} W/cm^2, the electron temperature is less than 10eV (Reference 25: 6). In this case, Equation 41 reduces to

$$\nu = 2.8 \times 10^{-8} n_{0T} T_e^{\frac{1}{2}} + 2.9 \times 10^{-5} T_e^{-3/2} n \tag{42}$$

The total heavy-particle density is a function of temperature. However, unless the pulse from the laser is extremely long, diffusion from the beam region is minimal during breakdown, and the particle density will remain near the room temperature value of $n_n = 2.5 \times 10^{19}$ atoms/cm^3. Using this value in Equation 42 results in

$$\nu = 7.0 \times 10^{11} T_e^{\frac{1}{2}} + 2.9 \times 10^{-5} n \tag{43}$$

The two terms on the right-hand side of Equation 43 correspond to the electron-neutral and the electron-ion collision frequency, respectively. Substituting Equation 43 into Equation 11 and assuming that ν is much less than ω results in the following expression for the microwave heating coefficient:

$$K = \frac{e^2 \left[7.0 \times 10^{11} T_e^{\frac{1}{2}} + 2.9 \times 10^{-5} n \right]}{m_e c \varepsilon_o \omega^2} \tag{44}$$

If the effects of ion collision are momentarily ignored, Equation 44 yields for CO_2 frequencies

$$K = 2.3 \times 10^{-18} T_e^{\frac{1}{2}} \text{ cm}^2 \tag{45}$$

Thus, it is seen that the selection of a given modified high-flux limit is tantamount to the specification of some electron temperature. Modifications A and B of Figure 7 correspond to temperatures of 1 eV and 0.025 eV (room temperature) respectively. Equations for the Modification A and B curves were acquired by specifying the temperature for each modification, solving Equation 45 for the appropriate value of K, and substituting the results into Equation 18. The resulting equation for S versus t_g was then plotted for each modification.

If electron-ion collisions are taken into account, Equation 44 must be replaced by

$$K = \frac{e^2}{m_e c \varepsilon_o} \frac{\nu}{\omega^2 + \nu^2} \tag{11}$$

where $$\nu = 7.0 \times 10^{11} T_e^{\frac{1}{2}} + 2.9 \times 10^{-5} n \tag{43}$$

In this case, K becomes dependent upon the electron density, and a transformation from one modified high-flux limit (K value) to another occurs as the electron density changes. Figure 8 shows the dependence of K on the electron density that results with T_e = 0.025 eV (K_B) and with T_e = 1 eV (K_A). It can be seen from the figure that at low electron densities K_A and K_B are below the true high-flux limit approximation of the heating coefficient. At higher electron densities, K_A and K_B increase in magnitude, and eventually reach the true high-flux limit approximation. In order for electron densities to be large, the laser flux intensity must be high. Hence, in establishing a relationship between K and n, Equations 11 and 43 implicitly relate K and S. The relationship is, of course, not exact. The electron temperature is a variable quantity; and a true expression for the heating coefficient must take this into account. The expressions for K_A and K_B are, however, an improvement over the high-flux limit, which consistently overestimates the electron growth rate.

Because K_A and K_B are approximations, the use of either in the electron distribution equation will lead to uncertainties in the results. To establish the magnitude of possible error, it is necessary to analyze carefully the specific physical situation on hand.

For example, if the laser flux intensity is low along the entire beam, the electron heating coefficient should be small. In this case K_B

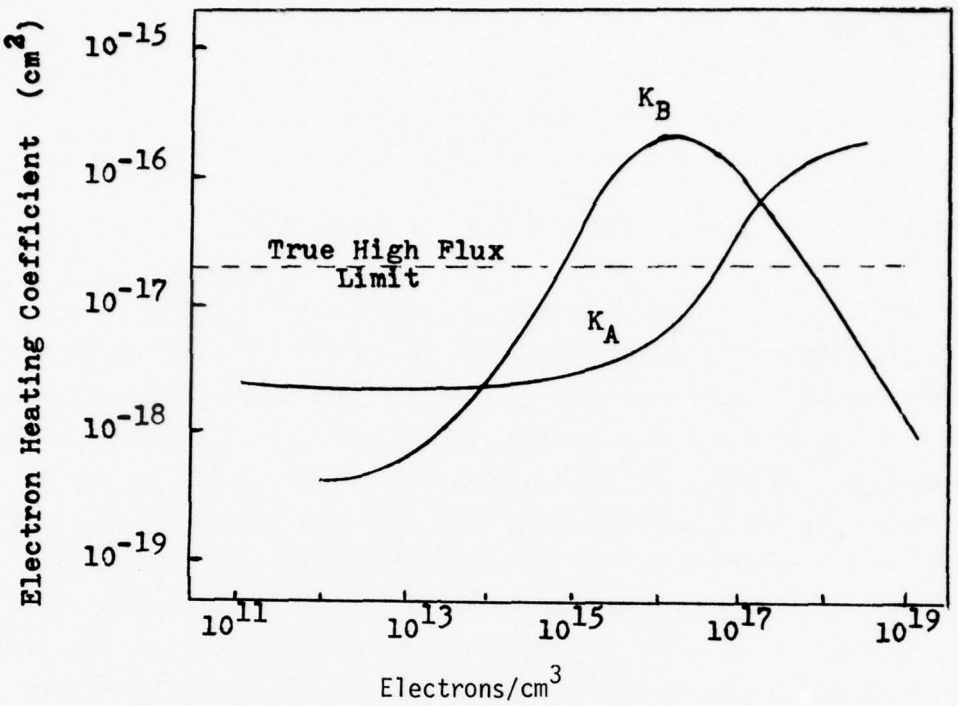

Figure 8. Modified Electron Heating Coefficients

would probably overestimate the electron density, whereas K_A might yield fairly accurate results. For a flux of extremely high intensity, K_B would be more accurate.

With a strongly focused laser beam, the situation is further complicated since the flux intensity may be extremely high in one region and low in another. In this case, each region of the beam must be analyzed separately. Since there is no precise mathematical tool available to perform the analysis, a strong measure of common sense must be used. Fortunately, for many laser-lightning-rod scenarios of interest, the electron distribution is relatively insensitive to the K value

chosen; and, in almost any scenario, the use of K_B will result in a good lower limit estimate of electron densities involved. Finally, it may be mentioned that an exact prediction of electron densities is not altogether necessary, so long as some confidence exists that the densities are high.

Perhaps more important than the actual electron numbers is the fact that the consistent use of a given K value enables an analysis of the effects of various other parameters on the electron distribution.

2. FOCUSING

The degree to which a laser beam of given power is focused determines the position at which air breakdown first begins, and the distribution of electrons beyond the breakdown initiation point. The term in the electron distribution equation which accounts for optical focusing is F(z). An expression for F(z) in terms of known laser beam parameters is easily acquired from simple laser beam diagnostic considerations. The same considerations also reveal optical limitations which can significantly influence the design of a laser lightning rod system.

a. Derivation of the Focusing Term

The instantaneous flux density of a laser beam as a function of distance z from an originating lens is given by

$$S(z,t) = \frac{P(t)}{\pi\,[w(z)]^2} \tag{46}$$

where P(t) is the instantaneous power at a time t after the beam encounters position z, and $\pi\,[w(z)]^2$ is the area of the beam at position z. The expression for the area, as given, is based on the assumption of a circular beam cross section.

The optical focusing contribution to the original radiation transfer equations (Equations 21 and 22) is acquired by taking a derivative of Equation 46 with respect to z. The result is

$$\frac{\partial S(z,t)}{\partial z} = F(z) = \frac{-2}{w(z)} \frac{\partial w(z)}{\partial z} \tag{47}$$

To recast Equation 47 in terms of easily measured beam parameters, the equation for the spot size of a gaussian laser beam as a function of z can be employed. The appropriate expression is, from Siegman (Reference 23: 309),

$$w(z) = w_F \left\{ 1 + \left[\frac{(z_F - z)}{\pi w_F^2} \right]^2 \right\}^{\frac{1}{2}} \tag{48}$$

where w_F is the spot size at the beam waist, and z_F is the distance of the waist from the lens originating the beam. Substituting Equation 48 into Equation 47 to eliminate w(z) results in

$$F(z) = \frac{2(z_F - z)}{a^2 + (z_F - z)^2} \tag{49}$$

where

$$a \approx \frac{\pi}{\lambda} w_F^2 \tag{50}$$

Although Equation 49 is derived on the assumption of a gaussian beam, the general form remains intact for any laser beam, since any beam can be expressed as the sum of a set of Hermite-gaussians. Many beams employed in high-power laser work are non-circular in cross section, and non-gaussian in form. For such beams, W_F and z_F would probably be most accurately determined through experimental measurements.

b. Limitations of Focusing

Focusing limitations arise in a laser lightning rod system because of the long focal lengths and high flux intensities required to produce an ionized column of air on the order of a kilometer in length. The parameter most affected is the size of the final optical element from which the beam originates.

A schematic of a laser lightning rod beam is shown in Figure 9. For the sake of analysis, the optical system which would be used to focus the beam has been symbolized by a single lens of focal length f. A coordinate system below the schematic establishes z = 0 at the lens. It is seen that the beam emerges from the laser and acquires a minimum spot size w_1 at a distance $-z_1$ from the lens. The beam then diverges and reaches a spot size w_L at z = 0. Passing through the lens, the beam is focused to a minimum spot size w_F at position z_F. Air breakdown begins enroute, at position z_B. The beam waist at the breakdown initiation point is w_B.

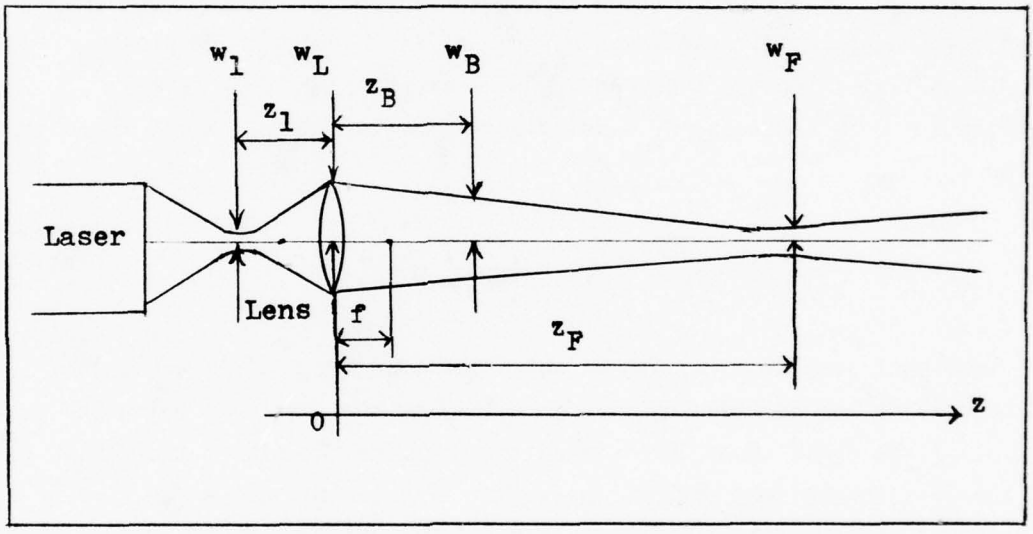

Figure 9. Laser Lightning Rod Beam Schematic

From laser beam diagnostic considerations, w_1, w_F, z_1, and z_F are related by (Reference 28: 152)

$$w_F^2 = \frac{w_1^2}{(1 + z_1/z_F)^2 + (\pi w_1^2/\lambda z_F)^2} \tag{51}$$

and

$$z_F = \frac{-f^2(z_1 + f)}{(z_1 + f)^2 + (\pi w_1^2/\lambda)^2} \tag{52}$$

It would appear from Equations 51 and 52 t a beam could be focused to an arbitrarily small waist at any given focal distance z_F, barring uncertainty principle matters. In practice, however, more severe limitations arise. The nature of the limitations can be seen from the following expression obtained straightforwardly from Equation 46:

$$S(z_F,t) = S(0,t)\ (w_L/w_F)^2 \tag{53}$$

It can be anticipated that the flux intensity at the beam waist, $S(z_F,t)$, must be large in order to maintain an electron cascade along the beam. To avoid air breakdown at the lens, however, $S(0,t)$ must be less than the threshold for the breakdown of air. Thus, to generate breakdown flux intensities beyond z_B, w_L must be large, or w_F small. By setting $z = 0$ in Equation 48, a relationship between w_L and w_F is found to be

$$w_L = \left[\ w_F^2 + \left(\frac{\lambda z_F}{\pi w_F}\right)^2\ \right]^{\frac{1}{2}} \tag{54}$$

The beam spot size at $z = 0$ can be no larger than the optical element through which the beam passes. Thus, w_L may be considered as being the radius of the lens. From this viewpoint, Equation 54 relates the radius of the lens to the spot size at the waist. The limitations arise, ultimately, because of unreasonably large lens radii.

To focus a laser beam at a given z_F, a certain minimum size of the lens is required. An expression for this minimum w_L can be obtained by taking a partial derivative of Equation 54 with respect to w_F, and setting the derivative equal to zero. The result is

$$w_{L\ min} = (2\lambda z_F/\pi)^{\frac{1}{2}} \tag{55}$$

The spot size at the beam waist when $w_L = w_{L\ min}$ is, from the same calculations,

$$w_{FC} = (\lambda z_F/\pi)^{\frac{1}{2}} \tag{56}$$

The relationships established by Equations 54, 55, and 56 are illustrated in Figures 10 and 11. By using the two figures in conjunction with Equation 53, it is possible to estimate the radius of the final optical element that will be needed in a laser lightning rod system.

To generate an ionized column of air from the ground to a cloud base would require that the laser beam be focused at about 1000 meters. From Figure 10, it is seen that the minimum lens radius for a beam focused at 1000 meters is 8.2 centimeters, for a CO_2 laser. The corresponding spot size at the waist is 5.8 centimeters. Assuming a flux intensity of one gigawatt at the lens, the flux intensity at the waist is, from Equation 53, approximately two gigawatts. At this point, the focusing limitations of a laser lightning rod system become obvious. The radius of the lens is already large at 8.2 centimeters. The flux at the lens is immense at one gigawatt. Despite this, the threshold for the breakdown of air, three gigawatts, is reached nowhere along the beam. To salvage the situation, the only alternatives are to increase the flux at the lens or to increase the radius of the lens. An enlargement of the lens can result in a significant increase in flux intensity along the beam. If w_L = 11 centimeters, for example, the spot size at the waist is, from Figure 11, 3.2 centimeters. From Equation 53, then, the flux intensity at the waist is 11.8 gigawatts, assuming the same flux at the lens as before. The spot size at the waist is, however, an increasingly weak function of $w_{L\ min}$, as can be seen from Figure 11.

A large lens, or mirror, at the end of the optical chain is fairly easy to accommodate. If the breakdown initiation point is brought fairly near the laser, however, the size of the laser aperture itself must be large. For example, a typical laser lightning rod beam might be focused at 1000 meters, with a desired breakdown initiation point at 100 meters from the laser. With this beam configuration, the laser might be located 90 meters from a metal tower, the beam run parallel to the ground from the laser to the base of the tower, and then turned vertically. The ionized air column would then run parallel to the metal tower, and upwards to an altitude of nearly 1000 meters. For this configuration, the beam spot size at the breakdown initiation point is, from

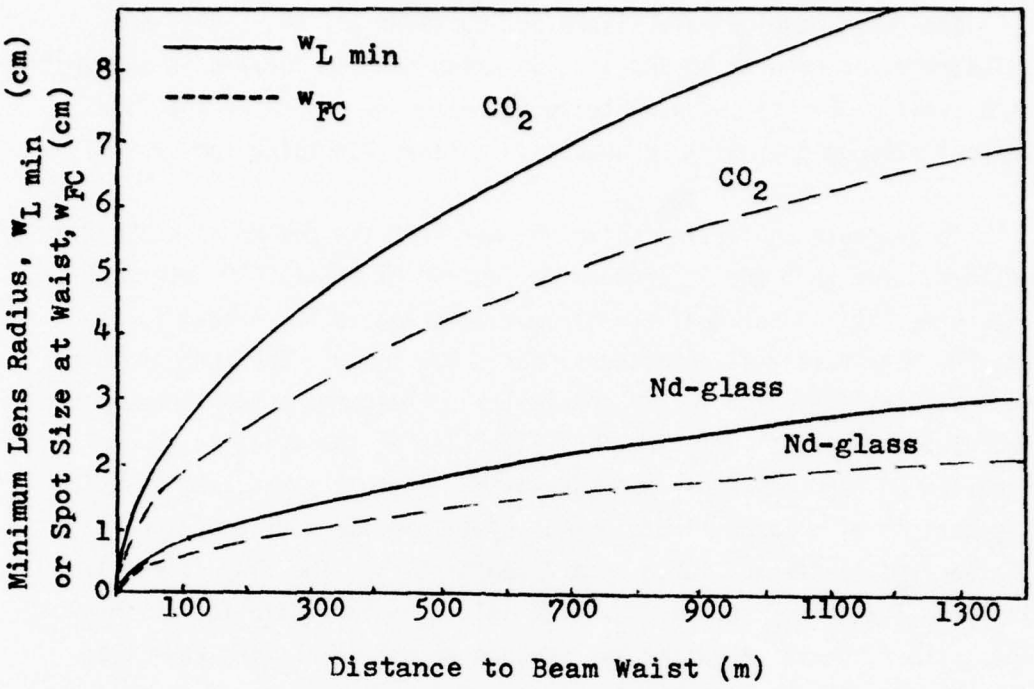

Figure 10. Effect of Focal Distance on Lens Radius and on Beam Waist Spot Size

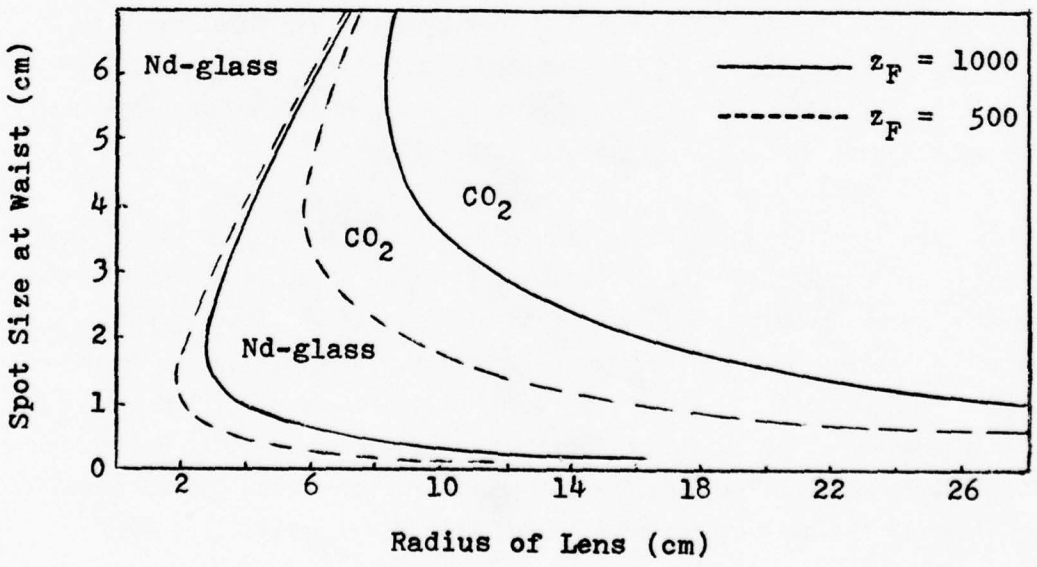

Figure 11. Effect of Lens Radius on Spot Size at Focal Point

Equation 48, 10 centimeters for the CO_2 laser with a lens radius of 11 centimeters. The spot size of the beam prior to the breakdown initiation point can be no larger than the spot size at the breakdown initiation point. Thus, the size of the laser aperture itself can not be less than 10 centimeters in radius. Furthermore, the beam spot size must remain larger than 10 centimeters throughout the optical chain used to focus and to direct the beam.

It becomes apparent from the preceding examples that laser fluxes on the order of gigawatts and laser aperture radii on the order of centimeters are required in a CO_2 laser lightning rod system. For the Nd-glass laser system, the aperture sizes required are not so large, as a glance at Figure 11 will show. However, for the Nd-glass wavelength, the breakdown threshold of air is a hundredfold larger than that for the CO_2 wavelength, from the λ^2 scaling law. As a result, the flux intensities required in a Nd-glass laser lightning rod system are much larger than those required in a CO_2 system.

3. PULSE SHAPES

Pulse shape information is carried by the Dt_1 and Dt_2 terms of the electron distribution equation. Although all pulse shapes can not be modeled, those that can be are extremely realistic. It is necessary to consider the leading and trailing edges of the pulse separately, however, in order to model any pulse shape. In forming a composite of the two parts, some difficulties arise which, under some conditions, affect the validity of the models.

a. Leading Edge

The pulse leading edge is defined here as that portion of the pulse which extends from $t = 0$ to $t = t_{max}$. The equation which carries leading edge information is, from Section IV,

$$Dt_1 = \frac{S(0,t_1)\ [\ A_T - F(z)\ ]}{\partial S(0,t_1)/\partial t_1} \tag{33}$$

To proceed with an analysis, it is necessary to specify a particular pulse shape leading edge. For the sake of computational simplicity, the linear leading edge is considered in the paragraph which follows. Results for other leading edges can be obtained by employing the same general approach.

The equation for a linear leading edge is

$$S(0,t) = \alpha t \qquad 0 < t < t_{max} \tag{57}$$

where α is some constant. At time t_1, Equation 57 and its derivative with respect to t_1 are

$$S(0,t_1) = \alpha t_1 \tag{58}$$

and

$$\frac{\partial S(0,t_1)}{\partial t_1} = \alpha \tag{59}$$

A substitution of Equation 59 into the expression for Dt_1 yields

$$Dt_1 = \frac{S(0,t_1)\ [\ A_T - F(z)\ ]}{\alpha} \tag{60}$$

From Equation 31

$$S(0,t_1) = S_T \exp \int_0^z [\ A_T - F(z')\ ]\, dz' \tag{31}$$

Thus, the final expression for Dt_1 can be written

$$Dt_1 = \frac{S_T}{\alpha} [\ A_T - F(z)\ ] \exp \int_0^z [\ A_T - F(z')\ ]\, dz' \tag{61}$$

Since $F(z)$ has been determined in the preceding section, and A_T will be approximated shortly as an empirical constant, Dt_1 has been completely

specified in terms of known laser beam, atmospheric, and pulse shape parameters. A similar analysis can be performed for the leading edge of other pulse shapes. Table 1 shows the results for sinusoidal and exponential leading edges. For ease in reference, the linear leading edge results are also tabulated. The constants A, B, α, β, and Ω are all determined by the leading edge shape at the final optical element.

TABLE 1

LEADING EDGES OF PULSES

S(0,t)	Dt_1
$Ae^{\beta t}$ (exponential)	$[A_t - F(z)]/\beta$
αt (linear)	$\frac{S_T}{\alpha}[A_T - F(z)] \exp \int_0^z [A_T - F(z')]\, dz'$
$B \sin \Omega t$ (sinusoidal)	$\frac{S_T [A_T - F(z)] \exp \int_0^z [A_T - F(z')]\, dz'}{\Omega \{ A_T^2 - S_T^2 \exp \int_0^z 2[A_T - F(z')]\, dz' \}^{\frac{1}{2}}}$

From geometric considerations, it is possible to acquire a numerical order-of-magnitude estimate of Dt_1 for a linear leading edge. Figure 12 shows a pulse with a linear leading edge as it may appear at the breakdown initiation point, z_B, and at the waist of the laser beam, z_F. The t_1 time, originally coincident with t_{max} when the pulse was at z_B, has moved to the left a time Δt as the pulse has moved from z_B to z_F. Thus, a rough estimate of Dt_1 can be found from

$$\frac{\partial t_1}{\partial z} \approx \frac{\Delta t}{z_F - z_B} \tag{62}$$

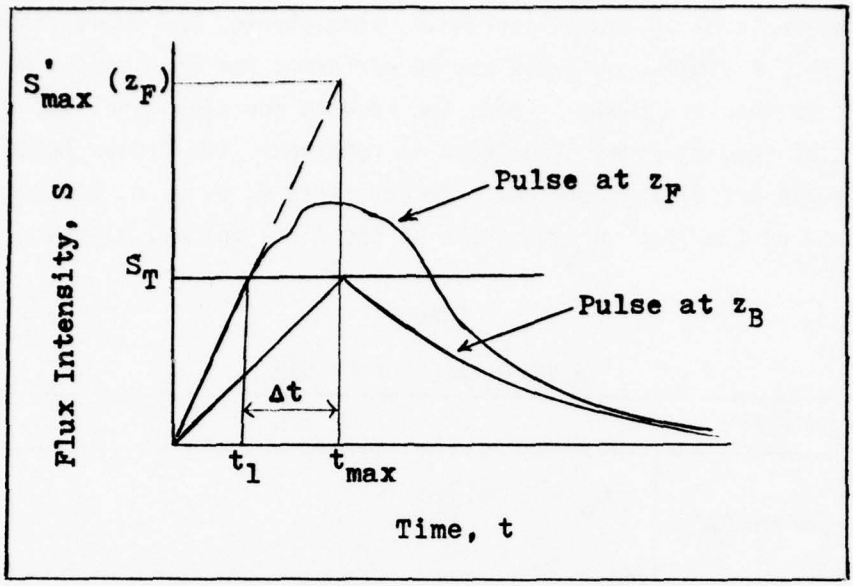

Figure 12. Pulse Shape for Estimating Dt_1

From the geometry of Figure 12,

$$\Delta t = \frac{S'_{max}(z_F) - S_T}{S'_{max}(z_F)} \; t_{max} \tag{63}$$

where $S'_{max}(z_F)$ is the maximum flux intensity the pulse would have reached had losses due to the electron cascade not occurred. From Equation 46,

$$S'_{max}(z_F) = S_T(w_B/w_F)^2 \tag{64}$$

where w_B is the spot size at z_B, and w_F is the spot size at z_f A substitution of Equations 63 and 64 into Equation 62 results in

$$\frac{\partial t_1}{\partial z} \approx \frac{(w_B/w_F)^2 - 1}{(w_B/w_F)^2 \; (z_F - z_B)} \; t_{max} \tag{65}$$

Borrowing from the examples employed in the section on Focusing, typical values for w_F, w_B, z_F, and z_B are 3.2 centimeters, 11 centimeters, 1000 meters, and 100 meters, respectively. Using these values in Equation 65, and assuming a t_{max} of 0.2 microseconds, results in

$$\frac{\partial t_1}{\partial z} \approx 2 \times 10^{-12} \text{ sec/cm} \tag{66}$$

The true value of Dt_1, given by Equation 61, can be monitored during the computer solutions of the electron distribution equation. A comparison with the estimated value of Equation 66 can then be made.

b. Trailing Edge

The pulse trailing edge extends from $t = t_{max}$ onward. An expression for Dt_2 is found in a method analogous to that for the determination of Dt_1. The variety of pulse shape trailing edges which can be modeled is, however, limited to a single functional form. The pertinent equation for evaluating Dt_2 is, from Section IV,

$$Dt_2 = \frac{S(0,\, t_2)\, [\, A_T - F(z) + Kn(z)\,]}{\partial S(0,t_2)/\partial t_2} \tag{38}$$

where, from Eq (36),

$$S(0,t_2) = S_T \exp \int_0^z [\, A_T - F(z')\,]\, dz' \exp \int_{z_B}^z Kn(z')\, dz' \tag{67}$$

The integral over Kn(z) in Equation 67 is an unknown which must be eliminated. The only obvious way this can be done is to use a function for $S(0,t_2)$ which cancels with its own derivative in Equation 38. The sole function with this property is the exponential. For an exponential trailing edge, then,

$$S(0,t) = B \exp(-\beta t) \qquad t_{max} < t < \infty \tag{68}$$

where B and β are constants. At time t_2, Equation 68 and its derivative with respect to t_2 are

$$S(0,t_2) = B \exp(-\beta t_2) \tag{69}$$

$$\frac{\partial S(0,t_2)}{\partial t_2} = - \beta B \exp(-\beta t_2) \tag{70}$$

Substituting Equations 69 and 70 into Equation 38 results in

$$Dt_2 = \frac{1}{\beta} [F(z) - A_T - Kn_e(z)] \tag{71}$$

Figure 17 of the next chapter illustrates a few of the many pulses which can be modeled using a linear or sinusoidal leading edge, and an exponential trailing edge. It can be seen that the pulses are extremely realistic (See Reference 2, for example). It is, in a sense, fortuitous that the modeling is limited to exponential trailing edges, since actual high-flux pulses have a decay of an exponential form.

c. Limits of Pulse Shape Model Validity

Pulse shape distortion affects the validity of the expressions for both Dt_1 and Dt_2. The following paragraphs discuss the nature of the invalidations, when they occur, and their effects.

The equation of Dt_1 was derived under the assumption that the pulse is optically magnified. As long as this is the case, t_1 is determined by the portion of the pulse below the threshold S_T. However, once the pulse passes the waist of the beam, the assumption is invalid, since the beam at this point is diverging. As the pulse intensity diminishes in magnitude beyond position z_F, the time t_1 must become dependent upon the distorted leading edge of the pulse which had been above threshold. Consequently, the equation for Dt_1 becomes inaccurate beyond z_F. The degree of inaccuracy depends upon the amount the pulse has been distorted, a factor which is not monitored using the methods here. It would be expected, however, that the degree of pulse distortion would be dependent

upon the number of electrons generated by the pulse. Thus, if the electron density generated in the breakdown region prior to z_F is small, the pulse would be only slightly distorted. The leading edge, in particular, would be little affected, since some time is required at a given position z for the electron cascade to become significant. The leading edge may be well beyond z before the cascade is large enough to produce a distortion in the pulse shape. If the electron density is high, however, the upper portion of the leading edge may become rounded, as shown in Figure 12. In this case, the expression for Dt_1 would become invalid, or at least inaccurate, as the rounded portion of the pulse falls below threshold. For a beam focused at a large distance, however, the upper portion of the pulse will remain above threshold until the pulse is well beyond the focal region, unless breakdown is initiated near the focal point, which would not usually be the case for the systems of interest here. From these considerations, it would appear that the theoretical value of Dt_1 would not differ much from the true value, even beyond the focal region. In any case, the expression for Dt_1 remains completely accurate over the portion of the beam of primary interest; namely, that portion from the laser to the focal point.

In the expression for Dt_2, the distortion in the pulse shape is taken into account by the Kn(z) term. A different source of difficulty arises, however, because of the composite nature of the pulse shape modeling. Figure 13 shows a pulse as it might appear at three different locations along the beam. The pulse as it emerges from the laser is identified by the label z_0. At a position z_1 downstream, the pulse has been magnified, and the t_2-time has moved to the right, away from t_{max}. Still further downstream, at position z_2, the pulse has been distorted by cumulative losses due to electron heating. The t_2-time has moved to the left, and rests at a t_2-equilibrium point, coincident with t_{max}. A further movement of t_2 to the left is impossible, since from Equation 38, Dt_2 will become positive if t_2 drifts to the leading edge side of the original pulse (assuming $F(z)<Kn(z) + A_T$). Consequently, the true value of Dt_2 is zero at the pulse position z_2, and all positions downstream.

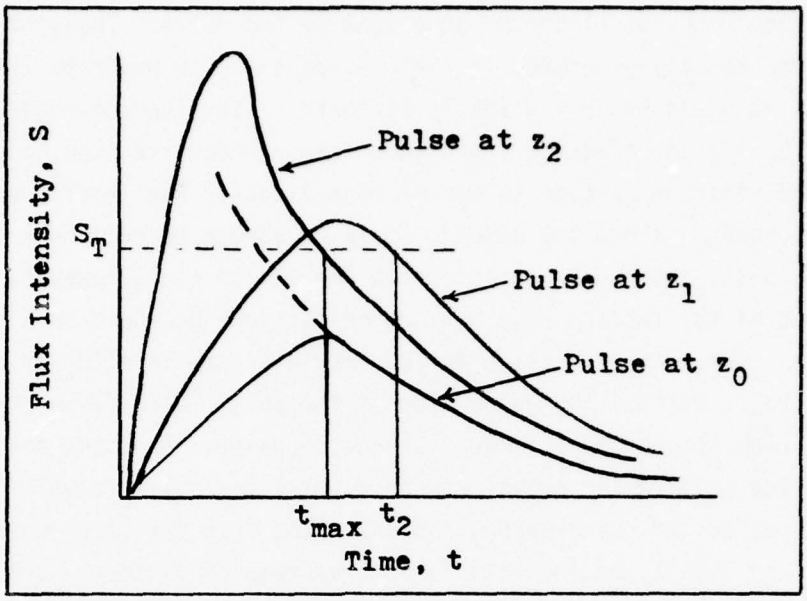

Figure 13. t_2-Equilibrium

Equation 71, however, is based on the formula for the exponential trailing edge of the original pulse, shown extended by the dashed line in Figure 13. Since the slope of the extended trailing edge is everywhere negative, Equation 38, and hence Equation 71, allows t_2 to continue a leftward drift. In summary, the true t_2 motion is determined by the shape of both the leading and trailing edges of the pulse, whereas Equation 71 is based on a formula for the trailing edge only. The result is an invalid expression for Dt_2 when the pulse becomes severely distorted, and t_2 drifts to the equilibrium point.

Fortunately, the same considerations which lead to the invalidity of Equation 71 also lend themselves to a derivation of a simplified relationship for the free electron distribution once t_2-equilibrium is reached. From Equation 38,

$$A_T - F(z) + Kn(z) = \frac{Dt_2}{S(0,t_2)} \frac{\partial S(0,t_2)}{\partial t_2} \tag{72}$$

Setting Dt_2 equal to zero results in

$$n(z) = \frac{1}{K} [\ F(z) - A_T\ ] \tag{73}$$

It will be possible during the computer solutions to monitor the motion of t_2, and to set $Dt_2 = 0$ when t_2-equilibrium is reached. The electron distribution given by Equation 73 can then be compared to the results of the more lengthy electron distribution equation (Equation 29), and a check for consistency made.

4. ATMOSPHERIC ATTENUATION

The attenuation of a laser beam due to molecular absorption and scattering is dependent upon a large number of atmospheric variables, including atmospheric pressure, temperature, aerosol concentration, water droplet concentration, and humidity. For the purpose of this report, however, only the simpler aspects of attenuation need be considered.

In the breakdown region of a laser beam, atmospheric attenuation is insignificant compared to the beam losses due to the microwave heating of electrons. Atmospheric attenuation does, however, affect the position z_B at which air breakdown is initiated, and can have a significant effect on the laser-generated free-electron densities beyond the breakdown initiation point.

The atmospheric attenuation coefficient as derived from computer models of the atmosphere is presented in Table 2, adapted from McClatchey (Reference 15: 21,24). In that table, A_{TA} and A_{TS} are the absorption coefficients due to molecular absorption and scattering, respectively, in a midlatitude summer atmosphere. The corresponding coefficients due to aerosol particles are given by A_{TA}^* and A_{TS}^*.

Table 2 does not take into account the effect of rain. Since a laser lightning rod system would likely be operating under rainfall

TABLE 2

ATMOSPHERIC ATTEN TION COEFFICIENT

Laser Wavelength (μm)	Height (km)	Atmosphere		Aerosol			
				Clear Day		Hazy Day	
		A_{TA} (km^{-1})	A_{TS} (km^{-1})	A_{TA}^* (km^{-1})	A_{TS}^* (km^{-1})	A_{TA}^* (km^{-1})	A_{TS}^* (km^{-1})
10.6	0	3.58 E-1	<1.0 E-6	5.48 E-3	4.65 E-3	2.67 E-2	2.27 E-2
	0 - 1	3.26 E-1		3.64 E-3	3.09 E-3	1.61 E-2	1.37 E-2
	1 - 2	1.88 E-1		1.58 E-3	1.34 E-3	5.90 E-3	5.01 E-3
	2 - 3	1.15 E-1		6.75 E-4	5.73 E-4	2.16 E-3	1.83 E-3
1.06	0	<1.0 E-6	8.20 E-4	1.98 E-2	6.79 E-2	9.63 E-2	3.31 E-1
	0 - 1		7.81 E-4	1.31 E-2	4.50 E-2	5.82 E-2	2.00 E-1
	1 - 2		7.06 E-4	5.71 E-3	1.96 E-2	2.13 E-2	7.31 E-2
	2 - 3		6.38 E-4	2.43 E-3	8.36 E-3	7.78 E-3	2.67 E-2

conditions, an estimate of the attenuation coefficient due to rain, A_{TR}, adapted from Chu and Hogg (Reference 5: 734), is provided in Figure 14.

The total attenuation coefficient is the sum of the contributing factors. Thus, for purposes of the electron distribution equation,

$$A_T = A_{TA} + A_{TS} + A_{TA}^* + A_{TS}^* + A_{TR} \tag{74}$$

Under sufficiently intense laser irradiation, aerosol particles and water droplets in the air will vaporize and form localized plasma spheres along the beam. The effect of these aerosol microplasmas on the propagation of the laser flux is discussed in Appendix C.

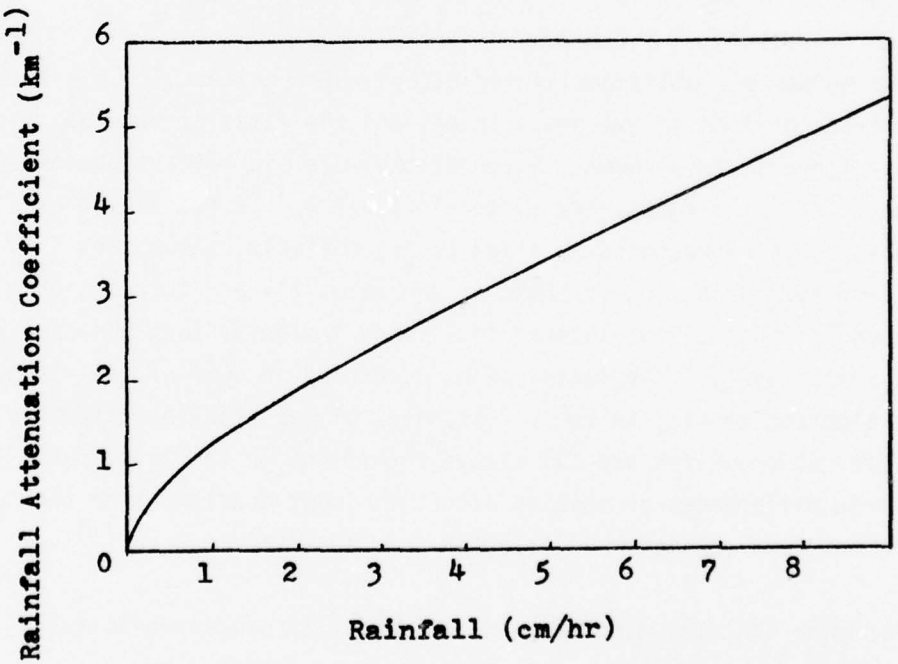

Figure 14. Rainfall Attenuation Coefficient

5. FREE ELECTRON LOSSES

The rate at which electrons and ions are lost by diffusion or by collisional interactions from the breakdown region of the beam establishes the persistence time of the ionized column of air. Losses due to free electron diffusion from the beam volume may be approximated by (Reference 14: 1889)

$$\frac{\partial n}{\partial t} = (845 + 171\ \varepsilon)\ n/L_D^2 \tag{75}$$

where ε is the electron energy in electron volts and L_D is a diffusion length, in centimeters, which may be taken as being the beam diameter. If electron densities exceed $10^6/L_D^2$ cm^{-3}, ambipolar diffusion dominates. In this case, an expression for diffusion is acquired by multiplying Equation 75 by a factor of 7.7×10^{-4} (Reference 14: 1886).

The number of collisional interactions which may result in a loss of electrons or ions is extremely large; and the rates of many of these are only approximately known. A few of the more significant processes, and their estimated rates, are listed in Table 3. In the table, electrons and photons are represented by e and p, respectively. Atoms are symbolized by A or B, and for most of the rates listed, correspond to oxygen and nitrogen. The superscripts + and * signify ions and excited atoms, respectively. The factor of n, occurring in some of the rates, is the electron density in cm^{-3}. Estimates of the reaction rates for the different processes are not always consistent in the literature. When large differences of opinion occur, the most consistent or the most recent rate estimate was selected for tabulation.

Assuming that the electron and ion densities are approximately equal, the loss rate of electrons from the beam is given by

$$\frac{dn}{dt} = -(845 + 171\ \varepsilon)/L_D^2 - \Sigma_i \langle R_i \rangle n^2 \tag{76}$$

TABLE 3

ELECTRON AND ION LOSS REACTIONS

Process Name	Reaction	Rate (cm^3/sec)	Source Ref, Page
Radiative Recombination	$e + A^+ \rightarrow A + p$	10^{-12}	16; 36
	$e + A^+ \rightarrow A^* + p$	$< 10^{-13}$	19; 53
Electron-Ion Recombination	$e + A_2^+ \rightarrow A + A$	3×10^{-7}	13; 5331
	$e + (AB)^+ \rightarrow A + B$	3×10^{-7}	13; 5331
	$e + e + A^+ \rightarrow A + e$	$10^{-20} n$	16; 36
	$e + A^+ + B \rightarrow A + B$	2×10^{-7}	16; 36
Dielectric Recombination	$e + (AB)^+ \rightarrow A + B$	10^{-7}	16; 36
Two-Body Attachments	$e + A_2 \rightarrow A^- + A$	$\approx 10^{-7}/n$	14; 1889
Three-Body Attachments	$e + A_2 + B_2 \rightarrow A_2^- + B_2$	$5 \times 10^{7}/n$	13; 5332
Ion-Ion Recombination	$A_2^+ + B_2^- \rightarrow A_2 + B_2$	7×10^{-7}	3; 190
	$A^+ + B^- \rightarrow AB + p$	$> 10^{-14}$	19; 55
	$A^+ + B^- \rightarrow A^* + B^*$	10^{-8}	19; 55

where $\langle R_i \rangle$ is the average loss rate for a given process, in cm^3/sec. Adding the electron loss rate terms from Table 3, Equation 76 becomes

$$\frac{\partial n}{\partial t} = -10^{-20} n^3 - 9 \times 10^{-7} n^2 - 6 \times 10^{7} n + (845 + 171\ \varepsilon) n / L_D^{\ 2} \qquad (77)$$

For a beam diameter on the order of centimeters, the diffusion term in Equation 77 is negligibly small, even at high electron energies (100 eV). The remaining portion of the equation may be solved in a piecemeal fashion, since each of the terms become significant at different electron densities. Figure 15 on page 78 shows the electron density dependence on time that results from the solution.

It is seen that the electron density falls to about 10^{14} electrons/cm^3 in less than 10^{-7} seconds, assuming an initial density of about 10^{19} electrons/cm^3 (full breakdown). This quick drop in electron density is due to electron-ion recombinations. Following recombinations, electron density diminishes more slowly. Electron loss mechanisms at this time are due primarily to electron attachment to neutral atoms. Although the attachments result in a loss of free electrons, the ion density is unaffected. Thus after a few tenths of a microsecond, the ionized channel consists of about 10^{14} ions and 10^{14} attached electrons. The attached electrons are easy to remove ($\approx$0.4 eV), so the channel at this point in time is still intact for laser lightning rod system purposes; and the persistence time of the channel now becomes dependent upon the rate of ion-ion recombinations. The ion loss rate is given by (from Table 3)

$$\frac{\partial n_I}{\partial t} = -\ 7 \times 10^{-7}\ n_I^{\ 2} \qquad (78)$$

which has the following solution:

$$n_{I(t)} = \frac{n_{Ii}}{1 + 7 \times 10^{-7}\ n_{Ii} t} \qquad (79)$$

where n_{Ii} is the initial ion density. Figure 16 shows the free-ion density as a function of time, as predicted by Equation 79.

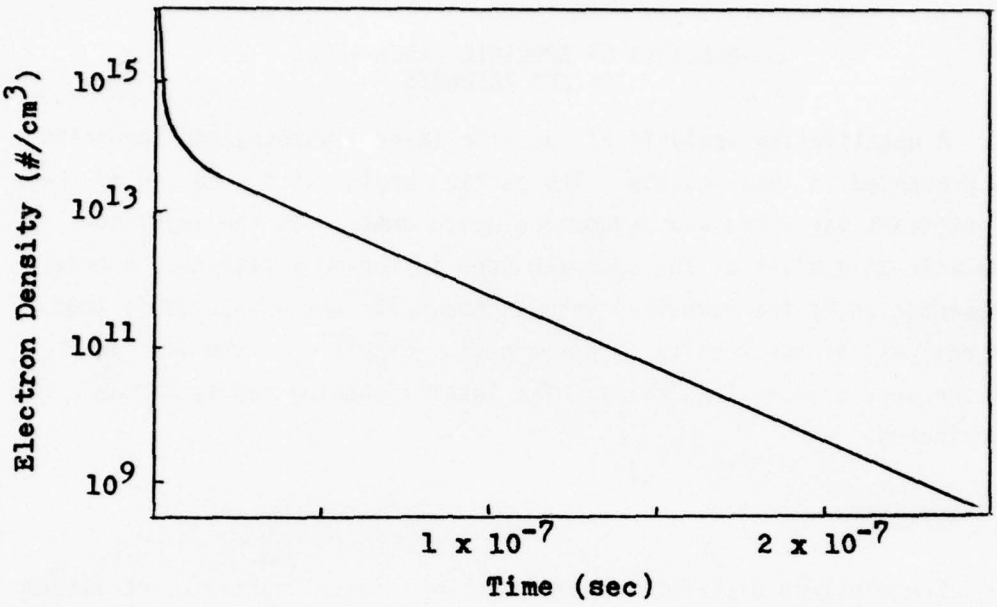

Figure 15. Electron Persistence Time in Channel

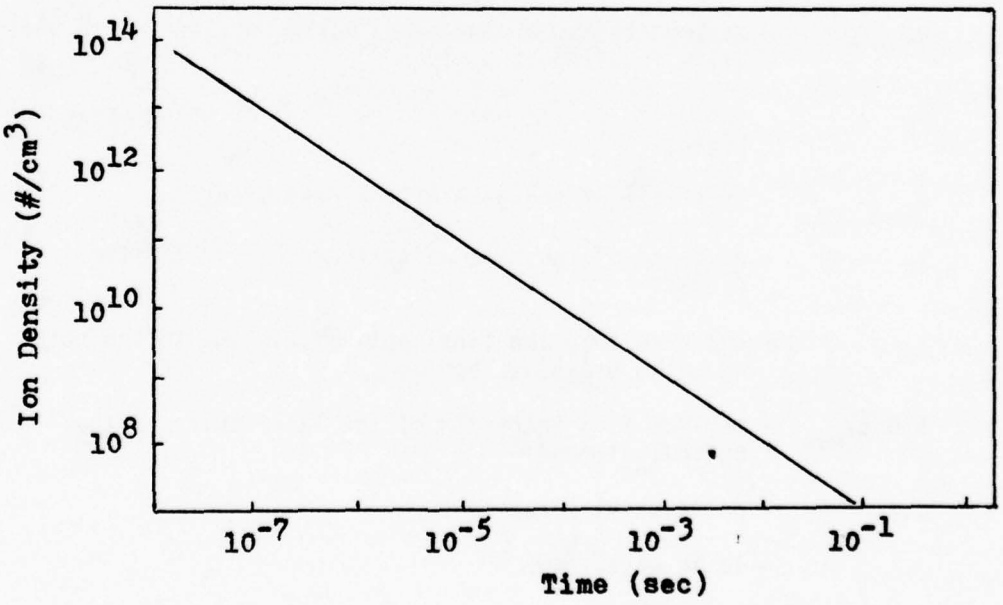

Figure 16. Ion Persistence Time in Channel

SECTION VI

ANALYSIS OF SPECIFIC LASER-INDUCED IONIZED PATHWAYS

A quantitative analysis of specific laser lightning rod scenarios is presented in this section. The section begins with a review of the significant variables and parameters which enter into the solutions, and with an outline of the approach used in the computations. A brief presentation of the numerical values chosen for the scenarios follows. An analysis of the results is given next. Finally, in the last part of the section, the feasibility of a laser lightning rod system is considered.

1. APPROACH

The electron distribution produced by a laser lightning rod system is dependent upon a large number of variables and parameters. Variables of specific interest are listed below for ease in reference.

- w_L - radius of the final mirror or lens of the optical system focusing the beam
- $w_{L\ min}$ - minimum radius of the final mirror or lens which will allow focusing at a given z_B
- w_B - spot size of the beam at the point at which breakdown begins
- w_F - spot size of the beam at the beam waist
- z_F - distance of the beam waist from the final optical element
- z_B - distance from the final optical element to the point at which breakdown begins
- $S(0,t)_{max}$ - maximum flux intensity of the laser pulse at the final optical element
- α,β - pulse shape parameters
- λ - laser wavelength

Parameters which must be specified are the following:

A_T - atmospheric attenuation coefficient

S_T - breakdown threshold of air

K - electron heating coefficient

The ten variables are interrelated by four independent equations. Consequently, six of the variables can be specified, and the remaining four solved. The four independent equations used to eliminate variables here were

$$w_F = \{ \tfrac{1}{2} w_L^2 - \tfrac{1}{2} \sqrt{w_L^4 - 4\left(\frac{\lambda z_F}{\pi}\right)^2} \}^{\frac{1}{2}} \tag{80}$$

$$W_{Lmin} = (2\lambda z_F/\pi)^{\frac{1}{2}} \tag{55}$$

$$w_B = [\, R^2 w_L^2 + (1 - R^2) w_F^2 \,]^{\frac{1}{2}} \tag{81}$$

and

$$S(0,t)_{max} = S_T \frac{a^2 + (z_F - z_B)^2}{a^2 + z_F^2} \exp(A_T z_B) \tag{82}$$

where

$$R = (z_F - z_B)/z_F \tag{83}$$

and

$$a = \frac{\pi}{\lambda} w_F^2 \tag{50}$$

Equations 80 and 81 result from a straightforward application of Equation 48. The equation for $S(0,t)_{max}$ is acquired by substituting F(z) given by Equation 49 into the breakdown initiation equation (Equation 24) and performing the integration.

To determine the electron distribution for a given laser lightning rod scenario, all of the variables and parameters except $w_{L\ min}$, w_B, w_F, and $S(0,t)_{max}$ were specified. The four unspecified variables were found using Equations 80, 55, 81, and 82. The electron distribution equation was computer programmed to solve for the electron density as a function of distance z from the final optical element. Computations began at $z = z_B$, and incremental steps Δz taken. The length of each step was adjusted by a method of leapfrog differencing to keep the error per step below one percent. For each scenario, 51 steps were taken. Six quantities, z, n, Dt_1, Dt_2, F(z), and K were printed on each step. At the end of each scenario, z_B, w_L, w_B, w_F, and S_{max} were printed, along with the location and value of the maximum electron count.

2. SCENARIOS

The electron distribution for over one thousand laser lightning rod scenarios was determined. Computer DO loops were used so that in a single computer run, 84 scenarios were tested. Parameters which were fixed in each set of 84 solutions are shown in Table 4. The pulse shapes identified by Roman numerals in Table 4 are shown in Figure 17. The time t_E in the pulse illustrations is the time at which the trailing edge of S(0,t) falls to e^{-1} x maximum intensity. In most of the computer runs, the heating term from the high flux limit modification A was used. However, the more conservative heating term, K_B, was tested in 252 scenarios. Atmospheric attenuation coefficients of 4.1×10^{-6} cm^{-1} for CO_2 radiation, and 4.3×10^{-6} cm^{-1} for neodymium radiation, were used in all but one scenario set. These values, from Table 2, correspond to a "hazy" midlatitude summer day. To determine the effect of moderate rainfall on the electron distribution, an A_T value of 2.72×10^{-5} cm^{-1} was used in a rerun of set 1. The initial electron density, n_0, was assumed to be one electron cm^{-3} in all solutions.

In each set of 84 scenarios, the breakdown initiation position, z_B, was incremented in steps one-eighth of the distance from the laser to z_F. Thus, for the focal distance of 1000 meters, breakdown initiation was

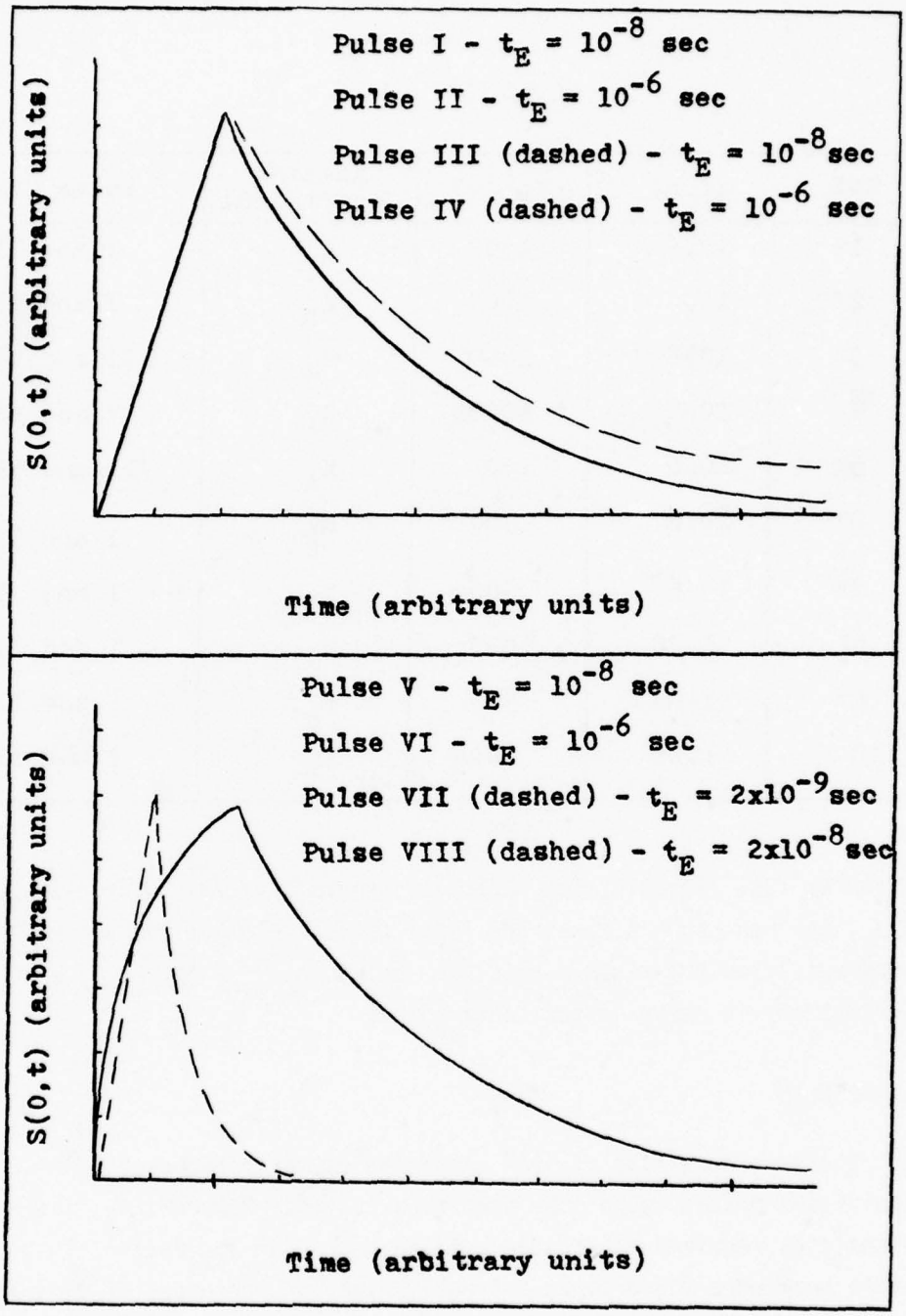

Figure 17. Scenario Pulse Shapes

TABLE 4

SCENARIO SETS

Set	$\lambda(\mu m)$	z_F (m)	Heating Coefficient	Pulse Shape
1*	10.6	1000	K_A	I and II
2*	10.6	1000	K_B	I and II
3	10.6	1000	K_A	III and IV
4	10.6	1000	K_A	V and VI
5*	10.6	1000	K_A	VII and VIII
6*	10.6	500	K_A	I and II
7*	10.6	500	K_B	I and II
8*	1.06	1000	K_A	I and II
9*	1.06	500	K_A	I and II
10	1.06	500	K_B	I and II

tested at 125, 250, 375, 500, 625, 750, and 875 meters. For each value of z_B, the beam spot size at the final optical element was increased by increments from the minimum possible radius, $w_{L\ min}$, to $w_{L\ min}$ + 10 centimeters, in steps of two centimeters.

3. RESULTS

Electron densities of 10^{14} electrons/cm^3 or more occurred in a significant percentage of the scenarios tested. However, th laser flux intensities required to produce a large degree of ionization along the entire beam were found to be extremely high: on the order of gigawatts. In addition, the radius required for the final optical element, w_L, was in many cases near the limits of current technology.

Results for 630 of the scenarios are tabulated in Appendix D. Those tabulated are indicated in Table 4 with an asterisk. Because of the impracticability of reproducing the entire distribution for each of the scenarios, the tabulations list only the critical information for each scenario and distribution. Consequently, much care must be taken in interpreting the data listed. The introduction to the tabulations discusses the approach which must be used to draw valid conclusions.

Many relationships could be seen between the electron distribution and the input parameters. The relationships found are discussed in the following paragraphs, along with some general comments concerning the solutions. The pulse shapes referred to in the narrative are those shown in Figure 17.

a. Final Optical Element Radius Dependence (w_L)

Figure 18 shows the electron distribution produced by a laser focused at 1000 meters, and power-adjusted to initiate breakdown at 125 meters. The solid lines apply to a 10 nanosecond pulse (Pulse shape I); and the dotted lines to a microsecond pulse (Pulse shape II). Open circles at the end of the distributions indicate the point at which computations stopped. It is seen from the figure that the size of w_L has a large influence on the electron distribution for the 10 nanosecond pulse. However, the degree of influence decreases rapidly with increasing w_L. Thus, changing w_L from 8.2 to 10.2 centimeters increases the maximum electron density by 11 orders of magnitude. A further increase to 16.2 centimeters has virtually no effect at all. For the microsecond pulse, a large electron density is produced almost immediately at z_B, and the size of w_L is unimportant. A physical interpretation here is that the high fluence of the longer pulse length becomes dominant over variations in w_L.

b. Pulse Length Dependence

The effect of a slight increase in pulse length can be seen in Figure 19, which illustrates the electron distribution for a laser focused

at 1000 meters and power-adjusted to initiate breakdown at 750 meters. The effects of the nearly identical pulse shapes I and III are compared. The slightly longer pulse III produces a higher electron density over the first part of the distribution; however, after about 150 meters, the longer pulse has dissipated more of its fluence than the shorter pulse, and the electron-generation capability of the two pulses becomes about equal.

c. Pulse Shape Dependence

The effect of pulse shape on the electron distribution was found to be minor compared to the effect of pulse length. Indeed, the distribution produced by pulse shape V (sinusoidal leading edge) was in many cases identical to that produced by pulse shape III (linear leading edge). In Figure 19, for example, the distribution labeled as Pulse Shape III is the same as the distribution for Pulse Shape V under the same focusing and laser power conditions.

d. Flux Intensity Dependence

The flux intensity required to produce an ionized column showed dependence on the breakdown initiation location, the size of the final optical element, and the laser wavelength. This dependence can be seen clearly in the tables in Appendix D. In General, the flux intensity required was found to be inversely proportional to z_B at a constant w_L, and inversely proportional to w_L at a constant z_B. The fluxes required in all scenarios were high. The range for CO_2 lasers was 0.11 to 2.79 gigawatts; that for Nd-glass lasers, 5.71 to 279 gigawatts.

e. Dependence on the Electron Heating Coefficient

The electron heating coefficient used in the computations had, as expected, a significant effect on the electron distribution. The upper part of Figure 20 shows typical distributions as predicted by K_A (dotted lines) and K_B (solid lines), for a 10 nanosecond pulse (Pulse I).

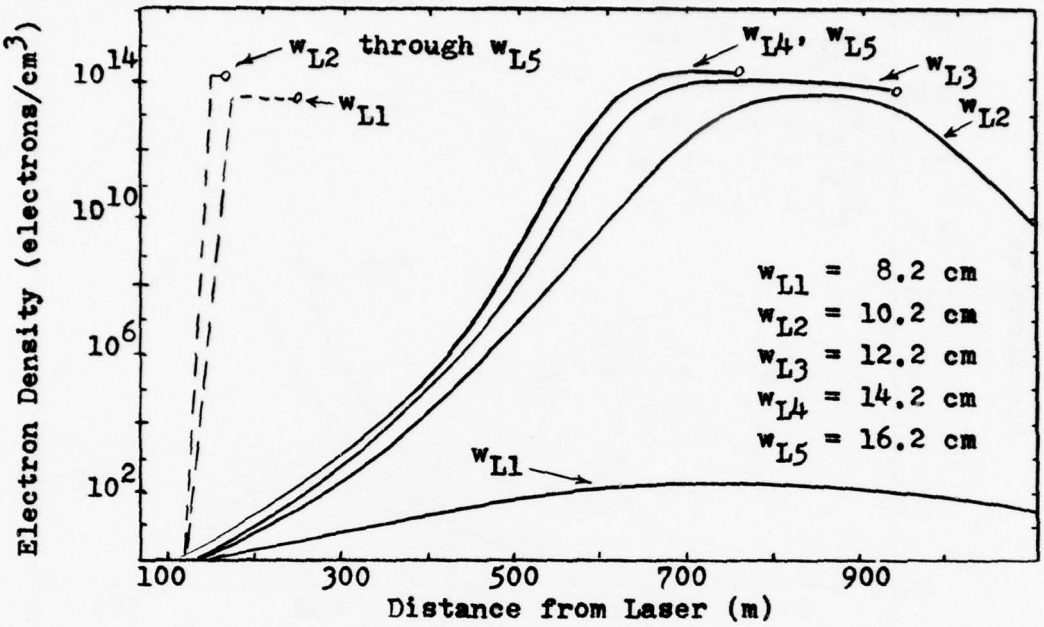

Figure 18. Effect of Lens Radius on Electron Distribution

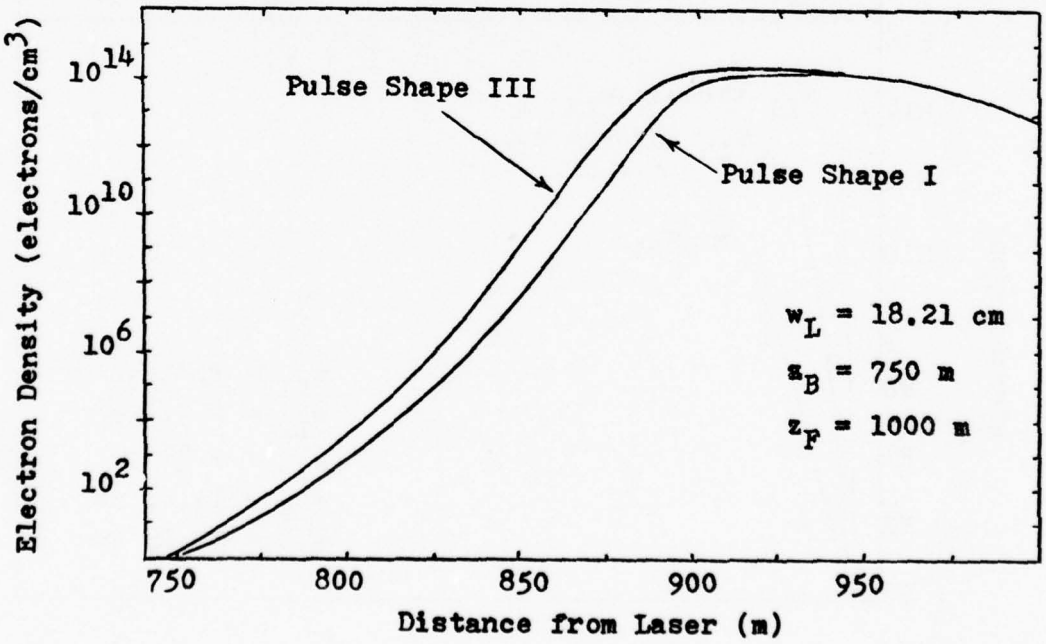

Figure 19. Effect of Pulse Length on Electron Distribution

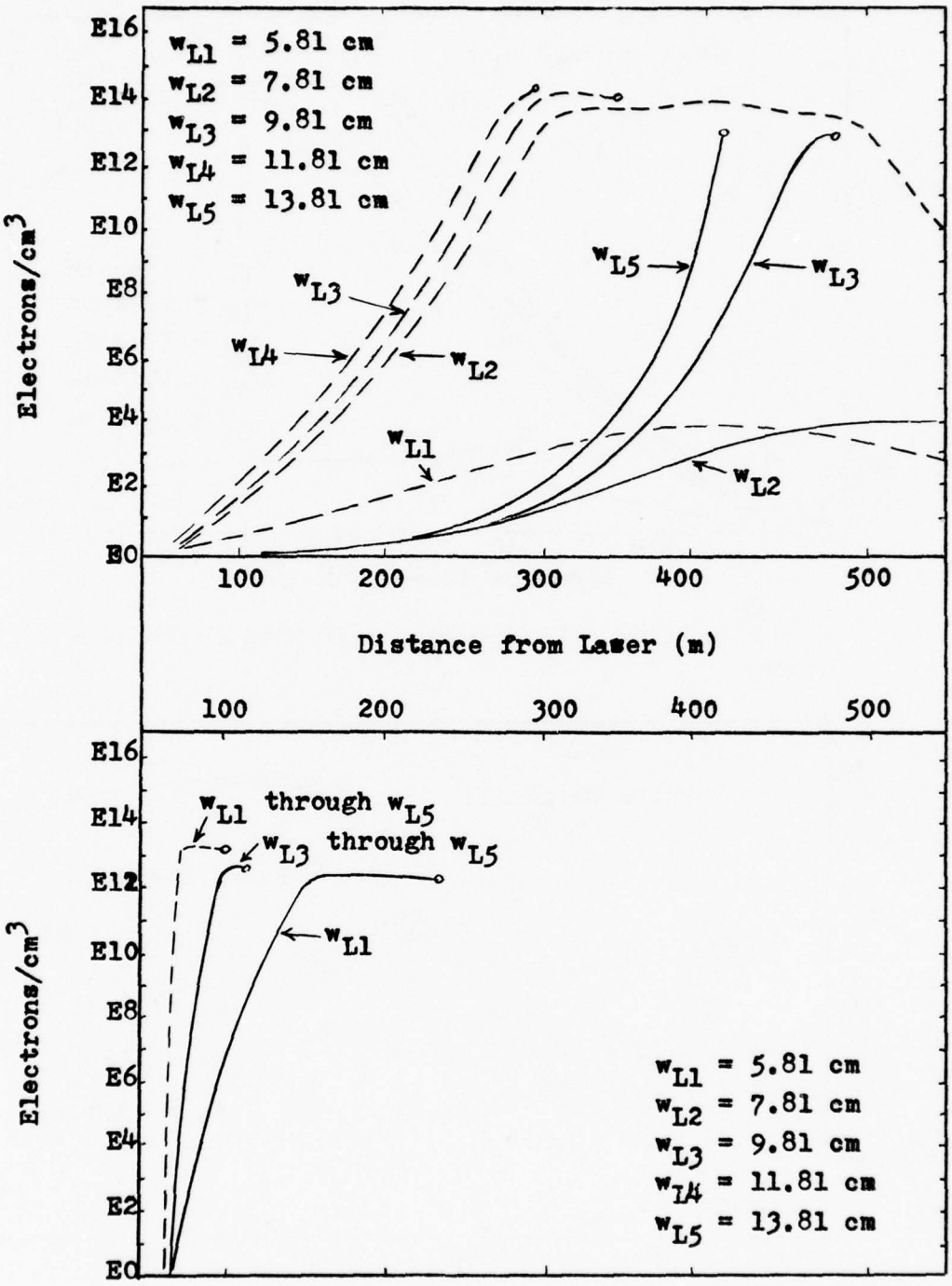

Figure 20. Effect of Heating Coefficient on Electron Distribution

The electron densities are consistently higher for K_A than for K_B at all values of w_L. As seen in the lower half of the figure, the effect is less significant for a microsecond pulse (Pulse III).

f. Dt_1 Value

The sign of Dt_1 consistently changed from positive to negative near the focal point in each scenario, as expected. Magnitudes of Dt_1 varied with position, z, and with scenario. For the CO_2 laser with z_F = 1000 meters, z_B = 125 meters, w_L = 10.21 centimeters, and w_F = 3.5 centimeters; the value of Dt_1 was approximately 3×10^{-12} seconds per centimeter over most of the path. This is in excellent agreement with the rough estimate made for a similar scenario elsewhere in this report.

g. t_2-Equilibrium

In Figure 21, a comparison is made between the results of the computer-solved electron distribution equation (Equation 29), and the t_2-approximation equation (Equation 73) of Section V. For the generation of both curves, the input parameters were w_L = 14.2 centimeters, z_F = 1000 meters, $t_p \approx 10^{-8}$ seconds, $z_B \approx 375$ meters, and λ = 10.6 μ. The discrepancy between the results of slightly more than one order of magnitude is relatively small at the orders of magnitude involved. The rise and decay rate of the electron density with distance is clearly consistent in the two solutions.

h. Atmospheric Attenuation Dependence

Forty-two scenarios were tested using an atmospheric attenuation coefficient corresponding to a moderate rainfall ($A_T = 2.27 \times 10^{-5}$ cm^{-1}). These results are tabulated in Appendix D, Table D-15. Results of the corresponding scenario set in which a "hazy day" attenuation coefficient ($A_T = 4.1 \times 10^{-6}$ cm^{-1}) was used appear in Table D-1. From a comparison of the two tables, it is evident that the free-electron distribution is strongly dependent upon the value of A_T. In particular, as the value of A_T increases, the length of the path over which a free-electron distribution

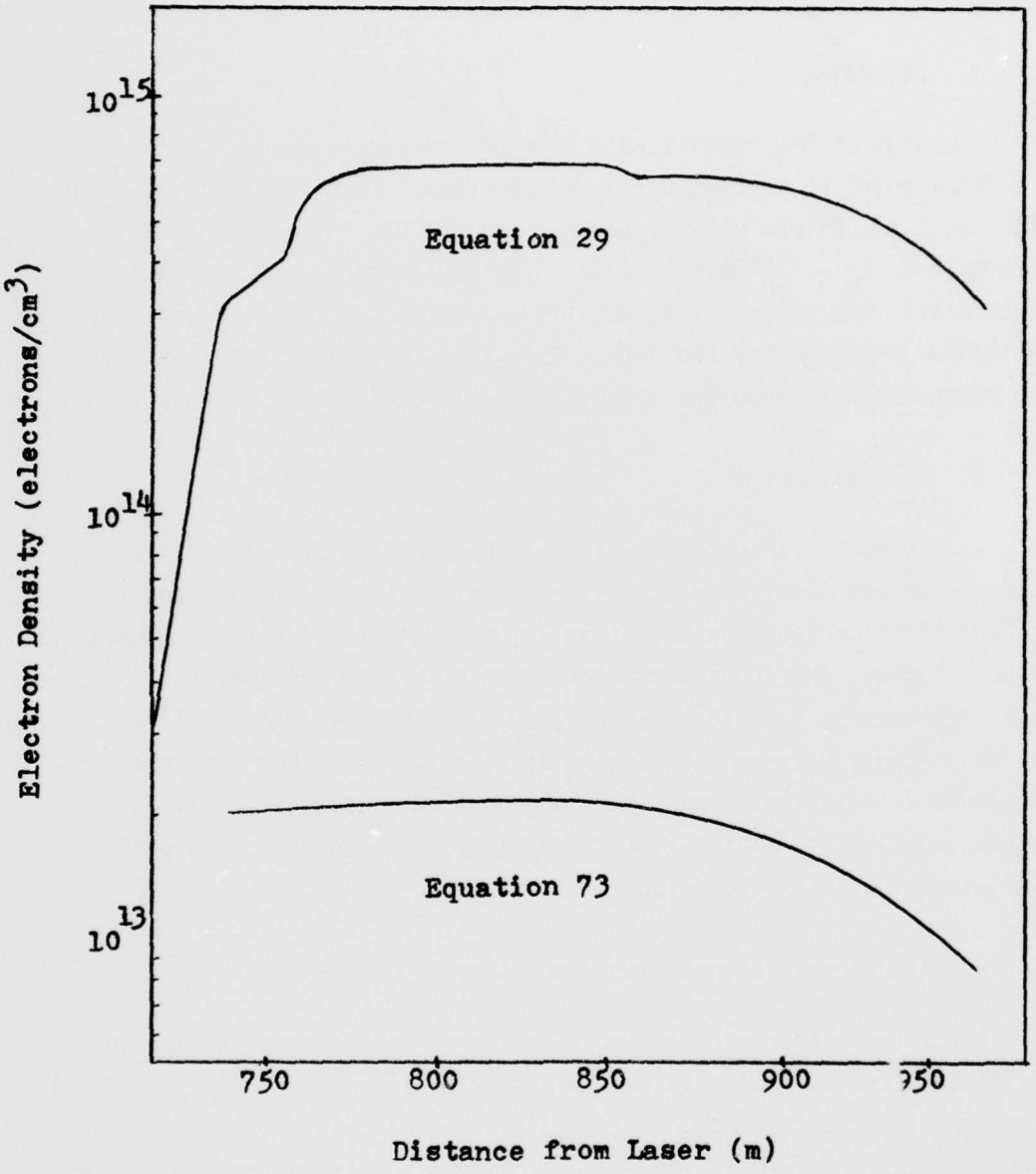

Figure 21. Comparison of Solutions of Different Electron Distribution Equations

can be maintained decreases. For the specific values of $A_T = 2.72 \times 10^{-5}$ cm^{-1}, and $z_F = 1000$ m, breakdown of the air can not be maintained at distances closer to the laser than 250 meters. Significant electron distributions beyond 250 meters occur only for laser aperture radii exceeding 12.21 centimeters.

i. Beam Radius

Table 5 shows the range of w_L and w_F for the scenarios tested. It can be seen that for the CO_2 laser, the beam radius was on the order of centimeters, or tens of centimeters; and for the Nd-glass laser, about an order of magnitude smaller.

j. Energy Conservation Considerations

For seven of the scenarios, the energy output of the laser, E_{LO}, was compared with the total energy, E_e, required to generate the electrons in the beam volume. To compute E_{LO}, the flux intensity of the appropriate pulse was integrated over time, and over the area of the laser aperture.

TABLE 5

SPOT SIZE AT WAIST FOR SCENARIOS TESTED

$\lambda = 10.6\ \mu$				$\lambda = 1.06\ \mu$			
$z_F = 1000$ m		$z_F = 500$ m		$z_F = 1000$ m		$z_F = 500$ m	
w_L (cm)	w_F (cm)	w_L (cm)	w_F (cm)	w_L (cm)	w_F (cm)	w_L (cm)	w_F (cm)
8.21	5.81	5.81	4.11	2.60	1.84	1.84	1.30
10.21	3.52	7.81	2.26	4.60	0.74	3.84	0.44
12.21	2.84	9.81	1.75	6.60	0.51	5.84	0.29
14.21	2.41	11.81	1.44	8.60	0.39	7.84	0.22
16.21	2.10	13.81	1.23	10.60	0.32	9.84	0.17
18.21	1.86	15.81	1.07	12.60	0.26	11.84	0.14

The value of E_e was approximated by the product of the beam volume, the maximum electron density within the beam, and the ionization potential of air. Scenarios with constant, or nearly constant, electron densities throughout were chosen for the computations. Ratios of E_e/E_{LO} ranging from 1.1×10^{-3} to 2.8×10^{-3} were obtained, with an average for the seven scenarios of 2.1×10^{-3}. The energy ratios of these seven scenarios may not be totally representative of all of the distributions. The low ratios obtained do, however, indicate that energy conservation requirements are easily met.

4. CONCLUSION

From the scenarios tested, it is clear that a laser beam can create an ionized column of air at least one kilometer long with electron densities on the order of 10^{13} to 10^{16} electrons/cm^3. The bulk of the electrons within such a column would attach to neutral atoms in about 10^{-7} seconds. The ions, however, would persist much longer. Consequently, from Figure 15, a charged column of 10^{10} ions/cm^3 and 10^{10} loosely attached electrons/cm^3 would remain after 10^{-4} seconds. Comparing these numbers with the feasibility criteria of Section II, it would appear that a laser lightning rod system is feasible, at least from the standpoint of the beam physics.

To generate an appropriate ionized channel, laser flux intensities on the order of gigawatts/cm^2 (for CO_2 radiation), or hundreds of gigawatts/cm^2 (For Nd radiation), over a laser aperture of centimeters or tens of centimeters in radius would be needed. In addition, short laser pulses, or a low atmospheric aerosol count, would be required to minimize beam losses due to aerosol breakdown.

Megawatt lasers, which may be used to generate rarified channels in air for the guidance of lightning (Appendix A), are presently available. Lasers capable of producing gigawatt pulses are currently in the experimental stage. Whether a gigawatt beam with the cross-sectional area and pulse length required to cause breakdown along a kilometer-long path can be engineered is a matter for further study.

APPENDIX A

LIGHTNING GUIDANCE BY LASER-INDUCED RAREFICATION CHANNELS IN AIR

Spark guidance experiments by Saum and Koopman (Reference 22: 2077-2079) suggest that a laser-induced rarefication channel in air may be used to guide lightning to a target on the ground. Laser flux intensities which would be required can be estimated from elementary considerations of thermodynamics.

The Saum and Koopman experiments indicate that the air density in a rarefied channel must be lowered to at least 0.67 ambient air density in order to guide a spark. Although it is not certain that the experiments are scalable to a laser-lightning-rod scenario, a rarefied-channel to ambient-air density ratio of 0.67 at least provides a starting point for rough calculations.

From pressure-balance considerations, the energy required to lower the density in a column of air of radius r and length z to a value of n_2 is given by

$$E_1 = (\pi r^2 z)\ (n_1 k T_1)\ \frac{n_1}{n_2} \tag{84}$$

where T_1 and n_1 are the ambient air temperature and density, respectively.

The energy deposited in the channel by a laser beam of initial constant flux S_o and pulse length t_p may be approximated by

$$E_1 = S_o\ [\ 1 - \exp(A_T z)\ ]\ \pi r^2 t_p \tag{85}$$

where A_T is the molecular absorption coefficient. Combining Equations 84 and 85 to eliminate E_1 gives the following relationship for the flux intensity required to guide an electrical discharge:

$$S_o = \frac{z n_1 k T_1}{[\ 1 - \exp(-A_T z)\ ]\ t_p}\ \left(\frac{n_1}{n_2}\right) \tag{86}$$

The time required for the laser-deposited energy to diffuse out of the channel is approximately (Reference 22: 2078)

$$t_D = c_p n_m r^2 / 2K_c \tag{87}$$

where c_p, n_m, and K_c are, respectively, the specific heat at constant pressure, the mass density of the air, and the thermal conductivity of the air. If the length of the laser pulse equals or exceeds t_D, energy deposition by the pulse is balanced by energy losses due to diffusion. Thus, the maximum effective pulse length for the maintenance of a given fractional rarefication is $t_p = t_D$. Substituting the expression for t_D given by Equation 87 into Equation 86 yields, for the long-pulse limit,

$$S_o = \frac{2zn_1 kT_1 K_c (n_1/n_2)}{[\ 1 - \exp(A_T z)\ ]\ c_p n_m r^2} \qquad t_p > t_D \tag{88}$$

For the parameter values

$n_2/n_1 \approx 0.67$

$z \approx 10^5$ cm

$n_1 \approx 2.5 \times 10^{19}$ cm^{-3}

$n_m \approx 1.3 \times 10^{-3}$ gm/cm^3

$K_c \approx 2.5 \times 10^{-4}$ joules/cm-sec-°K

$C_p \approx 1$ joule/gm-°K

$kT_1 \approx 4 \times 10^{-21}$ joules

$A_T \approx 3.6 \times 10^{-6}$ cm^{-1} (CO_2 radiation, Table 2)

Equations 86 and 88 become

$$S_o \approx \frac{5 \times 10^4}{t_p} \text{ watts/cm}^2 \qquad t_p < t_D \tag{89}$$

$$S_o \approx \frac{2 \times 10^4}{r^2} \text{ watts/cm}^2 \qquad t_p > t_D \tag{90}$$

The flux intensity versus pulse length criterion established by Equations 89 and 90 are illustrated in Figure 22. It is seen that for short pulse lengths, the flux intensity requirement is extremely high; reaching approximately 100 gigawatts for a microsecond pulse. For longer pulse lengths, the requirements are not so stringent. Maintenance of a rarefied channel by a laser beam of one centimeter radius and a pulse length of two seconds or longer can be accomplished with a rather modest flux intensity of 10^4 W/cm^2.

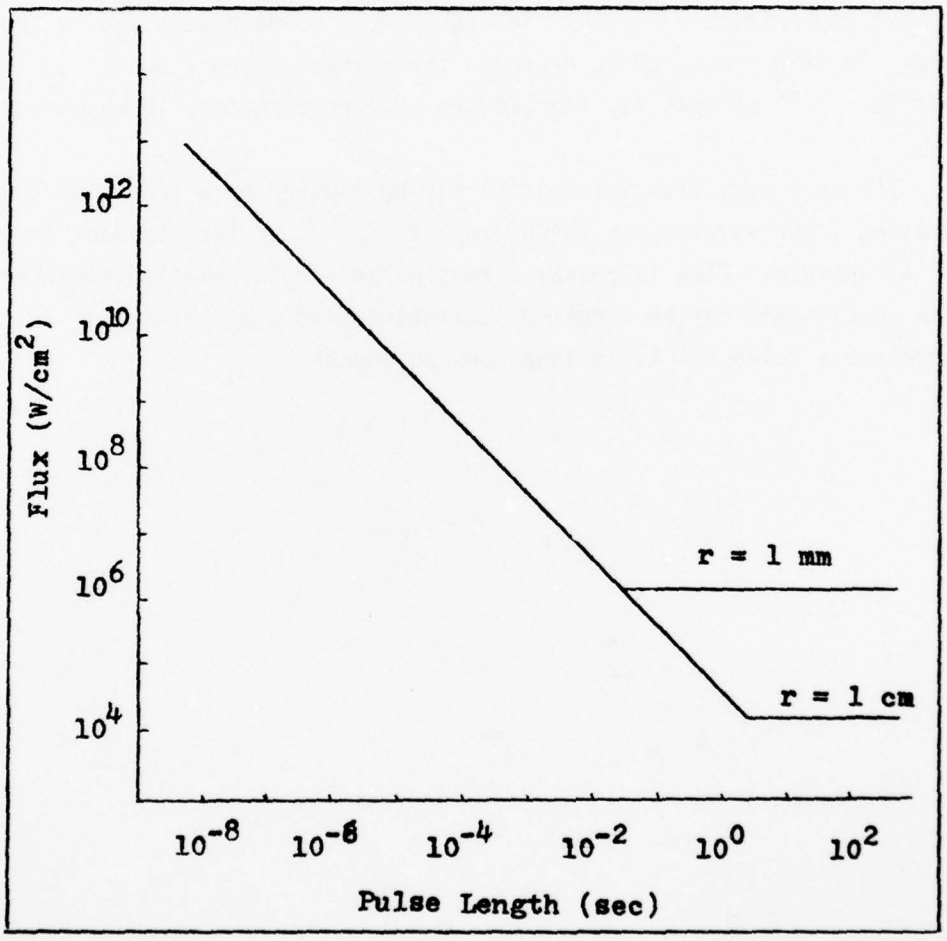

Figure 22. Flux Versus Pulse-Length Criterion for Maintenance of Rarefied Channel by CO_2 Radiation

The considerations so far, however, have neglected the effects of wind shear. If the laser pulse is excessively long, winds blowing across the beam in opposite directions may dissipate the channel before the rarefication can be fully established. In a shearing wind of velocity v_w, the persistence time of the channel, t_w, may be approximated by

$$t_w \approx r/v_w \tag{91}$$

Thus, in a wind of 44 cm/sec (10 mph), a one-centimeter channel will persist approximately 2×10^{-2} seconds before being dissipated by the wind. The flux required to generate the channel using a pulse length of less than 10^{-2} seconds is, from Figure 22, approximately 10 megawatts.

The necessary flux intensities may be lowered by a factor of ten or so using laser wavelengths which exhibit high molecular attenuation in the atmosphere. Flux intensity versus pulse-length relationships for such wavelengths may be acquired straightforwardly by using the appropriate value for A_T in Equations 86 and 88.

APPENDIX B

COLLISIONAL MOMENTS

Moments of the Boltzman equation collisional terms must be analyzed on a reaction-by-reaction basis. The derivations below apply for the specific process of electron-atom ionizations. For other processes, such as electron-atom attachments and electronic excitations, the mathematics will differ. However, the same general approach can be used.

1. ELECTRON-ATOM IONIZING COLLISIONS

Three possible modes exist by which an electron can enter or leave a distribution $f(\varepsilon)$ as a result of an ionizing collision. First, a free electron of energy ε may collide with an atom, produce an ionization, and emerge with some arbitrary energy y. Second, a free electron of energy y may collide with an atom, produce an ionization, and depart with an energy ε. Third, an electron of energy y may collide with an atom, release an electron of energy ε from the atom, and recoil with an energy $y-\varepsilon-I$. These three possibilities are illustrated in Figure 23.

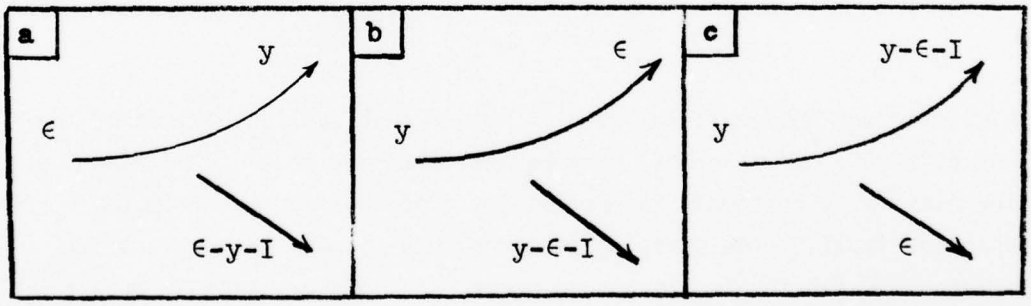

Figure 23. Modes of Ionization

If $R_I(A,B)$ is the rate at which a free electron of energy A recoils with an energy B upon ionizing an atom, and n_o is the density of atoms; the change in $f(\varepsilon)$ with time due to ionizing collisions is

$$\frac{\partial f(\varepsilon)}{\partial t}_{\text{I-coll}} = -\int_{y=0}^{\varepsilon-I} f(\varepsilon) n_o R_I(\varepsilon,y)dy + \int_{y=I+\varepsilon}^{\infty} f(y) n_o R_I(y,\varepsilon)dy + \int_{y=I+\varepsilon}^{\infty} f(y) n_o R_I(y,y-\varepsilon-I)dy \quad (92)$$

The zeroth moment, acquired by integrating Equation 92 over all energy, is then

$$\frac{\partial n}{\partial t}_{\text{I-coll}} = -\int_{\varepsilon=I}^{\infty} f(\varepsilon) \int_{y=0}^{\varepsilon-I} n_o R_I(\varepsilon,y)dyd\varepsilon + \int_{y=I}^{\infty} f(y) \int_{\varepsilon=0}^{y-I} n_o R_I(y,\varepsilon)d\varepsilon dy + \int_{y=I}^{\infty} f(y) \int_{\varepsilon=0}^{y-I} n_o R_I(y,y-\varepsilon-I)d\varepsilon dy \quad (93)$$

Limits to the integrals in Equation 93 are most easily obtained by the use of Figure 23. The last term on the left-hand side of the equation, for example, corresponds to possibility c of the figure. From the reaction implied, the ionizing electron must possess an energy of at least y = I for the ionization to occur. Thus, y can range from y = I to infinity. The same electron must emerge from the collision with an energy equal to, or greater than zero. Therefore, from Figure 23-c, $y-\varepsilon-I > 0$; and ε can thus range from $\varepsilon = 0$ to $\varepsilon = y-I$. Limits on the other integrals are established in the same manner.

The inner integrals of Equation 93 are of the form $\int_B R_I(A,B)dB$ or $\int_B R_I(B,A)dB$, and represent the total rate of ionization, $R_I(B)$, at electron energy B. Equation 93 can therefore be written

$$\frac{\partial n}{\partial t}_{I\text{-coll}} = -\int_{\varepsilon=I}^{\infty} f(\varepsilon)n_o R_I(\varepsilon)d\varepsilon + \int_{y=I}^{\infty} f(y)n_o R_I(y)dy + \int_{y=I}^{\infty} f(y)n_o R_I(y)dy \qquad (94)$$

Using the general relationship $\int_A f(A)R_I(A)dA = n\langle R_I\rangle$, where $\langle R_I\rangle$ is the energy-averaged ionization rate, Equation 94 yields for the zeroth moment

$$\frac{\partial n}{\partial t}_{I\text{-coll}} = \langle R_I\rangle n_o n \qquad (95)$$

The first moment is found by multiplying Equation 92 by ε, and setting up integrals over all energy as described in the preceding paragraphs. A change of variable $\varepsilon^* = y-\varepsilon-I$ on the term involving $R_I(y,y-\varepsilon-I)$, and an interchange of integrals permits a mutual cancellation of all but one term. Using the relationships for the total rate of ionization at a given energy and for the energy-averaged ionization rate on the remaining term yields for the first moment

$$\frac{\partial\langle\varepsilon\rangle}{\partial t}_{I\text{-coll}} = -In_o n\langle R_I\rangle \qquad (96)$$

APPENDIX C

AEROSOL BREAKDOWN

Microscopic particles, such as water droplets, salt, ash, spores, dust, and photochemical pollutants, are present to some degree in any given portion of the atmosphere. Under intense laser irradiation, these particles, or aerosols, vaporize and form localized plasma spheres within the beam volume. High free electron densities within each aerosol plasma sphere can cause, via microwave heating, severe attenuation of the laser flux intensity. Thus, if the number density of aerosol particles within the beam is large, the beam parameters must be chosen with some care if breakdown is to be extended over a kilometer-long path.

The radius of the plasma sphere formed about each aerosol particle may be approximated

$$r_p = v_p(t_p - t_v) \tag{97}$$

where v_p is the velocity of the plasma wave, t_v is the time required to vaporize the particle, and t_p is the time that the particle is irradiated by the laser pulse. The cross-sectional area of each plasma sphere is thus

$$K_{AER}(t) = \pi v_p^2(t - t_v)^2 \tag{98}$$

The radiation transfer equation (Equation 22) may be modified to include losses due to aerosol vaporization. The resultant equation is

$$\frac{dS(z,t)}{dz} = [\ F(z) - A_T\ ]\ S(z,t) - Kn(z,t)S(z,t)$$

$$- K_{AER}(t)n_{AER}S(z,t) \tag{99}$$

where n_{AER} is the aerosol particle density. An approximate solution of Equation 99, using the methods of Section IV, is not evident. The aerosol

term of Equation 99 can be ignored, however, if it is smaller than the least contributing of the remaining terms, namely A_T. A criterion for negligible aerosol contribution to the electron distribution equation is thus

$$K_{AER}(t)n_{AER} << A_T \tag{100}$$

Substituting Equation 98 into Equation 100, and rearranging the terms results in

$$t_p << \left(\frac{A_T}{\pi n_{AER} v_p^2}\right)^{\frac{1}{2}} + t_v \tag{101}$$

The energy required to vaporize a particle of mass density n_m and radius r_p is given by

$$E = \frac{4}{3}\pi r^3 n_m c_p \Delta T \tag{102}$$

where c_p is the specific heat of the particle at constant pressure, and ΔT is the change in temperature for the particle.

The energy added to the particle is, assuming a laser pulse of constant intensity,

$$E = \pi r^2 S t_v \tag{103}$$

Eliminating E from Equation 102 and 103, the time required to vaporize a particle is found to be

$$t_v = \frac{4 r_p n_m c_p \Delta T}{S} \tag{104}$$

The criterion for negligible flux losses due to aerosol plasmas (Equation 101) thus becomes

$$t_p << \left(\frac{A_T}{\pi n_{AER} v_p^2}\right)^{\frac{1}{2}} + \frac{4 r_p n_m c_p \Delta T}{S} \tag{105}$$

The atmospheric attenuation coefficient corresponding to a hazy day is, from Table 2, 4.1×10^{-6} cm^{-1}. Using typical values for n_m, $c_p \Delta T$, and v_p of 1 gm/cm^3, 10^4 joules/gm, and 10^5 cm/sec (Reference 18), Equation 105 becomes, for a laser flux intensity of 10^9 W/cm^3,

$$t_p << 10^{-8}(n_{AER})^{\frac{1}{2}} + 4 \times 10^{-5} r_p \tag{106}$$

The number density of aerosol particles in the atmosphere is highly variable. Particle sizes are typically in the micron range. Using a particle density of 10^4 cm^{-3} from the "hazy atmosphere" aerosol model of McClatchey, et al., and assuming a particle radius of 10^{-4} cm, Equation 106 yields

$$t_p << 10^{-10} \text{ sec} \tag{107}$$

An upper limit of 10^{-10} seconds for the pulse length in a laser lightning rod system poses severe constraints on the laser lightning rod system, since it is evident from Appendix D that short pulse lengths tend to generate the lower electron distributions along the beam. If the system is to be operated in a clean-air breakdown mode, it thus becomes important that the atmospheric aerosol count be as low as possible so that the pulse length can be maximized.

APPENDIX D

SUMMARY DATA FROM TESTED LASER LIGHTNING ROD SCENARIOS

Summary data for 630 laser lightning rod scenarios is listed in the following 16 tables. The information is organized so that each page contains data for 42 scenarios of common focal length, wavelength, pulse length, electron heating coefficient, and atmospheric attenuation. Each horizontal line of data represents a single scenario.

Definitions of the symbols which appear at the heading of the tables follows:

λ	= laser wavelength (μm)
z_F	= distance from final optical element to beam waist (m)
t_E	= approximate pulse length (sec). The specific pulse is indicated by the Roman numeral in parentheses, which corresponds to a pulse in Figure 17.
$K_A(K_B)$	= electron heating coefficient (cm^2) corresponding to Modification A (B) of the high flux limit. The numeric given is the approximate beginning heating coefficient value.
A_T	= atmospheric attenuation coefficient (km^{-1})
z_B	= distance from final optical element to the breakdown initiation point (m)
w_L	= radius of the final optical element (cm)
n_e max	= maximum electron density (electrons/cm^3)
n_e final	= electron density on the 51st, and final, step of the computations (electrons/cm^3)
z_{max}	= location of n_e max relative to the final optical element (m)
z_{end}	= location of n_e final relative to the final optical element (m)
S_{max}	= maximum flux intensity at the final optical element (GW/cm^2)
EDT	= distribution shape, to be discussed below.

AD-A063 847 AIR FORCE FLIGHT DYNAMICS LAB WRIGHT-PATTERSON AFB OHIO F/G 4/2
THE LASER LIGHTNING ROD SYSTEM: A FEASIBILITY STUDY.(U)
JUN 78 C W SCHUBERT

UNCLASSIFIED AFFDL-TR-78-60 NL

2 OF 2
AD
A063 847

END
DATE
FILMED
3--79
DDC

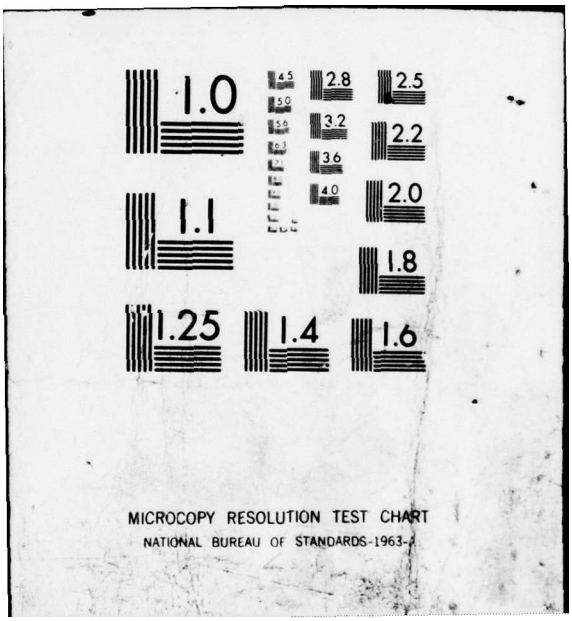
1.0
1.1
1.25
1.4
1.6
1.8
2.0
2.2
2.5
2.8
3.2
3.6
4.0
4.5
5.0
5.6
6.3
MICROCOPY RESOLUTION TEST CHART
NATIONAL BUREAU OF STANDARDS-1963-A

It is possible to categorize a given electron distribution into one of five general types illustrated in Figure 24, and defined as follows:

Type A - The electron density reaches a maximum at z_{max}, then falls to zero at z_{end}.

Type B - The electron density reaches a maximum at z_{max}, and shows a definite decrease from that point onward until computations stop at z_{end}.

Type C - The electron density reaches a maximum at z_{max} and maintains that density until computations stop at z_{end}.

Type D - The electron density increases until z_{end}.

Type E - The electron cascade is extinguished immediately. No free electrons are generated.

The approximate electron distribution can be sketched by plotting the electron densities at z_B, z_{max}, and z_{end} on semilog paper, and drawing a smooth line connecting the points.

To interpret the data for a given scenario, it is important to take all of the factors into consideration. It is possible, for example, for a beam with a low $n_{e\ max}$ to have a high total ionization along the beam, and for a beam with a high $n_{e\ max}$ to have a low total beam ionization. Thus, beam sketches, mental or real, should be made before attempting to draw conclusions.

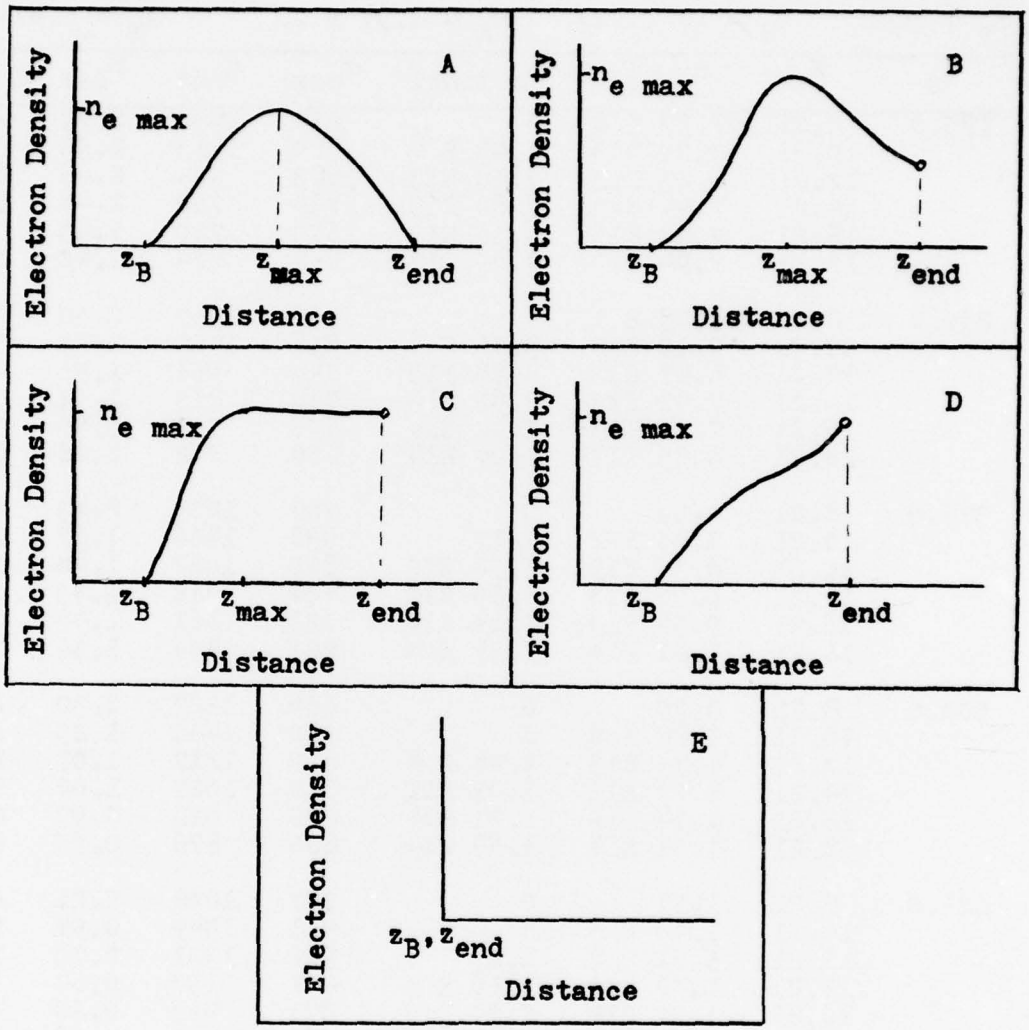

Figure 24. Electron Distribution Types

TABLE D-1

λ = 10.6
z_F = 1000 $t_E \approx 10^{-8}$ (I) $K_A \approx 2.35 \times 10^{-18}$ A_T = 0.41

Z_B	W_L	n_e max	n_e final	z_{max}	z_{end}	S_{max}	EDT
125.0	8.21	2.27 E 2	0	657	1430	2.79	A
	10.21	3.29 E13	1.05 E 4	770	1313	2.50	B
	12.21	6.21 E13	3.48 E13	683	939	2.46	C
	14.21	7.44 E13	7.80 E13	714	760	2.44	C
	16.21	7.99 E13	9.36 E13	673	729	2.43	C
	18.21	7.94 E13	9.09 E13	647	724	2.42	C
250.0	8.21	5.08 E 1	0	700	1353	2.60	A
	10.21	2.19 E13	3.46 E 1	864	1417	2.04	B
	12.21	6.47 E13	2.78 E13	747	951	1.95	C
	14.21	7.42 E13	9.02 E13	716	813	1.91	C
	16.21	7.99 E13	1.12 E14	670	798	1.89	C
	18.21	8.25 E13	1.07 E14	660	772	1.88	C
375.0	8.21	9.39	0	784	1289	2.43	A
	10.21	2.95 E12	2.17	938	1466	1.62	B
	12.21	6.35 E13	1.58 E10	810	1082	1.48	B
	14.21	8.08 E13	6.60 E13	744	912	1.43	C
	16.21	9.54 E13	1.14 E14	733	861	1.40	C
	18.21	1.01 E14	1.37 E14	723	836	1.39	C
500.0	8.21	3.70	0	664	1227	2.30	A
	10.21	1.78 E 9	0	940	1440	1.25	A
	12.21	4.74 E13	1.48 E 4	879	1217	1.07	B
	14.21	8.77 E13	7.05 E11	812	1027	1.00	B
	16.21	1.14 E14	1.21 E14	800	928	0.97	C
	18.21	1.31 E14	1.53 E14	800	876	0.95	C
625.0	8.21	1.51	0	707	1024	2.21	A
	10.21	1.48 E 5	0	901	1349	0.94	A
	12.21	5.62 E12	1.23	922	1331	0.72	B
	14.21	7.72 E13	3.10 E 5	891	1137	0.64	B
	16.21	1.27 E14	5.54 E13	871	973	0.60	B
	18.21	1.54 E14	1.54 E14	922	922	0.58	D
750.0	8.21	1.02	0	770	832	2.17	A
	10.21	3.21 E 2	0	924	1220	0.71	A
	12.21	2.63 E 6	0	955	1242	0.46	A
	14.21	8.00 E11	1.08	986	1256	0.36	B
	16.21	8.26 E13	3.68 E 2	944	1149	0.32	B
	18.21	1.54 E14	9.77 E 6	927	1067	0.30	B
875.0	8.21	0	0	875	875	2.18	E
	10.21	4.26	0	957	1107	0.57	A
	12.21	4.29 E 1	0	987	1137	0.30	A
	14.21	2.29 E 3	0	972	1129	0.19	A
	16.21	7.98 E 5	0	977	1130	0.14	A
	18.21	1.50 E 9	0	990	1134	0.11	A

TABLE D-2

λ = 10.6
z_F = 1000 $t_E \approx 10^{-6}$ (II) $K_A \approx 2.35 \times 10^{-18}$ A_T = 0.41

z_B	W_L	n_e max	n_e final	z_{max}	z_{end}	S_{max}	EDT
125.0	8.21	3.81 E12	3.46 E12	162	240	2.79	C
	10.21	1.05 E13	1.07 E13	140	168	2.50	C
	12.21	1.20 E13	1.18 E13	140	164	2.46	C
	14.21	1.25 E13	1.26 E13	140	162	2.44	C
	16.21	1.27 E13	1.29 E13	140	161	2.43	C
	18.21	1.29 E13	1.26 E13	140	160	2.42	C
250.0	8.21	3.45 E12	3.22 E12	288	377	2.60	C
	10.21	1.21 E13	1.13 E13	264	289	2.04	C
	12.21	1.41 E13	1.35 E13	279	283	1.95	C
	14.21	1.38 E13	1.40 E13	260	281	1.91	C
	16.21	1.40 E13	1.37 E13	260	280	1.89	C
	18.21	1.46 E13	1.46 E13	260	279	1.88	C
375.0	8.21	3.10 E12	2.26 E12	429	528	2.43	C
	10.21	1.37 E13	1.32 E13	392	408	1.62	C
	12.21	1.56 E13	1.48 E13	384	403	1.48	C
	14.21	1.76 E13	1.64 E13	384	401	1.43	C
	16.21	1.81 E13	1.76 E13	384	400	1.40	C
	18.21	1.87 E13	1.85 E13	384	400	1.39	C
500.0	8.21	2.18 E12	3.53 E11	558	765	2.30	B
	10.21	1.40 E13	1.38 E13	510	531	1.25	C
	12.21	1.95 E13	1.88 E13	508	524	1.07	C
	14.21	2.17 E13	2.00 E13	508	521	1.00	C
	16.21	2.31 E13	2.14 E13	508	521	0.97	C
	18.21	2.36 E13	2.40 E13	507	520	0.95	C
625.0	8.21	6.06 E11	0	732	927	2.21	A
	10.21	1.52 E13	1.46 E13	634	654	0.94	C
	12.21	2.30 E13	2.19 E13	632	646	0.72	C
	14.21	2.78 E13	2.65 E13	636	642	0.64	C
	16.21	2.82 E13	2.91 E13	630	641	0.60	C
	18.21	3.04 E13	3.02 E13	630	640	0.58	C
750.0	8.21	9.67	0	770	832	2.17	A
	10.21	1.39 E13	1.17 E13	770	783	0.71	C
	12.21	2.58 E13	2.38 E13	758	769	0.46	C
	14.21	3.40 E13	3.31 E13	755	764	0.36	C
	16.21	4.05 E13	4.02 E13	754	762	0.32	C
	18.21	4.45 E13	4.44 E13	754	761	0.30	C
875.0	8.21	0	0	875	875	2.18	E
	10.21	6.71 E12	8.24 E11	899	966	0.57	B
	12.21	1.95 E13	1.68 E13	883	900	0.30	C
	14.21	3.28 E13	3.13 E13	879	889	0.19	C
	16.21	4.91 E13	4.66 E13	879	885	0.14	C
	18.21	5.73 E13	5.95 E13	877	883	0.11	C

TABLE D-3

λ = 10.6
z_F = 1000 $t_E \approx 10^{-8}$ (I) $K_B \approx 3.72 \times 10^{-19}$ A_T = 0.41

z_B	W_L	n_e max	n_e final	z_{max}	z_{end}	S_{max}	EDT
125.0	8.21	2.36	0	658	1430	2.79	A
	10.21	3.88 E 3	3.04	944	1518	2.50	B
	12.21	1.79 E 8	9.09 E 3	965	1210	2.46	B
	14.21	1.90 E14	1.21 E14	924	965	2.44	C
	16.21	1.14 E14	9.74 E13	883	896	2.43	C
	18.21	1.37 E14	1.07 E14	852	864	2.42	C
250.0	8.21	1.86	0	701	1353	2.60	A
	10.21	6.39 E 2	1.50	946	1540	2.04	B
	12.21	4.17 E 6	1.04 E 3	936	1223	1.95	B
	14.21	5.78 E12	1.49 E 7	977	1141	1.91	B
	16.21	2.59 E14	8.99 E13	905	931	1.89	B
	18.21	4.90 E14	1.31 E14	875	895	1.88	B
375.0	8.21	1.43	0	785	1289	2.43	A
	10.21	1.33 E 2	1.11	938	1507	1.62	B
	12.21	7.51 E 4	9.02	948	1338	1.48	B
	14.21	9.51 E 8	3.73 E 3	989	1204	1.43	B
	16.21	3.13 E14	4.14 E13	938	989	1.40	B
	18.21	5.40 E14	1.31 E14	908	929	1.39	B
500.0	8.21	1.23	0	664	1227	2.30	A
	10.21	8.93 E 1	0	940	1437	1.25	A
	12.21	2.03 E 3	2.33	961	1350	1.07	B
	14.21	1.22 E 6	4.04 E 1	992	1248	1.00	B
	16.21	3.72 E10	1.91 E 4	981	1145	0.97	B
	18.21	2.78 E14	7.94 E14	951	973	0.95	B
625.0	8.21	1.07	0	707	1024	2.21	A
	10.21	6.60	0	902	1349	0.94	A
	12.21	1.06 E 2	1.04	963	1337	0.72	B
	14.21	5.89 E 3	3.86	988	1265	0.64	B
	16.21	3.49 E 6	2.47 E 2	968	1173	0.60	B
	18.21	5.10 E10	2.64 E 5	978	1091	0.58	B
750.0	8.21	1.00	0	770	832	2.17	A
	10.21	2.50	0	924	1220	0.71	A
	12.21	1.04 E 1	0	95[illegible]	1240	0.46	A
	14.21	7.84 E 1	1.02	9[illegible]6	1256	0.36	B
	16.21	1.53 E 3	1.48	970	1221	0.32	B
	18.21	7.18 E 4	3.78	996	1185	0.30	B
875.0	8.21	0	0	875	875	2.18	E
	10.21	1.26	0	957	1107	0.57	A
	12.21	1.82	0	988	1136	0.30	A
	14.21	3.41	0	972	1130	0.19	A
	16.21	8.63	0	977	1130	0.14	A
	18.21	2.81 E 1	0	990	1134	0.11	A

TABLE D-4

$\lambda = 10.6$
$z_F = 1000$ $t_B \approx 10^{-6}$ (II) $K_B \approx 3.72 \times 10^{-19}$ $A_T = 0.41$

z_B	W_L	n_e max	n_e final	z_{max}	z_{end}	S_{max}	EDT
125.0	8.21	1.19 E13	3.54 E 1	350	1134	2.79	B
	10.21	2.64 E13	2.68 E13	206	272	2.50	C
	12.21	2.80 E13	2.81 E13	197	254	2.46	C
	14.21	2.88 E13	2.90 E13	195	248	2.44	C
	16.21	2.90 E13	2.96 E13	194	246	2.43	C
	18.21	2.95 E13	2.97 E13	194	244	2.42	C
250.0	8.21	9.99 E12	0	511	1161	2.60	A
	10.21	2.81 E13	2.81 E13	322	381	2.04	C
	12.21	3.08 E13	3.07 E13	315	353	1.95	B
	14.21	3.06 E13	3.16 E13	308	349	1.91	C
	16.21	3.06 E13	3.24 E13	306	345	1.89	C
	18.21	3.29 E13	3.22 E13	306	345	1.88	C
375.0	8.21	4.04 E12	0	703	1158	2.43	A
	10.21	2.98 E13	2.96 E13	442	490	1.62	C
	12.21	3.32 E13	3.44 E13	427	464	1.48	C
	14.21	3.53 E13	3.58 E13	423	458	1.43	C
	16.21	3.58 E13	3.67 E13	421	454	1.40	C
	18.21	3.65 E13	3.67 E13	420	453	1.39	C
500.0	8.21	1.04 E 9	0	664	1227	2.30	A
	10.21	3.05 E13	3.05 E13	601	601	1.25	D
	12.21	3.69 E13	3.28 E13	544	576	1.07	C
	14.21	3.97 E13	3.44 E13	539	565	1.00	C
	16.21	4.11 E13	4.12 E13	543	560	0.97	B
	18.21	4.17 E13	3.96 E13	536	558	0.95	B
625.0	8.21	7.04 E 2	0	707	1024	2.21	A
	10.21	3.16 E13	2.60 E13	680	726	0.94	C
	12.21	4.06 E13	3.83 E13	665	688	0.72	C
	14.21	4.51 E13	4.58 E13	656	676	0.64	C
	16.21	4.65 E13	4.53 E13	654	671	0.60	C
	18.21	4.83 E13	4.89 E13	652	670	0.58	C
750.0	8.21	1.43	0	771	832	2.17	A
	10.21	2.73 E13	1.50 E13	814	925	0.71	B
	12.21	4.24 E13	3.52 E13	784	808	0.46	C
	14.21	5.07 E13	4.75 E13	775	790	0.36	C
	16.21	5.55 E13	5.20 E13	771	783	0.32	B
	18.21	5.84 E13	5.97 E13	769	779	0.30	C
875.0	8.21	0	0	875	875	2.18	E
	10.21	9.61 E 9	0	957	1107	0.57	A
	12.21	2.91 E13	1.37	924	1078	0.30	B
	14.21	4.73 E13	4.26 E13	901	923	0.19	C
	16.21	6.02 E13	5.90 E13	893	903	0.14	C
	18.21	6.96 E13	6.18 E13	890	896	0.11	C

TABLE D-5

λ = 10.6
z_F = 1000 $t_E \approx 2 \times 10^{-8}$ (VII) $K_A \approx 2.35 \times 10^{-18}$ A_T = 0.41

z_B	W_L	n_e max	n_e final	z_{max}	z_{end}	S_{max}	EDT
125.0	8.21	6.91 E 6	0	657	1425	2.79	A
	10.21	3.40 E13	1.73 E13	494	893	2.50	C
	12.21	4.25 E13	4.91 E13	478	683	2.46	C
	14.21	4.81 E13	5.58 E13	560	652	2.44	C
	16.21	4.73 E13	5.93 E13	514	637	2.43	C
	18.21	4.66 E13	6.11 E13	499	627	2.42	C
250.0	8.21	9.86 E 4	0	700	1351	2.60	A
	10.21	3.58 E13	5.24 E 9	583	1084	2.04	B
	12.21	4.84 E13	4.78 E13	680	762	1.95	B
	14.21	4.78 E13	6.23 E13	516	706	1.91	C
	16.21	4.70 E13	6.62 E13	491	690	1.89	C
	18.21	5.01 E13	7.23 E13	491	690	1.88	C
375.0	8.21	7.53 E 2	0	784	1286	2.43	A
	10.21	3.48 E13	3.19 E 5	672	1194	1.62	B
	12.21	4.94 E13	4.15 E13	605	856	1.48	C
	14.21	5.76 E13	6.90 E13	590	779	1.43	C
	16.21	5.92 E13	7.57 E13	580	754	1.40	C
	18.21	6.32 E13	8.65 E13	580	744	1.39	C
500.0	8.21	4.93 E 1	0	664	1227	2.30	A
	10.21	3.01 E13	7.35	787	1288	1.25	B
	12.21	5.52 E13	3.34 E12	700	1002	1.07	B
	14.21	6.90 E13	6.87 E13	684	869	1.00	C
	16.21	7.67 E13	9.11 E13	679	828	0.97	C
	18.21	8.09 E13	9.56 E13	674	797	0.95	C
625.0	8.21	3.45	0	707	1019	2.21	A
	10.21	7.36 E12	0	922	1288	0.94	A
	12.21	5.72 E13	1.67 E 5	804	1142	0.72	B
	14.21	8.15 E13	3.52 E13	781	960	0.64	B
	16.21	9.91 E13	9.91 E13	884	884	0.60	D
	18.21	9.84 E13	1.17 E14	753	858	0.58	C
750.0	8.21	1.07	0	770	832	2.17	A
	10.21	1.81 E 7	0	924	1217	0.71	A
	12.21	2.51 E13	0	934	1204	0.46	A
	14.21	7.88 E13	7.71 E 2	880	1131	0.36	B
	16.21	1.07 E14	2.50 E11	850	1019	0.32	B
	18.21	1.30 E14	4.82 E13	842	983	0.30	B
875.0	8.21	0	0	875	875	2.18	E
	10.21	7.46 E 1	0	957	1105	0.57	A
	12.21	6.10 E 4	0	988	1135	0.30	A
	14.21	4.28 E 9	0	972	1128	0.19	A
	16.21	3.06 E13	0	977	1116	0.14	A
	18.21	1.10 E14	1.95	947	1095	0.11	B

TABLE D-6

λ = 10.6
z_F = 1000 $t_E \approx 2 \times 10^{-9}$(VIII) $K_A \approx 2.35 \times 10^{-18}$ A_T = 0.41

z_B	W_L	n_e max	n_e final	z_{max}	z_{end}	S_{max}	EDT
125.0	8.21	4.83	0	657	1425	2.79	A
	10.21	9.11 E 5	6.90	944	1518	2.50	B
	12.21	2.07 E13	3.95 E 5	924	1231	2.46	B
	14.21	2.74 E14	2.56 E14	888	918	2.44	B
	16.21	3.93 E14	3.98 E14	842	857	2.43	C
	18.21	4.62 E14	4.15 E14	832	837	2.42	C
250.0	8.21	3.16	0	700	1351	2.60	A
	10.21	5.05 E 4	1.91	946	1540	2.04	B
	12.21	5.97 E10	1.05 E 5	936	1223	1.95	B
	14.21	2.13 E14	1.01 E14	936	977	1.91	B
	16.21	3.96 E14	3.83 E14	875	926	1.89	C
	18.21	5.05 E14	4.97 E14	867	887	1.88	C
375.0	8.21	1.94	0	784	1286	2.43	A
	10.21	2.87 E 3	1.17	959	1501	1.62	B
	12.21	7.05 E 7	6.13 E 1	969	1317	1.48	B
	14.21	5.03 E13	5.30 E 5	969	1174	1.43	B
	16.21	3.58 E14	3.84 E12	912	1020	1.40	B
	18.21	5.24 E14	5.07 E14	897	918	1.39	C
500.0	8.21	1.48	0	664	1227	2.30	A
	10.21	2.59 E 2	0	961	1433	1.25	A
	12.21	4.11 E 5	2.80	940	1381	1.07	B
	14.21	8.82 E 9	5.44 E 2	992	1248	1.00	B
	16.21	1.69 E14	1.49 E 8	961	1094	0.97	B
	18.21	4.88 E14	2.48 E14	928	979	0.95	B
625.0	8.21	1.13	0	707	1019	2.21	A
	10.21	3.17 E 1	0	963	1344	0.94	A
	12.21	2.35 E 3	1.04	973	1337	0.72	B
	14.21	3.41 E 6	7.32	978	1275	0.64	B
	16.21	4.55 E10	1.00 E 4	968	1173	0.60	B
	18.21	1.85 E14	2.56 E10	978	1050	0.58	B
750.0	8.21	1.01	0	770	832	2.17	A
	10.21	5.32	0	924	1217	0.71	A
	12.21	6.17 E 1	0	955	1239	0.46	A
	14.21	1.70 E 3	1.03	986	1252	0.36	B
	16.21	1.85 E 5	2.28	980	1216	0.32	B
	18.21	9.68 E 7	1.02 E 1	996	1185	0.30	B
875.0	8.21	0	0	875	875	2.18	E
	10.21	1.54	0	957	1105	0.57	A
	12.21	3.01	0	988	1135	0.30	A
	14.21	9.18	0	972	1128	0.19	A
	16.21	4.06 E 1	0	988	1130	0.14	A
	18.21	3.26 E 2	0	990	1132	0.11	A

TABLE D-7

λ = 10.6
z_F = 500 $t_E \approx 10^{-8}$ (I) $K_A \approx 2.35 \times 10^{-18}$ A_T = 0.41

z_B	W_L	n_e max	n_e final	z_{max}	z_{end}	S_{max}	EDT
62.5	5.81	6.74 E 3	0	370	848	2.72	A
	7.81	1.04 E14	3.07 E 9	339	559	2.42	B
	9.81	1.50 E14	1.61 E14	349	367	2.38	C
	11.81	1.56 E14	1.96 E14	316	365	2.37	C
	13.81	1.47 E14	2.05 E14	303	352	2.36	C
	15.81	1.60 E14	1.99 E14	306	349	2.36	C
125.0	5.81	5.75 E 2	0	412	801	2.47	A
	7.81	1.02 E14	1.54 E14	376	550	1.89	B
	9.81	1.56 E14	1.66 E14	350	407	1.82	C
	11.81	1.61 E14	2.17 E14	325	389	1.80	C
	13.81	1.71 E14	2.20 E14	322	384	1.79	C
	15.81	1.70 E14	2.53 E14	320	381	1.78	C
187.5	5.81	9.90 E 1	0	413	757	2.25	A
	7.81	8.50 E13	4.93 E 5	418	618	1.43	B
	9.81	1.67 E14	1.55 E14	369	459	1.33	C
	11.81	1.98 E14	2.66 E14	359	420	1.29	C
	13.81	2.14 E14	2.90 E14	356	410	1.28	C
	15.81	2.17 E14	2.97 E14	354	408	1.27	C
250.0	5.81	1.32 E 1	0	373	713	2.08	A
	7.81	2.12 E13	7.71	480	701	1.04	B
	9.81	1.74 E14	1.55 E10	406	534	0.91	B
	11.81	2.43 E14	2.58 E14	396	452	0.87	C
	13.81	3.00 E14	3.40 E14	419	433	0.51	C
	15.81	2.96 E14	3.46 E14	406	423	0.84	C
312.5	5.81	4.19	0	394	625	1.94	A
	7.81	9.14 E 8	0	461	709	0.72	A
	9.81	1.44 E14	2.91 E 5	453	576	0.57	B
	11.81	2.79 E14	1.93 E14	434	479	0.52	C
	13.81	3.12 E14	3.64 E14	419	456	0.50	C
	15.81	3.31 E14	4.04 E14	412	446	0.49	C
375.0	5.81	1.51	0	416	564	1.86	A
	7.81	2.61 E 4	0	467	632	0.49	A
	9.81	4.90 E11	1.06	493	636	0.32	B
	11.81	2.21 E14	1.88 E 4	467	559	0.27	B
	13.81	3.73 E14	5.13 E11	452	512	0.24	B
	15.81	4.69 E14	4.32 E14	449	481	0.23	C
437.5	5.81	1.01	0	448	457	1.82	A
	7.81	1.70 E 1	0	489	572	0.35	A
	9.81	1.76 E 3	0	486	569	0.17	A
	11.81	1.04 E 7	0	490	569	0.11	A
	13.81	8.86 E11	0	499	571	0.08	A
	15.81	3.04 E14	1.10 E 2	486	544	0.07	B

TABLE D-8

λ = 10.6
z_F = 500 $t_E \approx 10^{-6}$ (II) $K_A \approx 2.35 \times 10^{-18}$ A_T = 0.41

z_B	W_L	n_e max	n_e final	z_{max}	z_{end}	S_{max}	EDT
62.5	5.81	1.07 E13	9.43 E12	78	106	2.72	C
	7.81	2.55 E13	2.42 E13	70	81	2.42	C
	9.81	2.78 E13	2.64 E13	74	79	2.38	C
	11.81	2.84 E13	2.84 E13	79	79	2.37	D
	13.81	2.68 E13	2.68 E13	78	79	2.36	C
	15.81	2.64 E13	2.62 E13	75	79	2.36	C
125.0	5.81	1.00 E13	9.51 E12	140	171	2.47	C
	7.81	2.67 E13	2.77 E13	130	142	1.89	C
	9.81	2.98 E13	3.11 E13	130	140	1.82	C
	11.81	3.24 E13	3.01 E13	130	139	1.80	C
	13.81	3.14 E13	3.20 E13	130	139	1.79	C
	15.81	3.19 E13	3.09 E13	130	139	1.78	C
187.5	5.81	9.10 E12	8.11 E12	204	239	2.25	C
	7.81	3.22 E13	3.15 E13	192	202	1.43	C
	9.81	3.70 E13	3.66 E13	192	200	1.33	C
	11.81	3.85 E13	3.82 E13	192	200	1.29	C
	13.81	4.03 E13	3.93 E13	192	199	1.28	C
	15.81	3.99 E13	3.85 E13	192	199	1.27	C
250.0	5.81	7.18 E12	5.80 E12	269	318	2.08	C
	7.81	3.62 E13	3.42 E13	254	263	1.04	C
	9.81	4.61 E13	4.46 E13	254	261	0.91	C
	11.81	4.93 E13	4.92 E13	254	260	0.87	C
	13.81	5.09 E13	4.92 E13	254	260	0.85	C
	15.81	5.15 E13	5.15 E13	254	260	0.84	C
312.5	5.81	5.12 E12	1.27 E12	339	429	1.94	C
	7.81	4.16 E13	3.73 E13	317	324	0.72	C
	9.81	5.55 E13	5.55 E13	321	321	0.57	D
	11.81	5.98 E13	5.65 E13	315	320	0.52	C
	13.81	6.43 E13	6.60 E13	315	320	0.50	C
	15.81	6.39 E13	6.73 E13	315	320	0.49	C
375.0	5.81	1.05 E12	0	426	516	1.86	A
	7.81	4.02 E13	3.61 E13	379	387	0.49	C
	9.81	6.63 E13	6.44 E13	377	382	0.32	C
	11.81	8.57 E13	8.46 E13	377	381	0.27	C
	13.81	9.52 E13	9.09 E13	377	380	0.24	C
	15.81	9.97 E13	9.08 E13	377	380	0.23	C
437.5	5.81	2.46	0	448	458	1.82	A
	7.81	2.65 E13	1.85 E13	444	457	0.35	C
	9.81	6.53 E13	5.65 E13	440	445	0.17	C
	11.81	1.08 E14	9.94 E13	440	442	0.11	C
	13.81	1.37 E14	1.29 E14	439	441	0.08	C
	15.81	1.65 E14	1.48 E14	438	440	0.07	C

TABLE D-9

λ = 10.6
z_F = 500 $t_R \approx 10^{-8}$ (I) $K_B \approx 3.72 \times 10^{-19}$ A_T = 0.41

Z_B	W_L	n_e max	n_e final	z_{max}	z_{end}	S_{max}	EDT
62.5	5.81	4.05	0	534	848	2.72	A
	7.81	1.86 E 6	2.13 E 1	503	749	2.42	B
	9.81	9.56 E13	8.83 E13	472	472	2.38	B
	11.81	2.81 E14	1.34 E14	431	432	2.37	B
	13.81	4.76 E14	4.21 E14	421	421	2.36	B
	15.81	1.59 E14	1.43 E14	414	416	2.36	B
125.0	5.81	2.74	0	576	801	2.47	A
	7.81	6.44 E 4	1.49 E 1	499	724	1.89	B
	9.81	1.24 E13	4.15 E 7	534	576	1.82	B
	11.81	2.10 E14	1.35 E14	448	458	1.80	B
	13.81	1.63 E14	1.56 E14	433	458	1.79	B
	15.81	1.62 E14	1.72 E14	428	436	1.78	B
187.5	5.81	2.07	0	577	757	2.25	A
	7.81	3.11 E 3	2.68	577	751	1.43	B
	9.81	5.26 E 9	3.47 E 2	530	633	1.33	B
	11.81	2.38 E14	1.06 E14	469	479	1.29	B
	13.81	1.49 E14	1.55 E14	449	464	1.28	B
	15.81	6.08 E14	1.65 E14	443	449	1.27	B
250.0	5.81	1.51	0	455	713	2.08	A
	7.81	2.28 E 2	1.17	501	752	1.04	B
	9.81	2.94 E 6	2.39 E 1	532	644	0.91	B
	11.81	3.64 E13	1.97 E 7	506	552	0.87	B
	13.81	1.28 E15	2.03 E14	470	445	0.85	B
	15.81	2.82 E14	1.69 E14	457	462	0.84	B
312.5	5.81	1.26	0	476	625	1.94	A
	7.81	2.64 E 1	0	502	709	0.72	A
	9.81	5.79 E 3	3.21	535	648	0.57	B
	11.81	1.18 E 8	4.05 E 3	507	563	0.52	B
	13.81	8.28 E13	1.34 E 8	497	533	0.50	B
	15.81	1.74 E14	1.42 E14	475	487	0.49	B
375.0	5.81	1.07	0	457	564	1.86	A
	7.81	5.02	0	508	632	0.49	A
	9.81	7.17	1.01	534	636	0.32	B
	11.81	6.98 E 3	1.83	508	613	0.27	B
	13.81	1.32 E 7	5.32	518	595	0.24	B
	15.81	3.89 E11	6.01 E 4	506	539	0.23	B
437.5	5.81	1.00	0	448	457	1.82	A
	7.81	1.57	0	530	572	0.35	A
	9.81	3.27	0	507	569	0.17	A
	11.81	1.30 E 1	0	510	569	0.11	A
	13.81	7.89 E 1	0	519	569	0.08	A
	15.81	1.74 E 3	1.32	503	568	0.07	B

TABLE D-10

λ = 10.6
z_F = 500 $t_E \approx 10^{-6}$ (I?) $K_B \approx 3.72 \times 10^{-19}$ A_T = 0.41

z_B	W_L	n_e max	n_e final	z_{max}	z_{end}	S_{max}	EDT
62.5	5.81	2.44 E13	2.10 E13	146	229	2.72	C
	7.81	4.36 E13	4.34 E13	97	118	2.42	C
	9.81	4.53 E13	4.63 E13	94	113	2.38	C
	11.81	4.52 E13	4.67 E13	93	111	2.37	C
	13.81	4.51 E13	4.59 E13	93	110	2.36	C
	15.81	4.62 E13	4.36 E13	93	110	2.36	C
125.0	5.81	2.34 E13	1.15 E13	221	391	2.47	C
	7.81	4.66 E13	4.18 E13	155	173	1.89	C
	9.81	4.86 E13	4.35 E13	152	170	1.82	C
	11.81	5.05 E13	4.99 E13	152	168	1.80	C
	13.81	5.07 E13	5.11 E13	151	165	1.79	C
	15.81	5.11 E13	5.12 E13	151	165	1.78	C
187.5	5.81	1.95 E13	0	292	635	2.25	A
	7.81	5.01 E13	4.58 E13	214	231	1.43	C
	9.81	5.41 E13	5.44 E13	214	222	1.33	C
	11.81	5.39 E13	5.28 E13	209	220	1.29	C
	13.81	5.65 E13	5.35 E13	209	220	1.28	C
	15.81	5.55 E13	5.58 E13	209	221	1.27	C
250.0	5.81	1.10 E13	0	398	634	2.08	A
	7.81	5.31 E13	5.33 E13	274	287	1.04	C
	9.81	6.05 E13	5.69 E13	269	278	0.91	C
	11.81	6.28 E13	6.16 E13	268	276	0.87	C
	13.81	6.34 E13	6.06 E13	267	276	0.85	C
	15.81	6.38 E13	5.93 E13	267	276	0.84	C
312.5	5.81	7.42 E 9	0	476	625	1.94	A
	7.81	5.48 E13	5.31 E13	334	345	0.72	C
	9.81	6.73 E13	6.70 E13	328	336	0.57	C
	11.81	6.96 E13	6.93 E13	328	332	0.52	C
	13.81	7.46 E13	6.59 E13	326	332	0.50	C
	15.81	7.14 E13	7.39 E13	325	332	0.49	C
375.0	5.81	7.24 E 2	0	457	564	1.86	A
	7.81	5.37 E13	4.75 E13	397	411	0.49	C
	9.81	7.37 E13	6.80 E13	388	393	0.32	C
	11.81	8.37 E13	7.75 E13	385	390	0.27	C
	13.81	8.88 E13	8.88 E13	384	388	0.24	C
	15.81	9.17 E13	9.12 E13	384	387	0.23	C
437.5	5.81	1.15	0	448	458	1.82	A
	7.81	2.68 E13	0	480	551	0.35	A
	9.81	6.76 E13	6.30 E13	451	460	0.17	C
	11.81	9.30 E13	9.08 E13	446	449	0.11	C
	13.81	1.08 E14	1.00 E14	444	446	0.08	C
	15.81	1.19 E14	1.17 E14	443	444	0.07	C

TABLE D-11

λ = 1.06
z_F = 1000 $t_E \approx 10^{-8}$ (I) $K_A \approx 2.34 \times 10^{-20}$ A_T = 0.43

z_B	W_L	n_e max	n_e final	z_{max}	z_{end}	S_{max}	EDT
125.0	2.60	1.61 E 2	0	985	1392	279.47	A
	4.60	5.49 E15	6.22 E15	647	739	244.31	C
	6.60	6.13 E15	7.50 E15	627	719	242.82	C
	8.60	6.13 E15	7.34 E15	622	719	242.53	C
	10.60	6.22 E15	6.90 E15	622	714	242.44	C
	12.60	5.89 E15	7.32 E15	616	714	242.40	C
250.0	2.60	2.99 E 1	0	1069	1335	260.97	A
	4.60	6.17 E15	6.95 E15	706	818	191.72	C
	6.60	6.86 E15	8.41 E15	680	777	188.78	C
	8.60	6.96 E15	8.61 E15	675	767	188.21	C
	10.60	7.06 E15	8.48 E15	675	767	188.03	C
	12.60	7.10 E15	8.61 E15	675	765	187.97	C
375.0	2.60	8.06	0	785	1271	245.09	A
	4.60	6.23 E15	6.35 E15	764	897	143.31	C
	6.60	7.98 E15	9.76 E15	744	823	139.00	C
	8.60	8.70 E15	9.64 E15	774	805	138.14	C
	10.60	8.65 E15	1.00 E16	767	818	137.89	C
	12.60	8.64 E15	1.08 E16	767	818	137.79	C
500.0	2.60	3.32	0	828	1114	232.47	A
	4.60	7.18 E15	4.71 E12	840	1043	100.29	B
	6.60	8.50 E15	1.00 E16	792	864	94.68	C
	8.60	8.41 E15	1.12 E16	774	848	93.57	C
	10.60	8.76 E15	1.12 E16	771	838	93.24	C
	12.60	9.00 E15	1.17 E16	771	835	93.12	C
625.0	2.60	1.44	0	789	1004	233.85	A
	4.60	6.39 E15	8.04 E 6	906	1127	64.02	B
	6.60	1.00 E16	1.19 E16	840	904	57.23	C
	8.60	1.10 E16	1.34 E16	832	886	55.90	C
	10.60	1.12 E16	1.35 E16	830	881	55.50	C
	12.60	1.14 E16	1.32 E16	830	881	55.35	C
750.0	2.60	1.01	0	791	791	220.03	A
	4.60	2.41 E12	1.33	996	1254	36.04	B
	6.60	1.20 E16	5.13 E15	907	989	28.23	B
	8.60	1.38 E16	1.44 E16	890	932	26.70	C
	10.60	1.38 E16	1.71 E16	884	920	26.24	C
	12.60	1.39 E16	1.78 E16	883	919	26.06	C
875.0	2.60	0	0	875	875	221.94	E
	4.60	4.30 E 3	0	1018	1126	18.08	A
	6.60	5.10 E14	2.18	1000	1134	9.43	B
	8.60	1.70 E16	1.12 E10	957	1025	7.72	B
	10.60	1.93 E16	1.88 E16	950	973	7.22	B
	12.60	2.01 E16	2.50 E16	943	964	7.02	C

TABLE D-12

$\lambda = 1.06$
$z_F = 1000$ $t_E \approx 10^{-6}$ (II) $K_A \approx 2.34 \times 10^{-20}$ $A_T = 0.43$

z_B	W_L	n_e max	n_e final	z_{max}	z_{end}	S_{max}	EDT
125.0	2.60	3.60 E14	3.37 E14	170	247	279.47	C
	4.60	1.19 E15	1.13 E15	143	163	244.31	C
	6.60	1.23 E15	1.05 E15	144	162	242.82	C
	8.60	1.24 E15	1.24 E15	144	162	242.53	C
	10.60	1.24 E15	1.23 E15	144	162	242.44	C
	12.60	1.24 E15	1.23 E15	144	162	242.40	C
250.0	2.60	3.39 E14	2.84 E14	318	387	260.97	C
	4.60	1.35 E15	1.26 E15	262	282	191.72	C
	6.60	1.37 E15	1.28 E15	262	280	188.79	C
	8.60	1.41 E15	1.41 E15	262	280	188.21	C
	10.60	1.42 E15	1.40 E15	262	279	188.03	C
	12.60	1.42 E15	1.39 E15	262	279	187.97	C
375.0	2.60	2.87 E14	2.05 E14	435	550	245.09	C
	4.60	1.61 E15	1.48 E15	385	402	143.31	C
	6.60	1.74 E15	1.70 E15	385	401	139.00	C
	8.60	1.77 E15	1.57 E15	385	400	138.14	C
	10.60	1.76 E15	1.79 E15	385	400	137.89	C
	12.60	1.79 E15	1.72 E15	385	400	137.79	C
500.0	2.60	1.86 E14	5.09 E 5	572	834	232.47	B
	4.60	2.02 E15	1.98 E15	509	522	100.29	C
	6.60	2.22 E15	2.13 E15	509	520	94.68	C
	8.60	2.26 E15	2.16 E15	510	519	93.57	C
	10.60	2.27 E15	2.10 E15	510	519	93.24	C
	12.60	2.27 E15	2.19 E15	510	519	93.12	C
625.0	2.60	1.29 E13	0	768	932	223.85	A
	4.60	2.46 E15	2.27 E15	631	642	64.02	C
	6.60	2.82 E15	2.79 E15	630	639	57.23	C
	8.60	2.86 E15	2.84 E15	630	639	55.90	C
	10.60	2.92 E15	2.66 E15	630	639	55.50	C
	12.60	2.95 E15	3.01 E15	630	639	55.35	C
750.0	2.60	2.39	0	791	791	220.03	A
	4.60	3.14 E15	3.09 E15	755	763	36.04	C
	6.60	4.09 E15	3.42 E15	755	760	28.23	C
	8.60	4.01 E15	4.03 E15	754	759	26.70	C
	10.60	4.05 E15	3.94 E15	753	759	26.24	C
	12.60	4.17 E15	4.15 E15	753	759	26.06	C
875.0	2.60	0	0	875	875	221.94	E
	4.60	3.52 E15	2.97 E15	880	888	18.08	C
	6.60	6.12 E15	5.74 E15	878	881	9.43	C
	8.60	6.62 E15	6.44 E15	877	880	7.72	C
	10.60	7.51 E15	7.58 E15	877	880	7.22	C
	12.60	7.43 E15	7.78 E15	877	879	7.02	C

TABLE D-13

λ = 1.06
z_F = 500 $t_E \approx 10^{-8}$ (I) $K_A \approx 2.34 \times 10^{-20}$ A_T = 0.43

z_B	W_L	n_e max	n_e final	z_{max}	z_{end}	S_{max}	EDT
62.5	1.84	4.37 E 3	0	554	842	272.06	A
	3.84	9.89 E15	1.08 E16	306	360	236.90	C
	5.84	9.98 E15	1.18 E16	300	360	236.12	C
	7.84	1.01 E16	1.28 E16	300	357	236.00	C
	9.84	9.91 E15	1.06 E16	298	352	235.97	C
	11.84	1.00 E16	1.24 E16	298	349	235.96	C
125.0	1.84	4.68 E 2	0	576	794	247.32	A
	3.84	1.08 E16	1.28 E16	335	391	179.91	C
	5.84	1.13 E16	1.33 E16	330	381	178.41	C
	7.84	1.15 E16	1.32 E16	330	380	178.17	C
	9.84	1.15 E16	1.31 E16	330	380	178.11	C
	11.84	1.15 E16	1.30 E16	330	380	178.09	C
187.5	1.84	8.41 E 1	0	577	751	226.11	A
	3.84	1.20 E16	1.35 E16	367	417	129.66	C
	5.84	1.35 E16	1.62 E16	378	405	127.51	C
	7.84	1.34 E16	1.65 E16	376	404	127.18	C
	9.84	1.34 E16	1.66 E16	373	404	127.09	C
	11.84	1.33 E16	1.58 E16	374	404	127.06	C
250.0	1.84	1.22 E 1	0	455	708	208.78	A
	3.84	1.34 E16	1.37 E16	411	445	86.85	C
	5.84	1.45 E16	1.71 E16	384	420	84.13	C
	7.84	1.47 E16	1.64 E16	383	426	83.70	C
	9.84	1.44 E16	1.72 E16	382	413	83.59	C
	11.84	1.46 E16	1.56 E16	382	410	83.55	C
312.5	1.84	3.95	0	476	622	195.70	A
	3.84	1.44 E16	1.36 E16	426	466	52.18	C
	5.34	1.72 E16	2.00 E16	415	442	49.00	C
	7.84	1.75 E16	2.10 E16	414	442	48.48	C
	9.84	1.77 E16	2.02 E16	414	441	48.34	C
	11.84	1.78 E16	2.24 E16	414	441	48.30	C
375.0	1.84	1.48	0	457	559	187.26	A
	3.84	1.33 E16	4.73 E 3	470	568	26.43	B
	5.84	2.04 E16	2.15 E16	444	467	22.84	C
	7.84	2.17 E16	2.40 E16	442	460	22.28	C
	9.84	2.16 E16	2.52 E16	440	456	22.13	C
	11.84	2.22 E16	2.53 E16	440	456	22.08	C
437.5	1.84	1.00	0	448	458	183.88	A
	3.84	4.50 E 7	0	513	569	10.40	A
	5.84	2.46 E16	2.81 E10	479	514	6.53	B
	7.84	2.97 E16	3.01 E16	472	486	5.93	C
	9.84	3.10 E16	3.62 E16	471	481	5.77	C
	11.84	3.17 E16	3.35 E16	470	478	5.71	C

TABLE D-14

λ = 1.06
z_F = 500 $t_E \approx 10^{-6}$ (II) $K_A = 2.34 \times 10^{-20}$ A_T = 0.43

z_B	W_L	$n_{e\ max}$	$n_{e\ final}$	z_{max}	z_{end}	S_{max}	EDT
62.5	1.84	1.00 E15	9.15 E14	80	107	272.06	B
	3.84	2.30 E15	2.41 E15	69	79	236.90	C
	5.84	2.47 E15	2.54 E15	69	79	236.12	C
	7.84	2.50 E15	2.51 E15	69	79	236.00	C
	9.84	2.50 E15	2.51 E15	69	79	235.97	C
	11.84	2.50 E15	2.50 E15	69	79	235.96	C
125.0	1.84	9.50 E14	9.06 E14	142	172	247.32	C
	3.84	2.79 E15	2.94 E15	130	139	179.91	C
	5.84	2.94 E15	3.02 E15	130	139	178.41	C
	7.84	2.96 E15	3.00 E15	130	139	178.17	C
	9.84	2.96 E15	3.00 E15	130	139	178.11	C
	11.84	2.98 E15	2.83 E15	130	139	178.09	C
187.5	1.84	8.26 E14	7.32 E14	207	242	226.11	C
	3.84	3.43 E14	3.18 E15	192	199	129.67	C
	5.84	3.55 E15	3.62 E15	192	199	127.51	C
	7.84	3.58 E15	3.43 E15	192	199	127.18	C
	9.84	3.59 E15	3.42 E15	192	199	127.09	C
	11.84	3.59 E15	3.41 E15	192	199	127.06	C
250.0	1.84	6.95 E14	5.63 E14	272	318	208.78	C
	3.84	3.98 E15	3.96 E15	257	260	86.85	C
	5.84	4.13 E15	4.24 E15	253	259	84.13	C
	7.84	4.29 E15	4.19 E15	253	259	83.70	C
	9.84	4.32 E15	4.14 E15	253	259	83.59	C
	11.84	4.33 E15	4.09 E15	253	259	83.54	C
312.5	1.84	4.73 E14	1.28 E11	345	463	195.70	B
	3.84	5.21 E15	5.12 E15	315	320	52.18	C
	5.84	5.60 E15	5.57 E15	315	319	48.98	C
	7.84	5.70 E15	5.22 E15	315	319	48.48	C
	9.84	5.72 E15	4.95 E15	315	319	48.34	C
	11.84	5.73 E15	5.78 E15	315	319	48.30	C
375.0	1.84	3.06 E13	0	447	518	187.26	A
	3.84	6.87 E15	6.86 E15	378	380	26.43	C
	5.84	7.62 E15	7.68 E15	377	379	22.84	C
	7.84	7.85 E15	7.02 E15	377	379	22.28	C
	9.84	7.60 E15	7.32 E15	377	379	22.13	C
	11.84	7.68 E15	7.16 E15	377	379	22.08	C
437.5	1.84	1.72	0	448	458	183.88	A
	3.84	8.37 E15	7.98 E15	439	441	10.40	C
	5.84	1.24 E16	1.21 E16	438	440	6.35	C
	7.84	1.33 E16	1.32 E16	438	440	5.93	C
	9.84	1.33 E16	1.33 E16	438	440	5.77	C
	11.84	1.36 E16	1.19 E16	438	440	5.71	C

TABLE D-15

λ = 10.6
z_F = 1000 $t_F \approx 10^{-8}$ (I) $K_A \approx 2.35 \times 10^{-18}$ A_T = 2.72

z_B	W_L	n_e max	n_e final	z_{max}	z_{end}	S_{max}	EDT
125.0	8.21	0	0	0	125	3.72	E
	10.21	0	0	0	125	3.34	E
	12.21	0	0	0	125	3.28	E
	14.21	0	0	0	125	3.26	E
	16.21	0	0	0	125	3.24	E
	18.21	0	0	0	125	3.24	E
250.0	8.21	0	0	0	250	4.63	E
	10.21	0	0	0	250	3.64	E
	12.21	0	0	0	250	3.47	E
	14.21	0	0	0	250	3.40	E
	16.21	0	0	0	250	3.37	E
	18.21	0	0	0	250	3.36	E
375.0	8.21	0	0	0	375	5.78	E
	10.21	0	0	0	375	3.85	E
	12.21	7.07 E 3	0	866	1102	3.52	A
	14.21	7.50 E10	1.73	928	1161	3.40	B
	16.21	6.60 E13	2.92 E 4	918	1092	3.34	B
	18.21	1.21 E14	2.62 E12	892	1002	3.30	B
500.0	8.21	0	0	0	500	7.30	E
	10.21	0	0	0	500	3.96	E
	12.21	4.09 E 3	0	869	1098	3.40	A
	14.21	1.51 E10	1.53	930	1158	3.17	B
	16.21	6.26 E13	5.69 E 3	940	1099	3.07	B
	18.21	1.21 E14	9.16 E 9	899	1027	3.01	B
625.0	8.21	0	0	0	625	9.37	E
	10.21	1.00	0	645	666	3.98	A
	12.21	5.98 E 2	0	891	1081	3.07	A
	14.21	1.26 E 8	0	932	1144	2.71	A
	16.21	2.10 E13	2.02	963	1145	2.55	B
	18.21	1.14 E 6	5.54 E 6	919	1058	2.46	B
750.0	8.21	0	0	0	750	12.25	E
	10.21	0	0	0	750	4.01	E
	12.21	3.80 E 1	0	873	1047	2.61	A
	14.21	6.30 E 4	0	944	1114	2.06	A
	16.21	1.90 E 9	0	955	1130	1.80	A
	18.21	4.05 E13	3.34 E 1	970	1106	1.67	B
875.0	8.21	0	0	0	875	16.46	E
	10.21	0	0	0	875	4.29	E
	12.21	1.34	0	895	967	2.23	A
	14.21	1.67 E 1	0	947	1041	1.42	A
	16.21	8.38 E 2	0	972	1070	1.04	A
	18.21	4.39 E 5	0	977	1085	0.84	A

BIBLIOGRAPHY

1. Ball, L. M. "The Laser Lightning Rod System: Thunderstorm Domestication." Applied Optics, 13: 2292-2295 (October, 1974).

2. Boni, A. A., et al. Theoretical Study of Laser-Target Interactions. DARPA ORDER 3056. Science Applications, Inc.: La Jolla, California, 1977.

3. Brown, S. C. Basic Data of Plasma Physics. New York: John Wiley and Sons, Inc., 1959.

4. Chen, F. F. Introduction to Plasma Physics. New York: Plenum Press, 1976.

5. Chu, T. S., and D. C. Hogg. "Effects of Precipitation on Propagation at 0.63, 3.5, and 10.6 Microns." Bell System Technical Journal, 47: 723-759 (May-June, 1968).

6. Dawson, G., et al. "Lightning Modification" in Weather and Climate Modification, edited by W. N. Hess. New York: John Wiley and Sons, Inc., 1974.

7. Fieux, R., and C. Gary. "Artificially Triggered Lightning Above Land." Nature, 257: 212-214 (September, 1975).

8. Fitzgerald, D. R. Experimental Studies of Thunderstorm Electrification. AFGL-TR-76-0128. Hanson Air Force Base: AFSC, June, 1976.

9. Fitzgerald, D. R. "Possible Aircraft 'Triggering' of Lightning in Certain Thunderstorms." Monthly Weather Review, 95: 835-842 (December, 1967).

10. Gunn. "Electrical Field Intensity Inside of Natural Clouds." Journal of Applied Physics, 19: 481-484 (May, 1948).

11. Kasemir, H. W. "Theory and Experiments to the Problem of Rocket-Triggered Lightning Discharge" in Third Conference on Weather Modification. Boston: American Meteorological Society, 1972.

12. Klingbeil, R., and D. A. Tidman. "Theory and Computer Model of the Lightning Stepped Leader." Journal of Geophysical Research, 79: 865-869 (February 20, 1974).

13. Koopman, D. W., and K. A. Saum. "Formation and Guiding of High-Velocity Electrical Streamers by Laser-Induced Ionization." Journal of Applied Physics, 44: 5328-5336 (December, 1973).

14. Kroll, N., and K. M. Watson. "Theoretical Study of Ionization of Air by Intense Laser Pulses." Physical Review A, 5: 1883-1905 (April, 1972).

BIBLIOGRAPHY (CONTINUED)

15. McClatchey, R. A., et al. Optical Properties of the Atmosphere (Third Edition). AFCRL-72-0497. L. G. Hanscom Field, Massachusetts: August, 1972.

16. Mitchner, M., and C. H. Kruger, Jr. Partially Ionized Gases. New York: John Wiley and Sons, Inc., 1973.

17. Newman, M. M., et al. "Triggered Lightning Strokes at Very Close Range." Journal of Geophysical Research, 72: 4761-4764 (September 15, 1967).

18. Nielsen, P. E. "Notes on Gas Breakdown." Unpublished.

19. Papoular, R. Electrical Phenomena in Gases. New York: American Elsevier Publishing Co., Inc., 1965.

20. Poehler, H. A. Measured Electric Field Intensities Near Electrical Cloud Discharges Detected by the Kennedy Space Center's Lightning Detection and Ranging System, LDAR. FEC 720-7154. Kennedy Space Center: FEC, 1977.

21. Raizer, Y. P. "Breakdown and Heating of Gases Under the Influence of a Laser Beam." Soviet Physics USPEKHI, 8: 650-672 (March-April, 1965).

22. Saum, K. A., and D. W. Koopman. "Discharges Guided by Laser-Induced Rarefication Channels." The Physics of Fluids, 15: 2077-2079 (November, 1972).

23. Siegman, A. E. Introduction to Lasers and Masers. New York: McGraw-Hill Book Co., 1971.

24. Tannenbaum, B. S. Plasma Physics. New York: McGraw-Hill Book Co., 1971.

25. Triplett, J. R. Laser-Controlled Lightning Discharge Processes. SSS Report SSS-R-76-2749. Hayward, California: Systems, Science, and Software, 1975.

26. Uman, M. A. Lightning. New York: McGraw-Hill Book Co., 1969.

27. Viemeiser, P. E. The Lightning Book. Cambridge, Massachusetts: MIT Press, 1972.

28. Weichel, H. High Energy Lasers. Wright-Patterson AFB, Ohio.

☆U.S.Government Printing Office: 1978 — 757-080/56